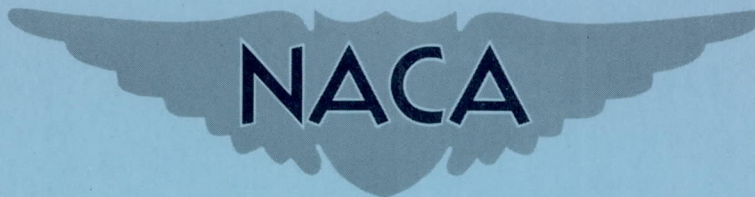


CASE FILE
COPY

RM L54B18

NACA RM L54B18



RESEARCH MEMORANDUM

INVESTIGATION AT HIGH SUBSONIC SPEEDS OF FINNED
AND UNFINNED BODIES MOUNTED AT VARIOUS LOCATIONS FROM
THE WINGS OF UNSWEPT- AND SWEPT-WING—FUSELAGE MODELS,
INCLUDING MEASUREMENTS OF BODY LOADS

By William J. Alford, Jr., and H. Norman Silvers

Langley Aeronautical Laboratory
Langley Field, Va.

NATIONAL ADVISORY COMMITTEE
FOR AERONAUTICS
WASHINGTON

April 1, 1954
Declassified February 26, 1958

NATIONAL ADVISORY COMMITTEE FOR AERONAUTICS

RESEARCH MEMORANDUM

INVESTIGATION AT HIGH SUBSONIC SPEEDS OF FINNED
AND UNFINNED BODIES MOUNTED AT VARIOUS LOCATIONS FROM
THE WINGS OF UNSWEPT- AND SWEEP-WING—FUSELAGE MODELS,
INCLUDING MEASUREMENTS OF BODY LOADS

By William J. Alford, Jr., and H. Norman Silvers

SUMMARY

An investigation has been made to determine the effects of location of bodies (finned and unfinned) on the aerodynamic characteristics of unswept- and swept-wing—fuselage models, and to determine the aerodynamic loads on the bodies in the presence of the wings. Pylon-mounted bodies at 0.33 semispan and tip-mounted bodies at 1.04 semispan were investigated.

The results indicated that the most significant effects of the bodies on the aerodynamic characteristics of the model were produced by the wing-tip-mounted body, which gave large increases in model lift-curve slope and reductions in drag due to lift, and, particularly for the swept-wing model, caused rearward shifts of the aerodynamic center.

The largest changes in the body longitudinal forces and moments were shown with the tip-mounted body, where increases in angle of attack caused substantial increases in the body normal-force and pitching-moment coefficients. Body fins effectively neutralized the body pitching-moments for the unswept-wing model, but only partially neutralized the body pitching moments for the swept-wing model. The fins increased the pitching moments on the inboard short-pylon-mounted bodies, but this effect was decreased on the swept-wing model by tilting the body axes down.

Some of the most important changes in the body lateral characteristics were shown with the inboard body, where an increase in wing sweep angle gave increases in body yawing moments and side force. Body fins partially neutralized these yawing moments.

INTRODUCTION

The National Advisory Committee for Aeronautics is conducting investigations of nacelles and external stores for use on high-speed aircraft. These investigations are primarily concerned with the performance characteristics of configurations having various store arrangements (refs. 1 to 5). In the present paper (where the external stores are referred to as bodies) the overall model forces and moments, as well as the loading characteristics of finned and unfinned bodies in the presence of both unswept and sweptback wings, are shown. A summary of information on aerodynamic loading due to external stores is presented in reference 6, wherein data from references 7 and 8, as well as from the present investigation, have been discussed. The present paper also includes some of the results presented in reference 7 for comparison with the results of the present investigation.

The results presented herein were obtained, generally, at Mach numbers from 0.50 to 0.91 over an angle-of-attack range which was dependent upon the limiting load factors of the strain-gage-balance measuring system of the body.

SYMBOLS

C_L	lift coefficient, $Lift/qS_w$
C_D	drag coefficient, $Drag/qS_w$
C_m	pitching-moment coefficient referred to $0.25\bar{c}$, $\frac{\text{Pitching moment}}{qS_w\bar{c}}$
$C_{N_b\lambda}$	body normal-force coefficient, $\frac{\text{Body normal force}}{qS_b}$
$C_{c_b\lambda}$	body axial-force coefficient, $\frac{\text{Body axial force}}{qS_b}$
$C_{m_b\lambda}$	body pitching-moment coefficient referred to $0.462l_b$, $\frac{\text{Body pitching moment}}{qS_b l_b}$
$C_{n_b\lambda}$	body yawing-moment coefficient referred to $0.462l_b$, $\frac{\text{Body yawing moment}}{qS_b l_b}$

C_{l_b}	body rolling-moment coefficient referred to body center line, $\frac{\text{Body rolling moment}}{qS_b l_b}$
C_{Y_b}	body side-force coefficient, $\frac{\text{Body side force}}{qS_b}$
q	free-stream dynamic pressure, lb/sq ft
R	Reynolds number based on \bar{c}
S_w	wing area, 2.25 sq ft
S_b	maximum frontal area of body, 0.0215 sq ft
\bar{c}	mean aerodynamic chord of wing, 0.765 ft, $\frac{2}{S_w} \int_0^{b/2} c^2 dy$ (using theoretical tip)
c	local wing chord, ft
c_p	pylon chord, 0.53 ft
b	wing span, 3.0 ft
l_b	body length, 1.544 ft
l	fuselage length, 4.10 ft
d_b	body diameter, ft
d	fuselage diameter, ft
y	spanwise distance from plane of symmetry of complete model, ft
z	vertical distance from wing chord plane to body center line, ft
M	Mach number
α	angle of attack, deg
i_b	angle of body tilt measured from wing chord line, deg
Λ	sweep angle of c/4 line, deg

ϕ_b angle of body center line with respect to plane of symmetry of complete model, deg

$C_{L\alpha}$ lift-curve slope at $C_L = 0$ for a given Mach number, $\frac{\partial C_L}{\partial \alpha}$

C_{MC_L} pitching-moment-curve slope at $C_L = 0$ for a given Mach number, $\frac{\partial C_m}{\partial C_L}$

$\frac{\partial C_{mbz}}{\partial \alpha}$ body pitching-moment-curve slope at $\alpha = 0^\circ$

MODELS AND APPARATUS

The wings utilized in this investigation were constructed of aluminum with an aspect ratio of 4, a taper ratio of 0.6, and NACA 65A006 airfoil sections parallel to the free stream. Two sweep angles were employed: one wing had its quarter-chord line swept back 3.6° and the other 46.7° . Drawings of the models are presented in figures 1 and 2, and photographs of a typical setup in the tunnel are presented in figure 3.

The fuselage was constructed of aluminum and was formed by parabolic-arc segments, ordinates for which are given in table I. The bodies were generated by revolution of a profile made up of ogival nose and tail sections, between which was located a constant-radius section. Ordinates of the body, which had a fineness ratio of 9.34, are presented in table II.

The pylons were unswept and had NACA 64A010 airfoil sections parallel to the free stream, except for one configuration with the 46.7° swept-back wing which employed a flat-sided pylon of 6.2-percent thickness, ordinates for which are presented in table III. Details of the body fins used are shown in figure 2. The fins were orientated at 45° from the vertical and horizontal.

Two spanwise locations of the body were investigated on both the 3.6° sweptback wing which, in the remainder of the paper, will be called the unswept wing, and the 46.7° sweptback wing which will be referred to as the swept wing. Table IV presents a summary of the positions employed. For all body configurations tested, symmetrical spanwise locations about the fuselage center line were employed.

In the case of the unswept-wing--fuselage combinations, the unfinned-body data of reference 7 are presented again for comparison with the finned configurations of this paper.

The complete model, consisting of the wing and fuselage with or without the bodies, was attached to the supporting sting by an internal strain-gage balance. The model forces and moments were measured by the balance and were recorded automatically.

The body, instrumented with a six-component strain-gage balance, was mounted from the left wing, while a solid wooden body was attached to the right wing. The body housing the balance was constructed of plastic impregnated with fiber glass. A cutaway drawing showing the installation of the balance with the clearance gaps between the pylon or wing tip and the body is presented in figure 4.

The origin of the axis of the body balance remained fixed with respect to the body length for all spanwise positions of the body. The location of the pitching-moment axis relative to the local wing chord changed slightly for each body location because of wing taper. Tabulated below are the locations of the pitching-moment axis for each of the body positions, based on both the local wing chord and the body length:

Installation designation	Spanwise location, $2y/b$	Pitching-moment axis, percent c	Pitching-moment axis, percent l_b
Inboard Tip	0.33	45.6	46.2
	1.04	43.6	46.2

The alinement of the bodies in the pitch plane and the bodies and pylons in the yaw plane was checked and found to be within 0.10° of the design angular positions. Because centering pins were employed on all components of each configuration, the repeatability of angular alinement was good.

TESTS AND RESULTS

The tests were conducted in the Langley high-speed 7- by 10-foot tunnel through a Mach number range that usually extended from 0.50 to 0.91. The angle-of-attack range investigated was restricted by the load limits of the body balance and therefore varied with the loading measured for each position of the body. A model yaw angle of zero was maintained for all tests of this investigation.

The results obtained on the complete model are presented as the lift, drag, and pitching-moment coefficients of the model with and without the two bodies, finned and unfinned, in the two locations on the wing of the model. Forces and moments of the complete model are presented with respect to the wind axes, with the pitching moment being presented about the 0.25-chord point of the mean aerodynamic chord.

The characteristics of the bodies in the presence of the model are given as six-component force and moment measurements varying with model angle of attack. These force and moment results are presented relative to the body axes as shown in figure 5. The body coefficients are based upon the maximum frontal area of the body and, in the case of moments, also upon the body length.

The body coefficients are the forces and moments of the body in the presence of the wing, fuselage, and pylons, and hence include the interference of these parts on the body as well as the forces and moments of the body alone.

The variation with Mach number of the Reynolds number based on the mean aerodynamic chord of the models is shown in figure 6.

CORRECTIONS

Blocking corrections applied to Mach number and dynamic pressure were determined by the velocity-ratio method of reference 9, which utilizes experimental pressures measured at the tunnel wall opposite the model. Over the Mach number range investigated, good agreement was obtained between these corrections and those obtained theoretically by the method of reference 10. The correction to Mach number increased slightly with increase in speed, and at $M = 0.90$ it was 0.01.

The jet-boundary corrections applied to the angle-of-attack and drag data for the complete model were calculated by the method of reference 11. Corrections to the pitching moments were considered negligible. No support tares have been applied but, as indicated in reference 12, they are believed to be small. Drag data have been corrected to correspond to a pressure at the base of the fuselage equal to free-stream static pressure. Base pressure was determined by measuring the pressure at a point inside the fuselage about 9 inches forward of the base. This correction, which was added to the measured drag coefficient, amounted to 0.0010 at $M = 0.50$ and increased to 0.0030 at $M = 0.91$. As indicated in reference 7, the presence of the bodies had no effect on the fuselage base pressure. A buoyancy correction, determined from static-pressure surveys, was added to the drag data of this investigation as well as to the drag data that were taken from reference 7, to account for the static-pressure gradient

that exists along the tunnel center line. The increment in drag due to buoyancy amounted to 0.0016 throughout the Mach number range investigated.

Corrections have been applied to the angle of attack of the model to account for the deflection of the support system under load. No correction has, however, been applied to the results presented in this paper to account for aeroelastic distortion of the wings. Shown in figure 7 is a summary of the aeroelastic characteristics of the test wings without the bodies; these characteristics have previously been discussed in reference 13.

No correction has been made to the body angles of attack or yaw to account for the deflection of the body balance under load. A deflection calibration has, however, been made and the results are presented in moment-coefficient form in figure 8 for Mach numbers giving maximum and minimum dynamic pressures. These results indicate that the body deflection due to a body pitching moment is usually less than 0.15° and due to a yawing moment less than 0.25° .

Subsequent to this investigation, it was found that the sweptback wing had an average of about 1° of washout in each wing panel. This washout is believed to have come from overloading the wing in other investigations. No correction of the present results was made to account for the washout since it is small and will not have any important effect upon the conclusions of the present paper.

DISCUSSION

Complete-Model Characteristics

The data are presented in figures 9 to 26, and a detailed listing of the data is presented in table IV. Lift-curve and pitching-moment-curve slopes of the model with and without the bodies were taken at zero lift coefficient. The body pitching-moment-curve slopes were taken at zero angle of attack.

Of the two spanwise locations of the body investigated, the tip-mounted body configurations produced the most pronounced effect on the longitudinal characteristics of the complete model (fig. 18). The inboard body configurations produced only minor variations to the model characteristics.

It is well known that the addition of bodies at the wing tip produces end-plate effects that are equivalent to increases in aspect ratio and result in additional loading at the wing tip. Such changes are also indicated for the tip-mounted body configurations of the present paper

by increases in lift-curve slope and reductions in the drag due to lift at the higher lift coefficients (fig. 18). In the case of the swept-wing model with tip-mounted bodies, large rearward shifts in aerodynamic-center location are also a result of the additional wing-tip loading. The addition of the fins to the tip-mounted bodies generally increases these effects.

Methods of calculating the effects of tip-mounted bodies on wing loading characteristics in incompressible flow are reported in references 14 and 15. An estimate by these methods has been made and is presented in the following table for comparison with the results of the present investigation. The results shown in this table are in the form of the ratio of the lift-curve slope of the model with the tip bodies to the lift-curve slope of the model without the bodies. For comparison with the incompressible-flow calculations, the experimental results are shown for the lowest available Mach number ($M = 0.50$).

Source	$(C_{L\alpha})_{\text{model + tip bodies}} / (C_{L\alpha})_{\text{model}}$	
	Unswept wing	Swept wing
Present investigation (experimental)	1.20	1.09
Reference 14 (calculated)	1.21	1.13
Reference 15 (calculated)	1.12	1.12

As can be seen from the table, the experimental ratios of the present investigation, for the unswept-wing model, are in good agreement with the calculated values of reference 14. The estimated value obtained by the method of reference 15 appears to be low in predicting the effects of the tip-mounted body on the unswept wing; however, both methods indicate fairly well the effects of the tip-mounted bodies on the lift-curve slope of the swept-wing model.

The increase in the drag of the models due to the body installations at zero lift (fig. 18) is primarily a function of the wetted area of the installation in this speed range. Thus, the highest drag of the models with the bodies was obtained with the inboard body and the longest pylon, and the lowest drag was obtained with the tip-mounted bodies. An increase in model lift coefficient reduces the increment in drag due to the tip-mounted body installations. This effect, however, is probably due to overall reduction in the drag due to lift of the complete model because of the end-plate action of the tip body rather than to any specific change in the drag of the body installation.

Body Characteristics

In interpreting the body forces and moments, it should be kept in mind that the measurements were made with the instrumented body on the left wing of the model. It is also well to remember that the lines of action of the forces and moments are as indicated in figure 5.

For comparison with the present results, the unfinned-body results, obtained on the unswept-wing model reported in reference 7, have been incorporated in this paper. It should be noted that the body lift and drag data of reference 7 have been transferred to the body axes to be consistent with the data presented in the present paper.

In general, changes in Mach number had less effect on the body characteristics than did changes in angle of attack (figs. 19 to 25). A similar effect has been reported in reference 7.

Some of the largest changes in the body longitudinal force and moment characteristics due to change in angle of attack exist for the bodies in the wing-tip location (figs. 21 and 25). These changes are in the form of substantial increases in the body normal force and in the positive pitching-moment coefficient of the unfinned body with increase in angle of attack for both wing sweep angles. An estimate of the slopes of the normal-force curves of the body mounted at the wing tip has been made by the method of reference 15 and was found to be in good agreement with the experimental results. For the inboard body, the normal-force coefficient was not large enough to be considered of primary concern in this discussion.

The stabilizing effect of the body fins was sufficient to cause all of the inboard-mounted bodies to become stable (fig. 26). In providing this stability, however, the fins generally caused increases in the absolute values of the pitching-moment coefficients throughout the angle-of-attack range. A reduction in the pitching-moment coefficients of the finned inboard body was accomplished by a -5° tilt of the body axes (fig. 23). The effect of body tilt was obtained on the swept-wing model. It should be noted that tilt of the finned body also increases substantially the normal-force loads of the body (figs. 22 and 23).

The stabilizing effect of the fins on the tip-mounted bodies (figs. 21, 25, and 26) was sufficient to cause the tip-mounted body on the unswept wing to become stable and to decrease the absolute values of the pitching-moment coefficients. The increased stability was attended by increased body normal force. In the case of the tip-mounted body on the swept wing, some reduction in pitching moment was accomplished but the body remained unstable.

Presented in figure 26 is a summary of the pitching-moment characteristics of all body configurations investigated. Included in this summary are estimates of the stability for the tip-mounted body obtained by the method of reference 15. The estimated value of $\frac{\partial C_{m_b} z}{\partial \alpha}$ for the tip-mounted body on the unswept-wing model is in good agreement with the experimental results at Mach numbers where compressibility can be neglected. Although the agreement between theory and experiment is not as satisfactory for the tip body on the swept-wing model, it is evident that this procedure gives a better indication of experimental results than the body-alone results calculated by the method of reference 16 (fig. 26). Until recently, body-alone calculations were the only available means of estimating the body force and moment characteristics.

Increasing the wing sweep angle produced some of the most significant changes in the lateral force and moment characteristics of the inboard body. With the instrumented body on the left wing, these changes are indicated as large increases in negative side force (outboard direction) and negative yawing moment (nose-outboard direction). (See figs. 20 and 22.) These characteristics, previously reported in reference 6, are interesting because they occur at zero angle of sideslip. They are important because the lateral plane of the supporting pylon is the plane of least structural strength. There are, however, no calculation procedures which indicate that lateral loading of this magnitude should be expected.

Although the addition of fins to the bodies reduced somewhat these severe lateral loads, they did not reduce them to an insignificant level throughout the Mach number range. It is not clearly understood why the decreased yawing-moment coefficient due to the addition of the fins to the body is accompanied by a decrease in side force. It is presumed that these characteristics are due to a complicated flow phenomenon caused by interference effects of the wing, fuselage, pylon, body, and fins.

The addition of the fins to the bodies also resulted in substantial positive increases in body rolling-moment coefficients. The fin rolling-moment effect, as may be anticipated from vorticity considerations, is particularly large for the tip-mounted body.

Changes in body tilt did not result in any significant changes in the body lateral force or moment characteristics.

Change in pylon shape from an NACA 64A010 airfoil section to a 6.2-percent-thick flat pylon produced no significant changes on any of the body or complete-model characteristics (figs. 16 and 24).

CONCLUSIONS

An investigation at high subsonic speeds of finned and unfinned bodies mounted from unswept- and swept-wing fuselage models, including measurements of body loads, indicates the following conclusions:

1. The most significant effects of the bodies on the aerodynamic characteristics of the model were produced by the wing-tip-mounted bodies, which gave large increases in lift-curve slope of the complete model and reductions in drag due to lift, and, particularly for the swept-wing model, caused rearward shifts in the model aerodynamic-center location. The addition of the fins to the bodies generally increased these effects.

2. The largest changes in the longitudinal force and moment coefficients of the body were shown with the tip-mounted body, where increases in model angle of attack gave substantial increases in the normal-force and pitching-moment coefficients. Body fins effectively neutralized the pitching moments of the tip body on the unswept wing but only partially neutralized the pitching moments on the tip body on the swept-wing model.

3. The addition of fins to the inboard pylon-mounted bodies generally increased the absolute value of the pitching-moment coefficients. This increase was reduced considerably for the inboard pylon-mounted body on the swept wing by tilting the body axis down.

4. Increasing the wing sweep angle produced some of the most significant changes in the lateral force and moment characteristics of the inboard body. These changes were indicated as large side-force increases in an outboard direction and large yawing-moment increases in a nose-out direction. The addition of body fins partially neutralized the yawing moments.

Langley Aeronautical Laboratory,
National Advisory Committee for Aeronautics,
Langley Field, Va., February 1, 1954.

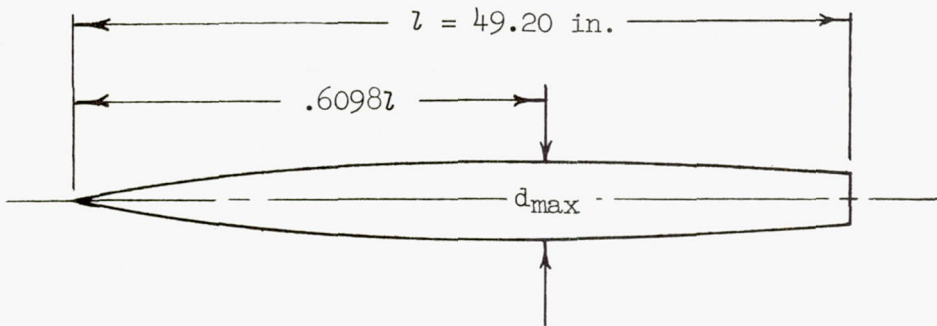
REFERENCES

1. Pepper, William B., Jr., and Hoffman, Sherwood: Transonic Flight Tests To Compare the Zero-Lift Drag of Underslung and Symmetrical Nacelles Varied Chordwise at 40 Percent Semispan of a 45° Sweptback, Tapered Wing. NACA RM L50G17a, 1950.
2. Hoffman, Sherwood: Comparison of Zero-Lift Drag Determined by Flight Tests at Transonic Speeds of Pylon, Underslung, and Symmetrically Mounted Nacelles at 40 Percent Semispan of a 45° Sweptback Wing and Body Combination. NACA RM L51D26, 1951.
3. Silvers, H. Norman, King, Thomas J., Jr., and Pasteur, Thomas B., Jr.: Investigation of the Effect of a Nacelle at Various Chordwise and Vertical Positions on the Aerodynamic Characteristics at High Subsonic Speeds of a 45° Sweptback Wing With and Without a Fuselage. NACA RM L51H16, 1951.
4. Hoffman, Sherwood, and Pepper, William B., Jr.: Transonic Flight Tests To Determine Zero-Lift Drag and Pressure Recovery of Nacelles Located at the Wing Tips on a 45° Sweptback Wing and Body Combination. NACA RM L51K02, 1952.
5. Spreeman, Kenneth P., and Alford, William J., Jr.: Investigation of the Effects of Geometric Changes in an Underwing Pylon-Suspended External-Store Installation on the Aerodynamic Characteristics of a 45° Sweptback Wing at High Subsonic Speeds. NACA RM L50L12, 1951.
6. Silvers, H. Norman, and O'Bryan, Thomas C.: Some Notes on the Aerodynamic Loads Associated With External-Store Installations. NACA RM L53E06a, 1953.
7. Silvers, H. Norman, and King, Thomas J., Jr.: Investigation at High Subsonic Speeds of Bodies Mounted From the Wing of an Unswept-Wing-Fuselage Model, Including Measurements of Body Loads. NACA RM L52J08, 1952.
8. Silvers, H. Norman, King, Thomas J., Jr., and Alford, William J., Jr.: Wind-Tunnel Investigation at High Subsonic Speeds of the Effects of Wing-Mounted External Stores on the Loading and Aerodynamic Characteristics in Pitch of a 45° Sweptback Wing Combined With a Fuselage. NACA RM L54A21, 1954.
9. Hensel, Rudolf W.: Rectangular-Wind-Tunnel Blocking Corrections Using the Velocity-Ratio Method. NACA TN 2372, 1951.

10. Herriot, John G.: Blockage Corrections for Three-Dimensional-Flow Closed-Throat Wind Tunnels, With Consideration of the Effect of Compressibility. NACA Rep. 955, 1950. (Supersedes NACA RM A7B28.)
11. Gillis, Clarence L., Polhamus, Edward C., and Gray, Joseph L., Jr.: Charts for Determining Jet-Boundary Corrections for Complete Models in 7- by 10-Foot Closed Rectangular Wind Tunnels. NACA WR L-123, 1945. (Formerly NACA ARR L5G31.)
12. Osborne, Robert S.: High-Speed Wind-Tunnel Investigation of the Longitudinal Stability and Control Characteristics of a 1/16-Scale Model of the D-558-2 Research Airplane at High Subsonic Mach Numbers and at a Mach Number of 1.2. NACA RM L9C04, 1949.
13. Wiggins, James W., and Kuhn, Richard E.: Wind-Tunnel Investigation of the Aerodynamic Characteristics in Pitch of Wing-Fuselage Combinations at High-Subsonic Speeds. Sweep Series. NACA RM L52D18, 1952.
14. Hartley, D. E.: Theoretical Load Distributions on Wings With Tip-Tanks. Rep. No. Aero. 2469, British R.A.E., June 1952.
15. Robinson, Samuel W., Jr., and Zlotnick, Martin: A Method for Calculating the Aerodynamic Loading on Wing-Tip-Tank Combinations in Subsonic Flow. NACA RM L53B18, 1953.
16. Allen, H. Julian: Estimation of the Forces and Moments Acting on Inclined Bodies of Revolution of High Fineness Ratio. NACA RM A9I26, 1949.

TABLE I.- FUSELAGE ORDINATES

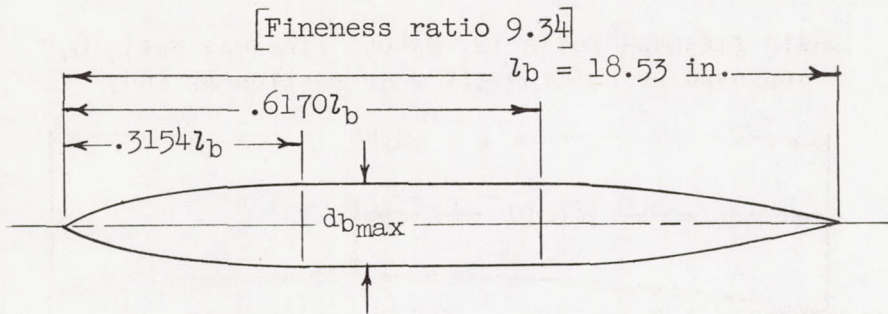
[Basic fineness ratio 12, actual fineness ratio 9.8
achieved by cutting off rear portion of body]



Ordinates, percent length	
Station	Radius
0	0
.61	.28
.91	.36
1.52	.52
3.05	.88
6.10	1.47
9.15	1.97
12.20	2.40
18.29	3.16
24.39	3.77
30.49	4.23
36.59	4.56
42.68	4.80
48.78	4.95
54.88	5.05
60.98	5.08
67.07	5.04
73.17	4.91
79.27	4.69
85.37	4.34
91.46	3.81
100.00	3.35

L. E. radius = 0.00067

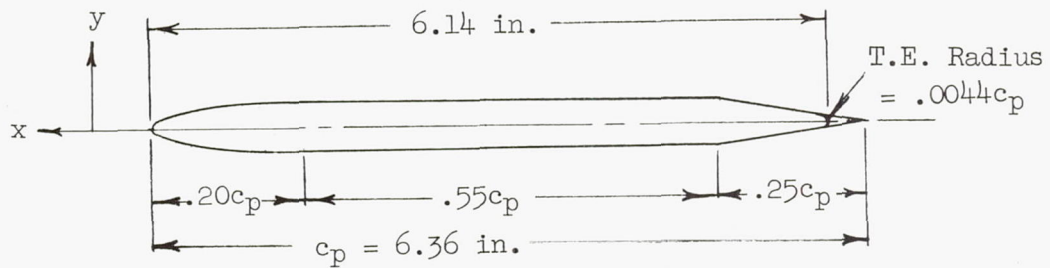
TABLE II.- BODY ORDINATES



Ordinates, percent length	
Station	Radius
0	0
.36	.30
1.21	.73
3.04	1.44
4.87	2.09
6.71	2.65
8.26	3.07
9.15	3.29
9.69	3.44
10.84	3.70
11.99	3.94
13.14	4.12
14.29	4.30
15.44	4.44
17.74	4.70
20.04	4.92
22.34	5.08
24.64	5.20
26.94	5.30
29.24	5.34
31.54	5.36
61.70	5.36
68.69	5.20
74.95	4.76
81.22	3.94
87.48	2.76
90.60	2.11
93.75	1.42
96.89	.72
98.44	.36
100.00	0


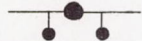




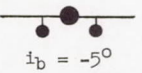
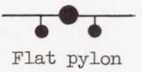

TABLE III.- FLAT-PYLON ORDINATES

[Basic thickness ratio 6.0 percent; actual thickness ratio 6.2 percent, based on actual chord length of 6.14 inches]

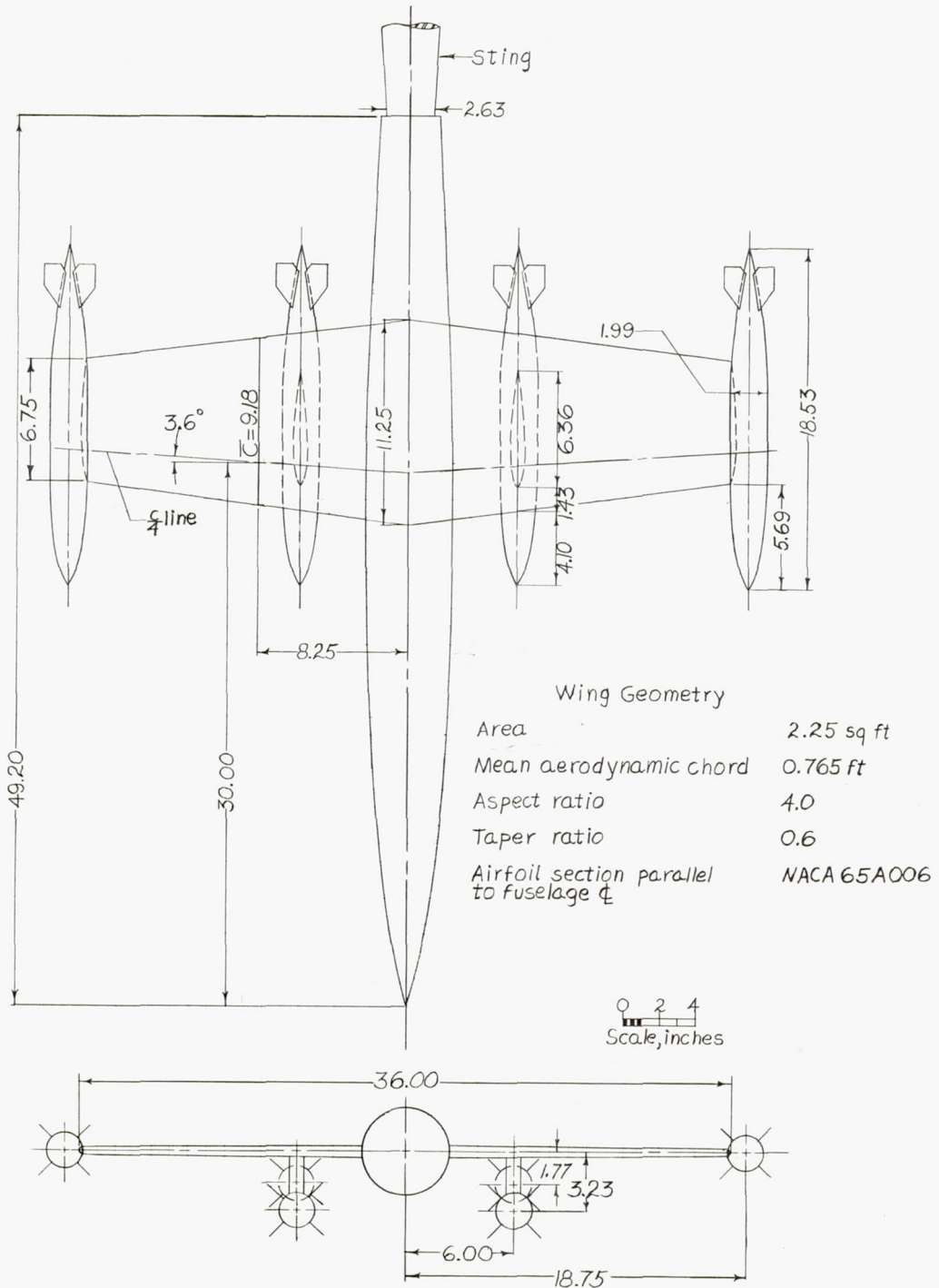


Ordinates, percent chord	
x	ty
0	0
2.5	.46
5.0	2.00
15.0	2.90
20.0	3.00
75.0	3.00
Straight taper	
100.0	0

TABLE IV.- LIST OF FIGURES PRESENTING DATA^a

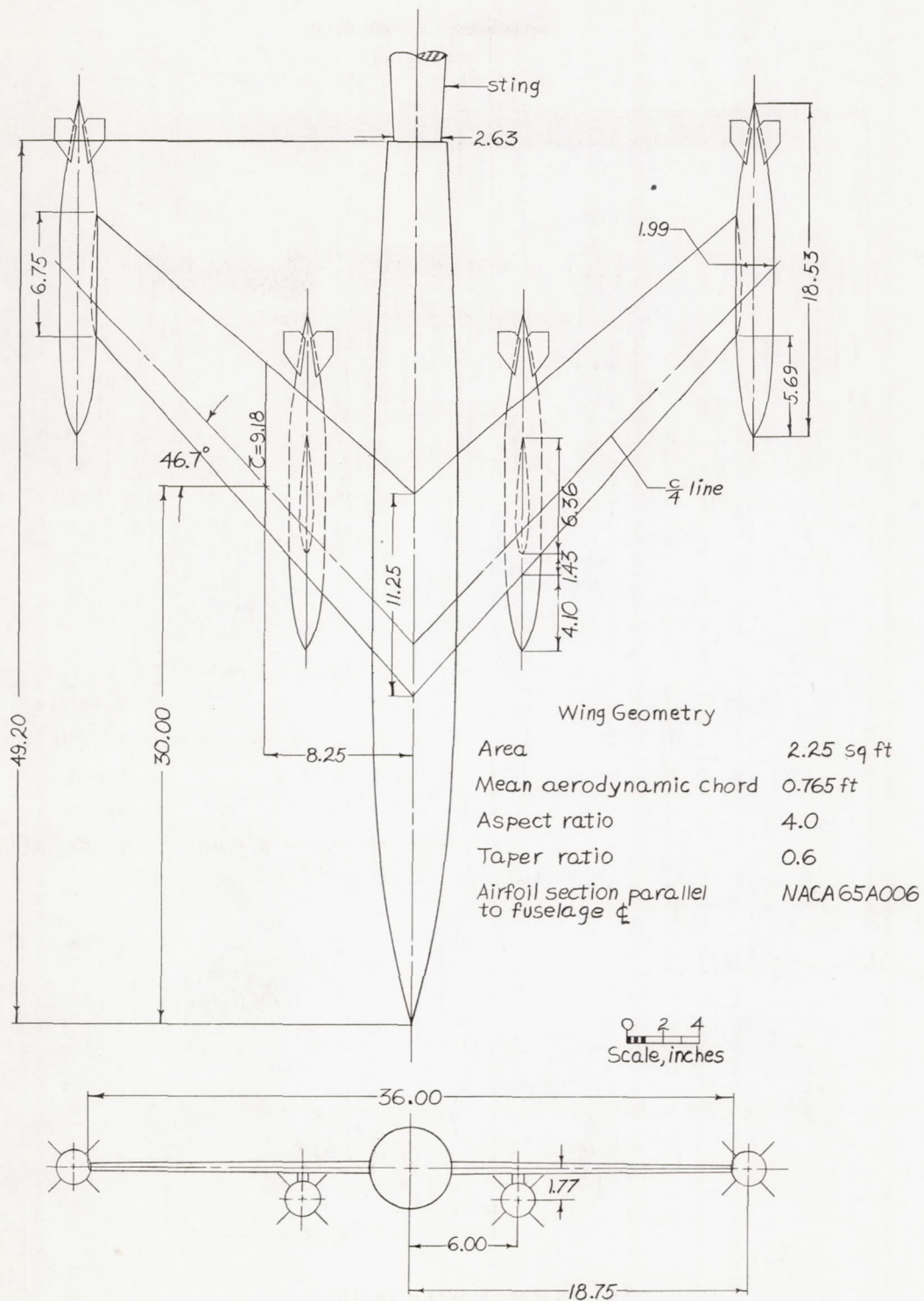
Λ , deg	Model configuration	Body $2y/b$	Pylon designation	z/d_b	Figure presenting basic data for -	
					Complete model	Body loads
3.6		----	-----	----	9	--
		.33	Long	1.62	10	19
		.33	Short	.89	11	20
		1.04	-----	----	12	21
46.7		----	-----	----	13	--
		.33	Short	.89	14	22
		.33	Short	.89	15	23
		.33	Short	.89	16	24
		1.04	-----	----	17	25
3.6 and 46.7	All	All	All	All	Figure presenting summary data for -	
					Complete model	Body loads
					18	26

^aFinned and unfinned data were obtained for all configurations except the one using a flat pylon, for which only finned conditions were tested.



(a) Unswept-wing model.

Figure 1.- Sketch of wing, fuselage, and bodies showing various locations of the bodies as tested on the sting-support system in the Langley high-speed 7- by 10-foot tunnel.



(b) Swept-wing model.

Figure 1.- Concluded.

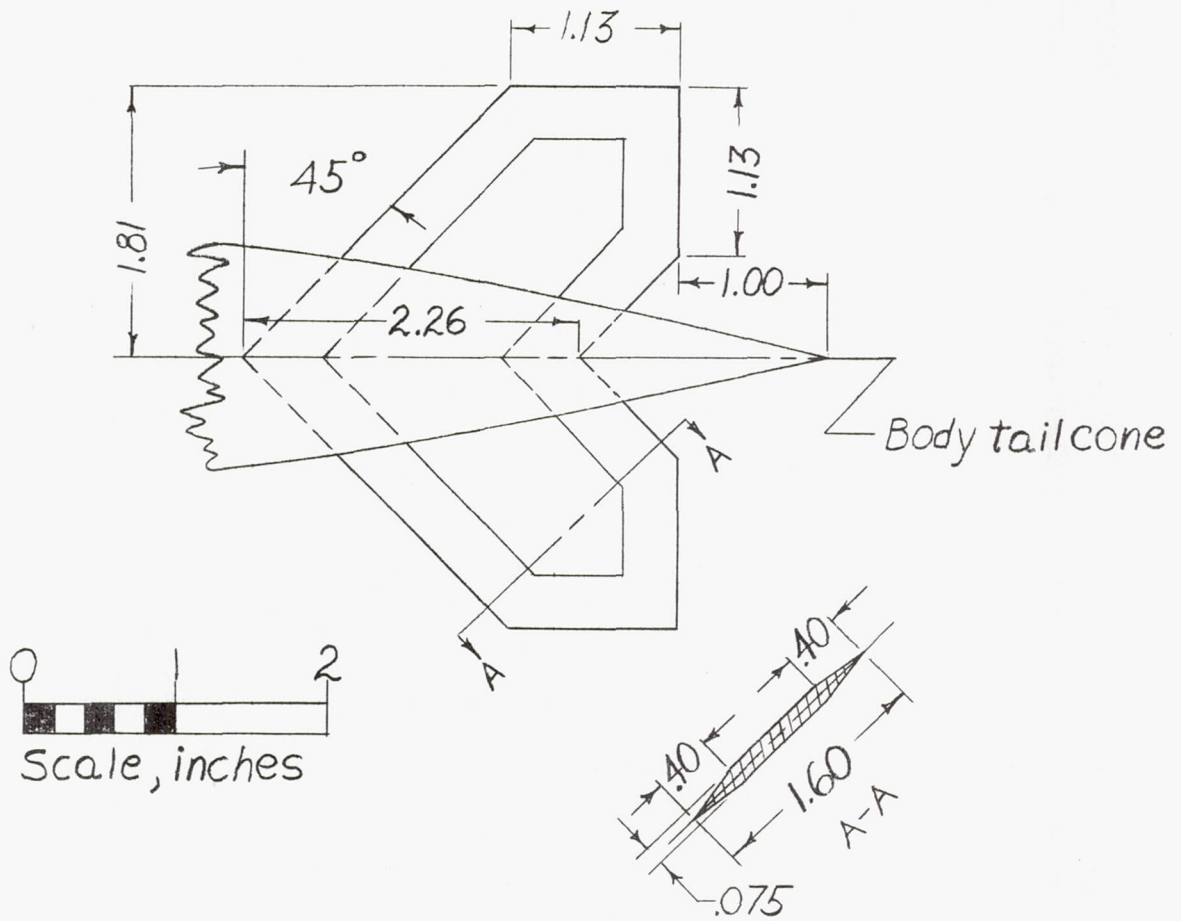
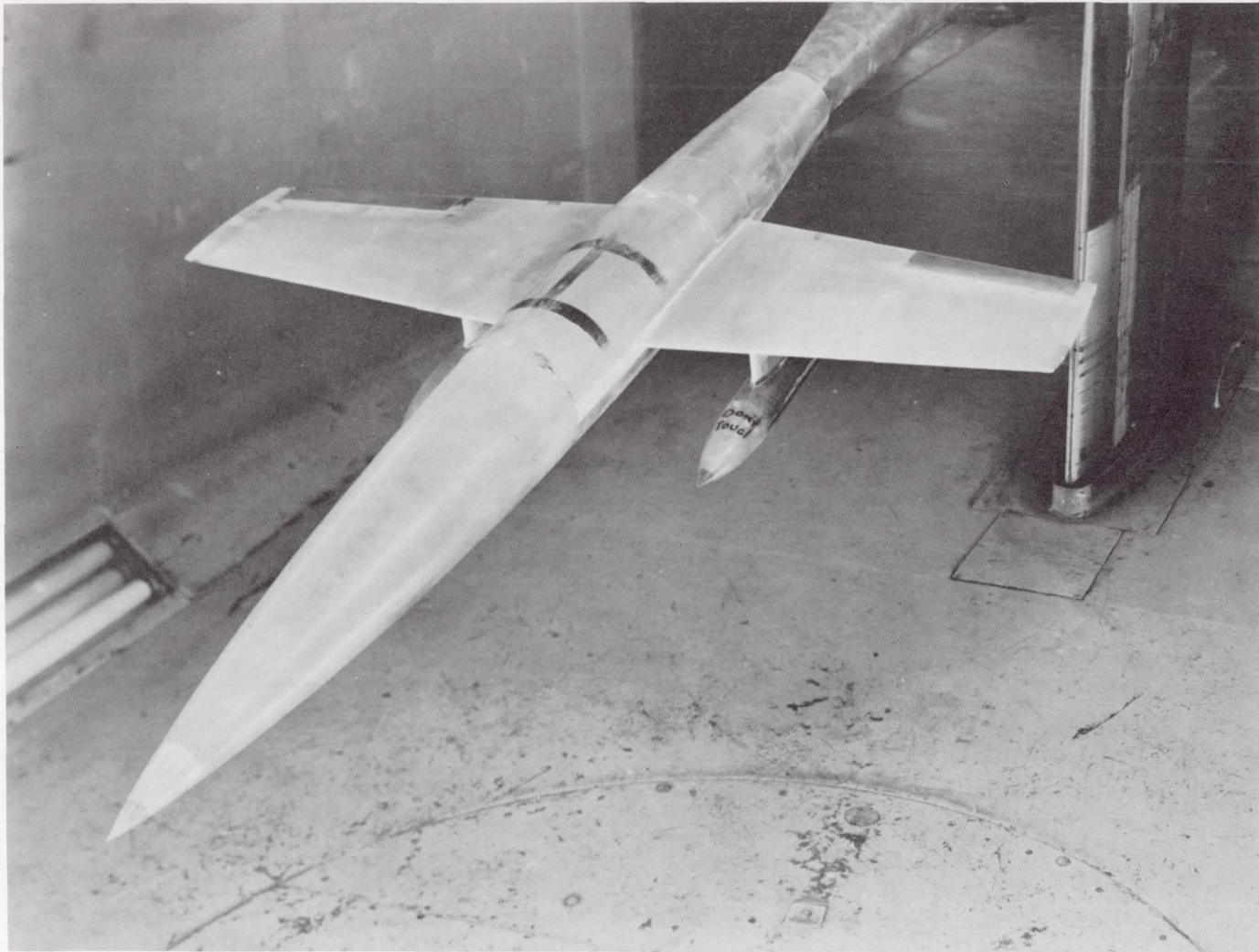
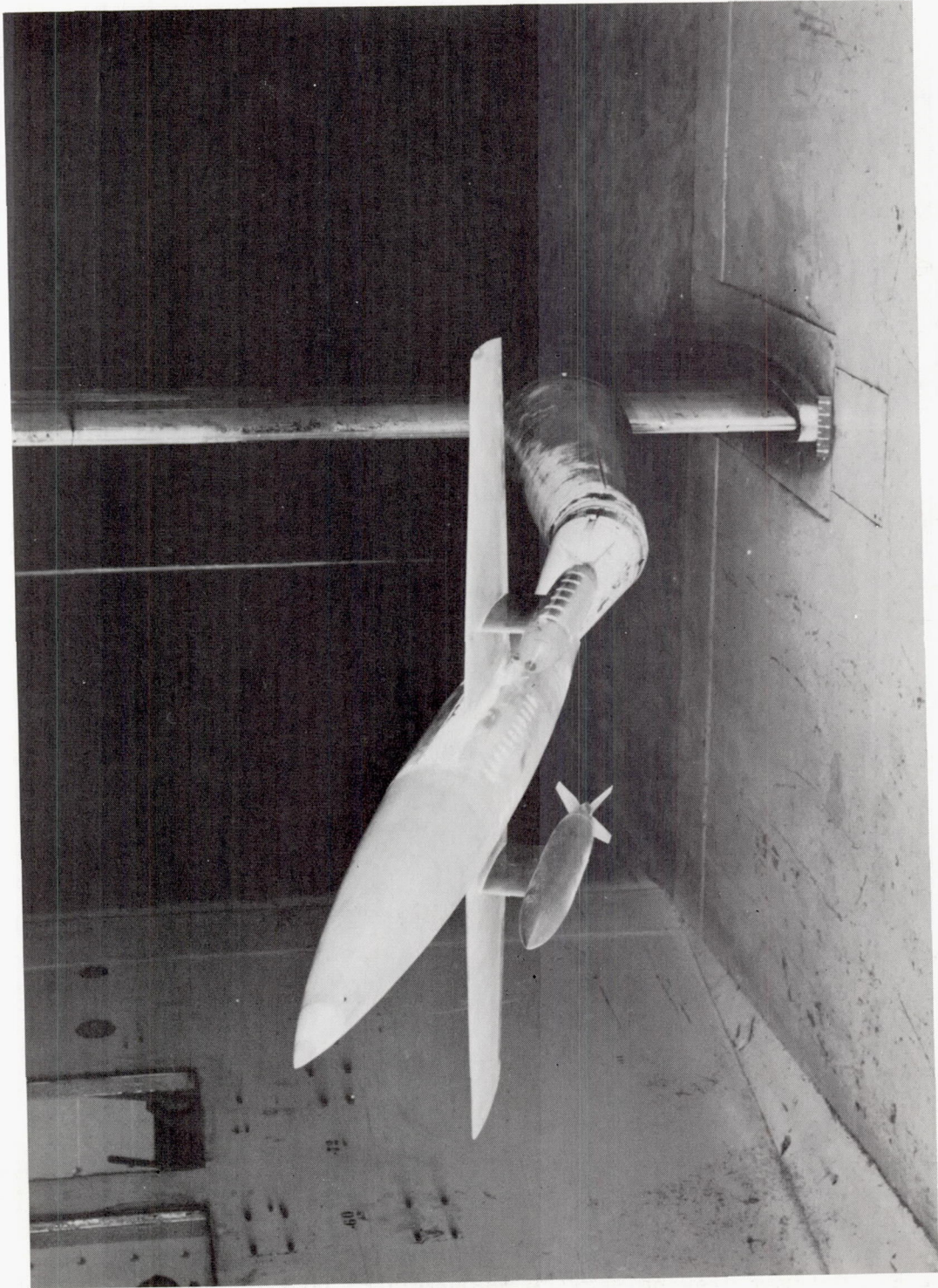


Figure 2.- Details of stabilizing fins.



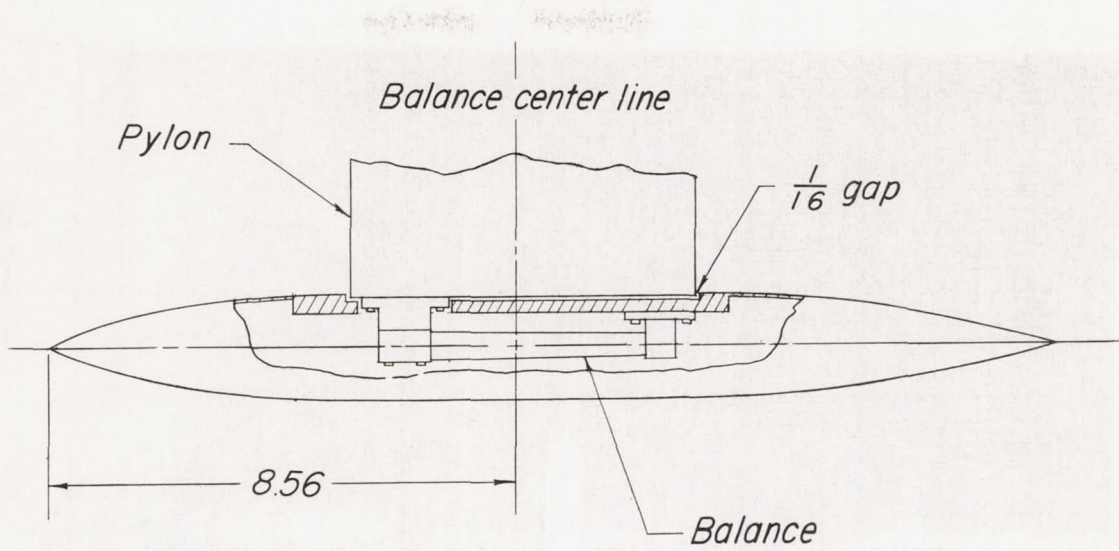
L-71861

Figure 3.- Unswept-wing model with bodies mounted under wing on long pylons.

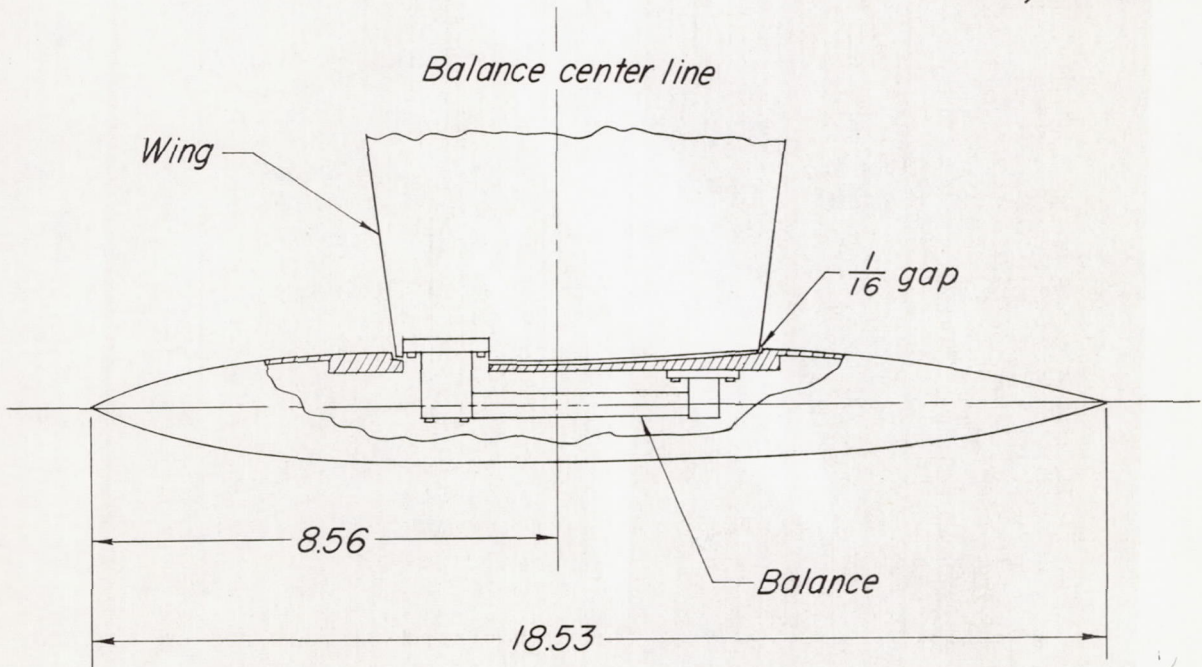
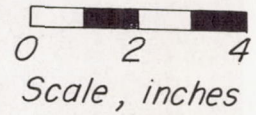


L-77843

Figure 3.- Concluded.



Pylon mounted



Wing-tip mounted

Figure 4.- Cutaway drawing showing instrumented body as mounted on pylons and on wing tip.

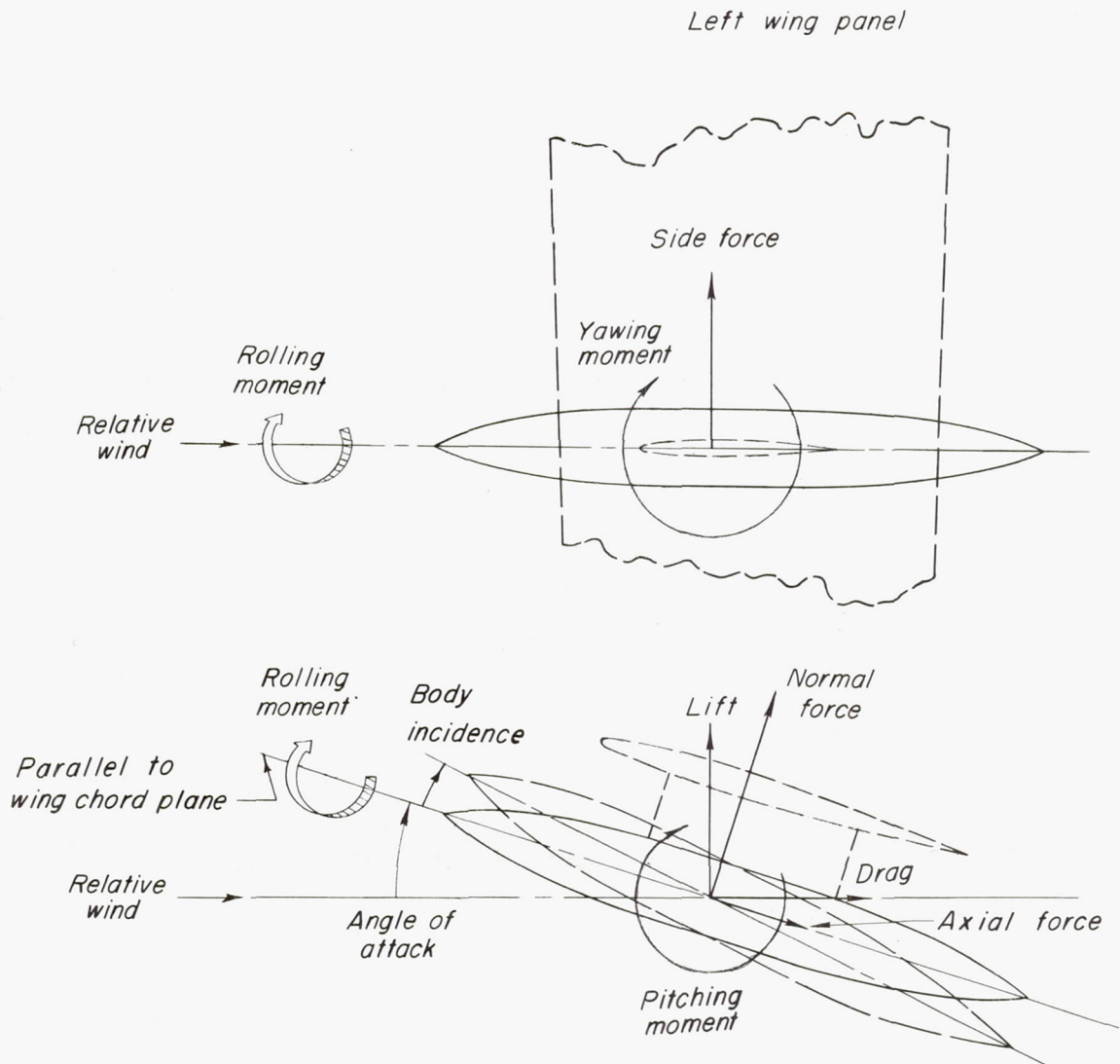


Figure 5.- Positive directions of forces and moments measured on the body and used in presentation of results.

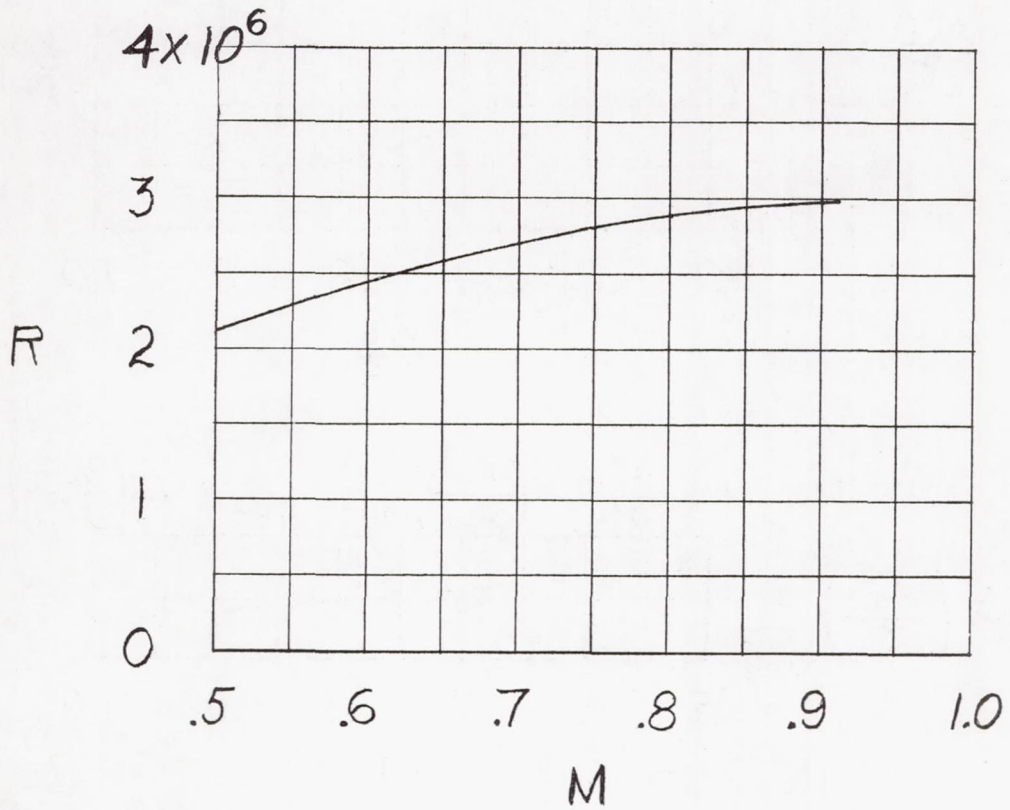


Figure 6.- Variation of average Reynolds number with Mach number for test models.

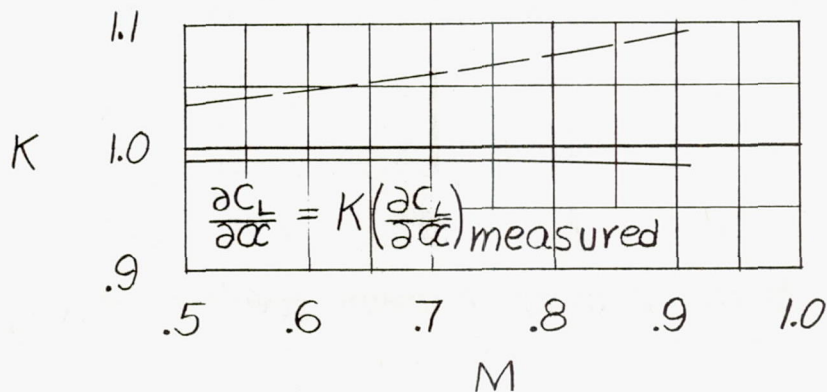
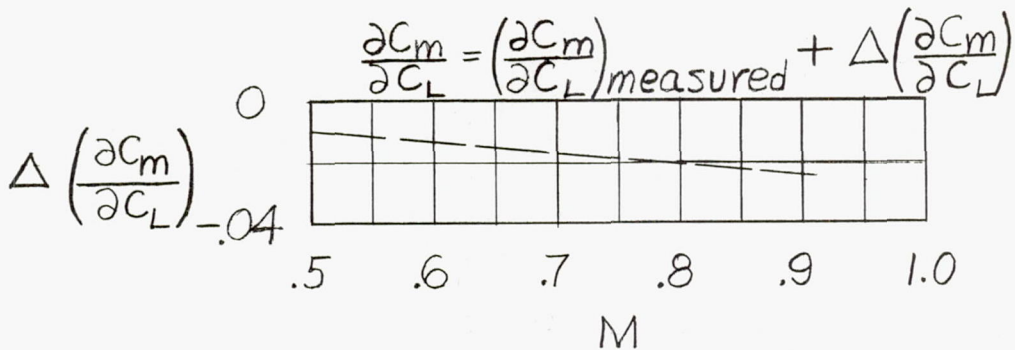
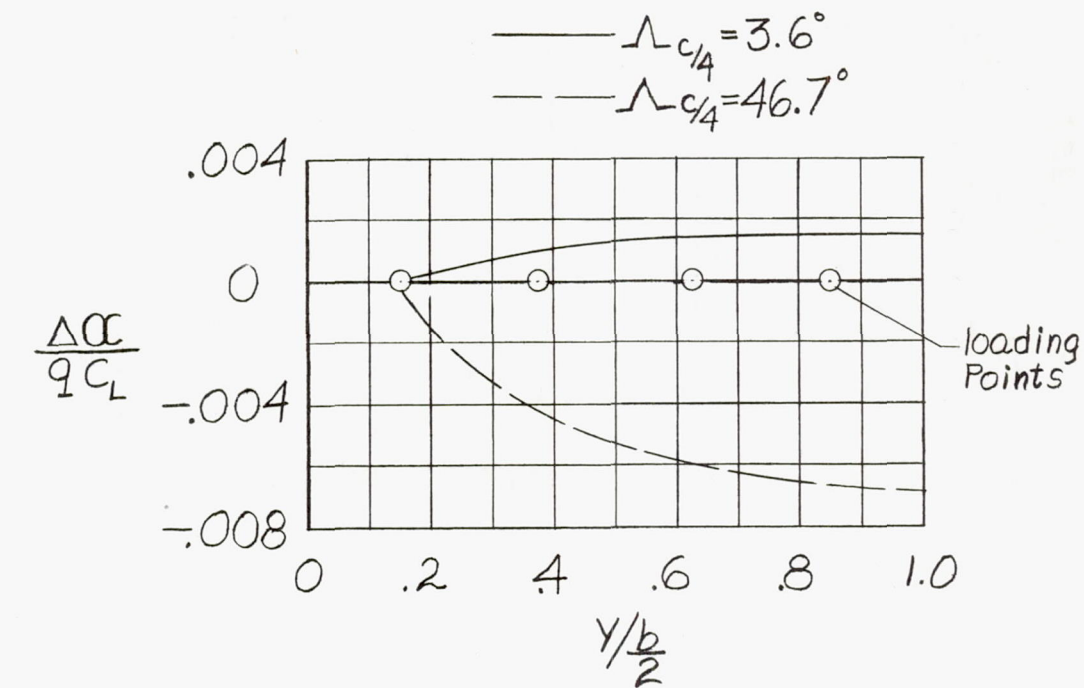


Figure 7.- Summary of aeroelastic characteristics of model wings.

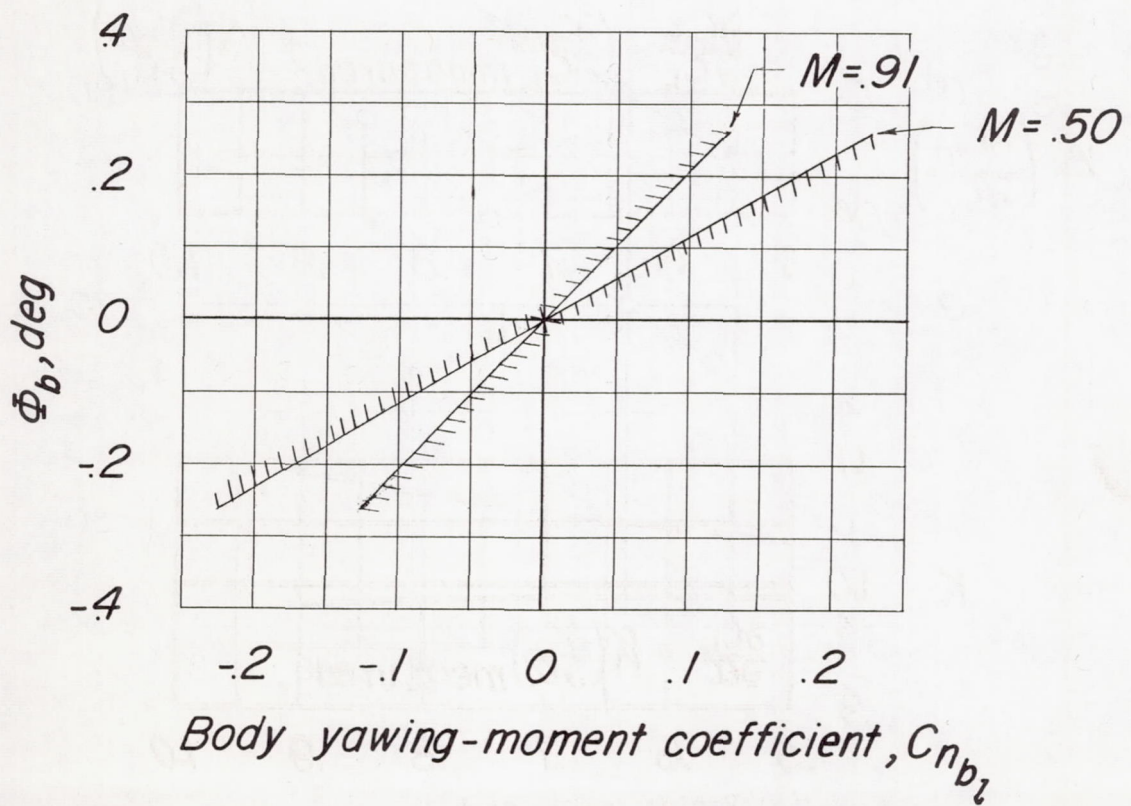
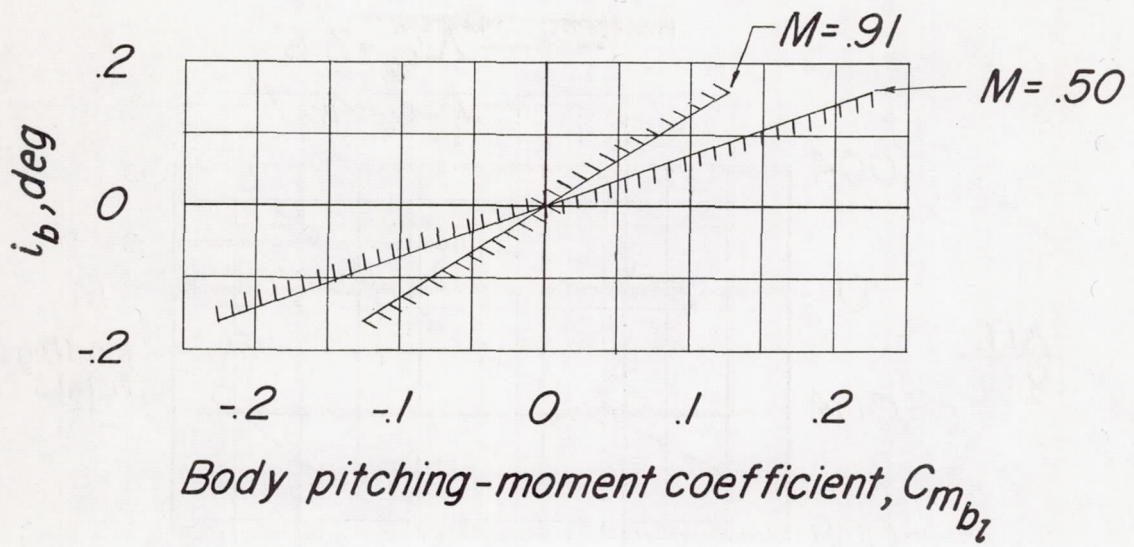
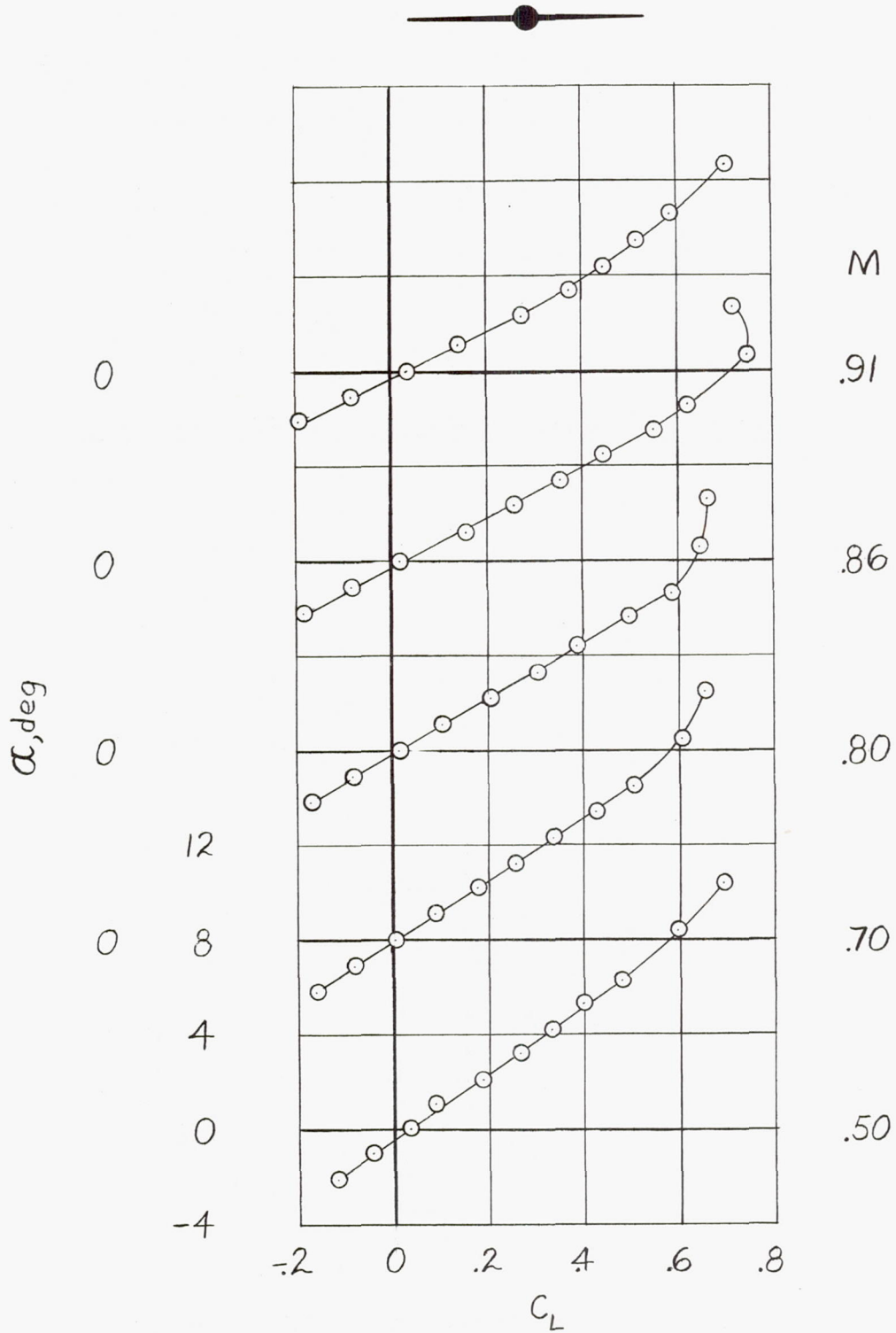
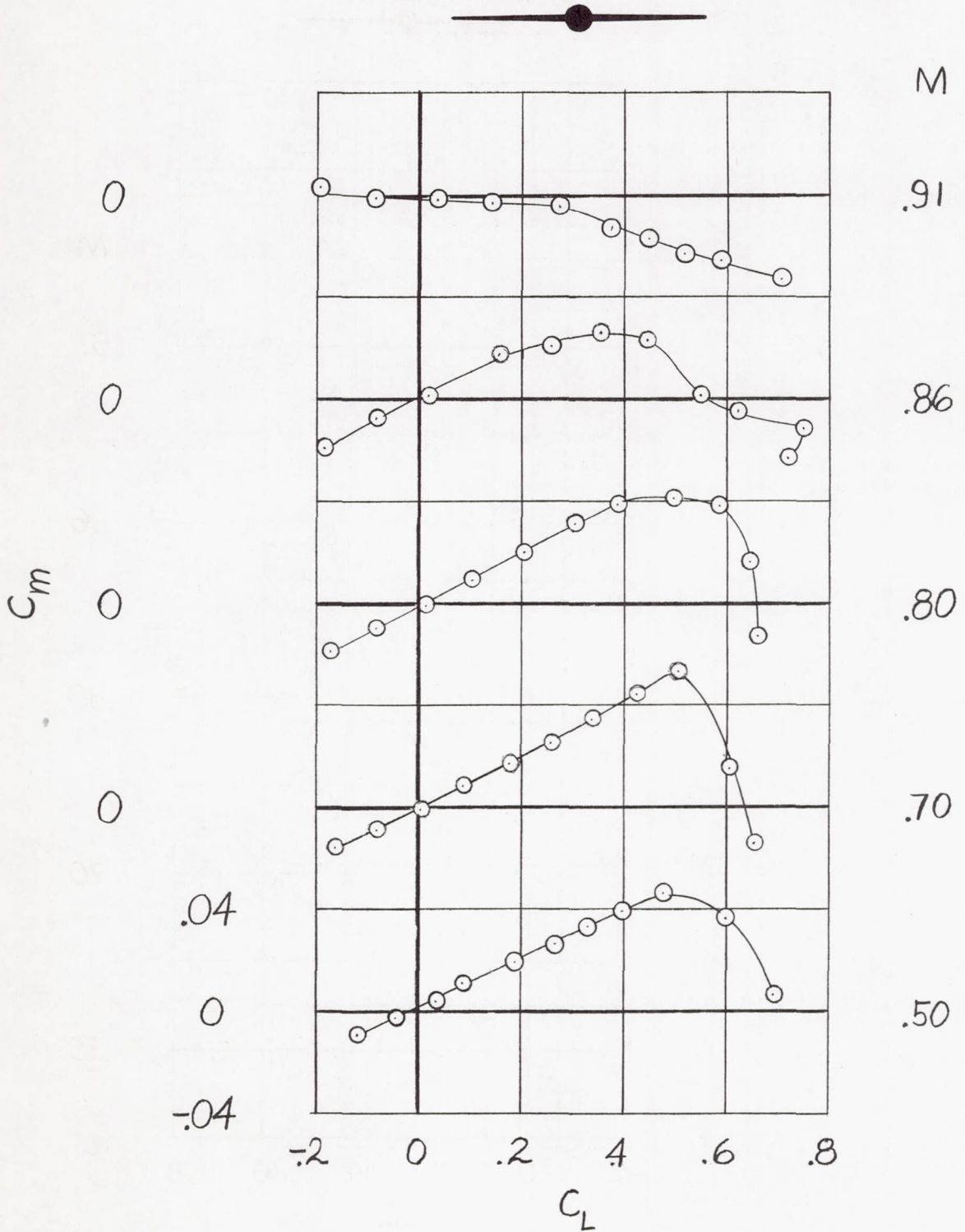


Figure 8.- Deflection characteristics of body under load.



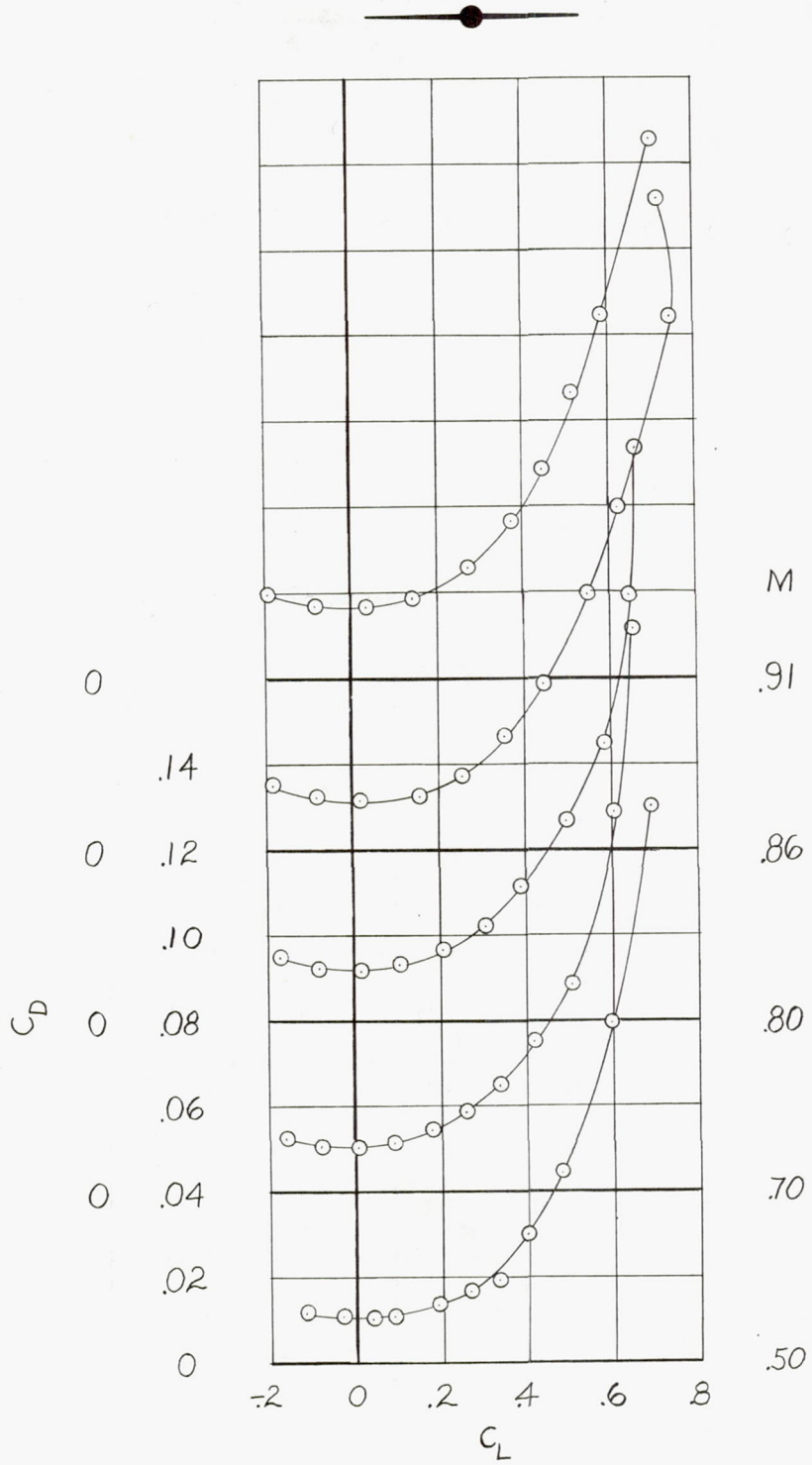
(a) Variation of α with C_L .

Figure 9.- Aerodynamic characteristics of basic unswept-wing model.



(b) Variation of C_m with C_L .

Figure 9.- Continued.

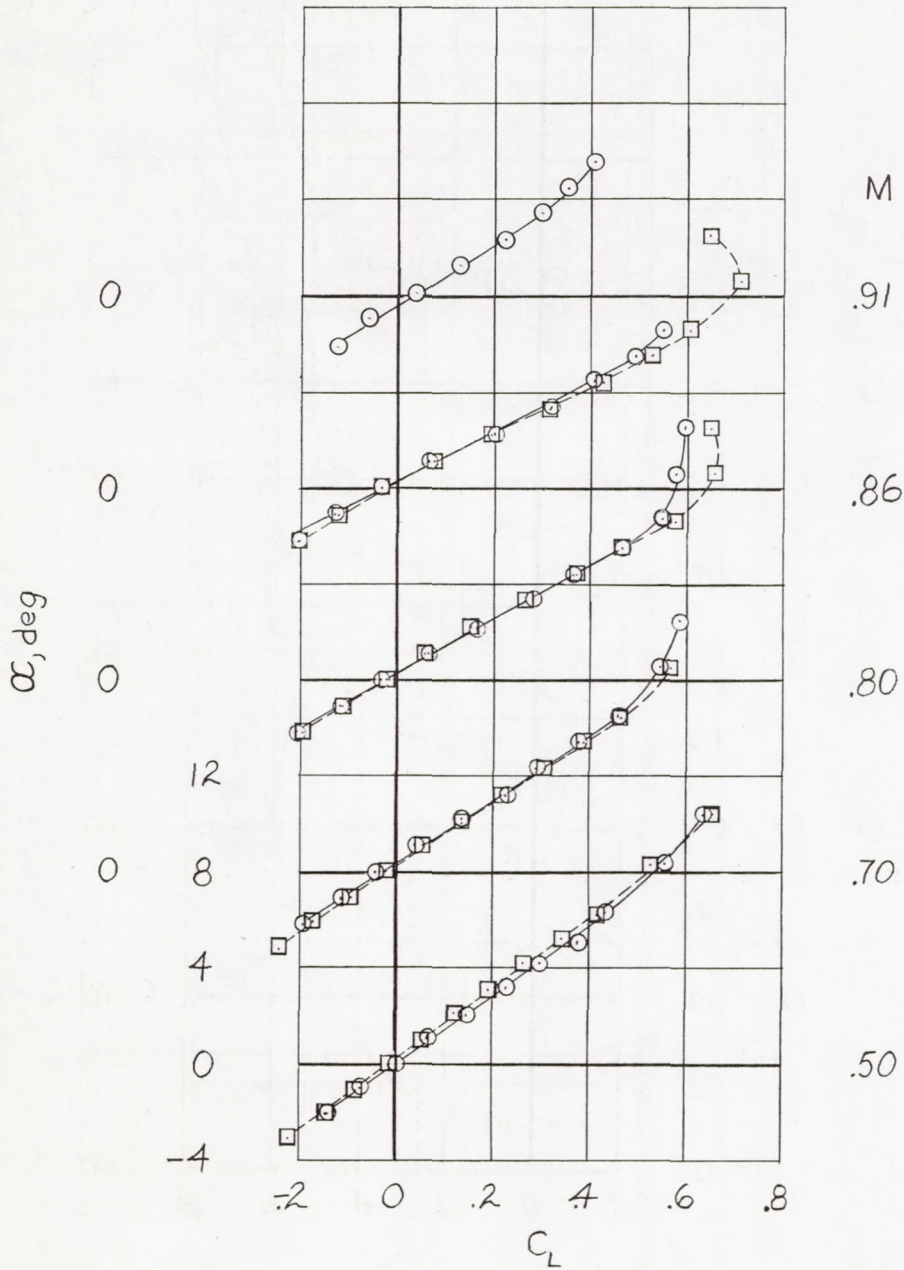


(c) Variation of C_D with C_L .

Figure 9.- Concluded.



○ — Fins off
 □ — Fins on



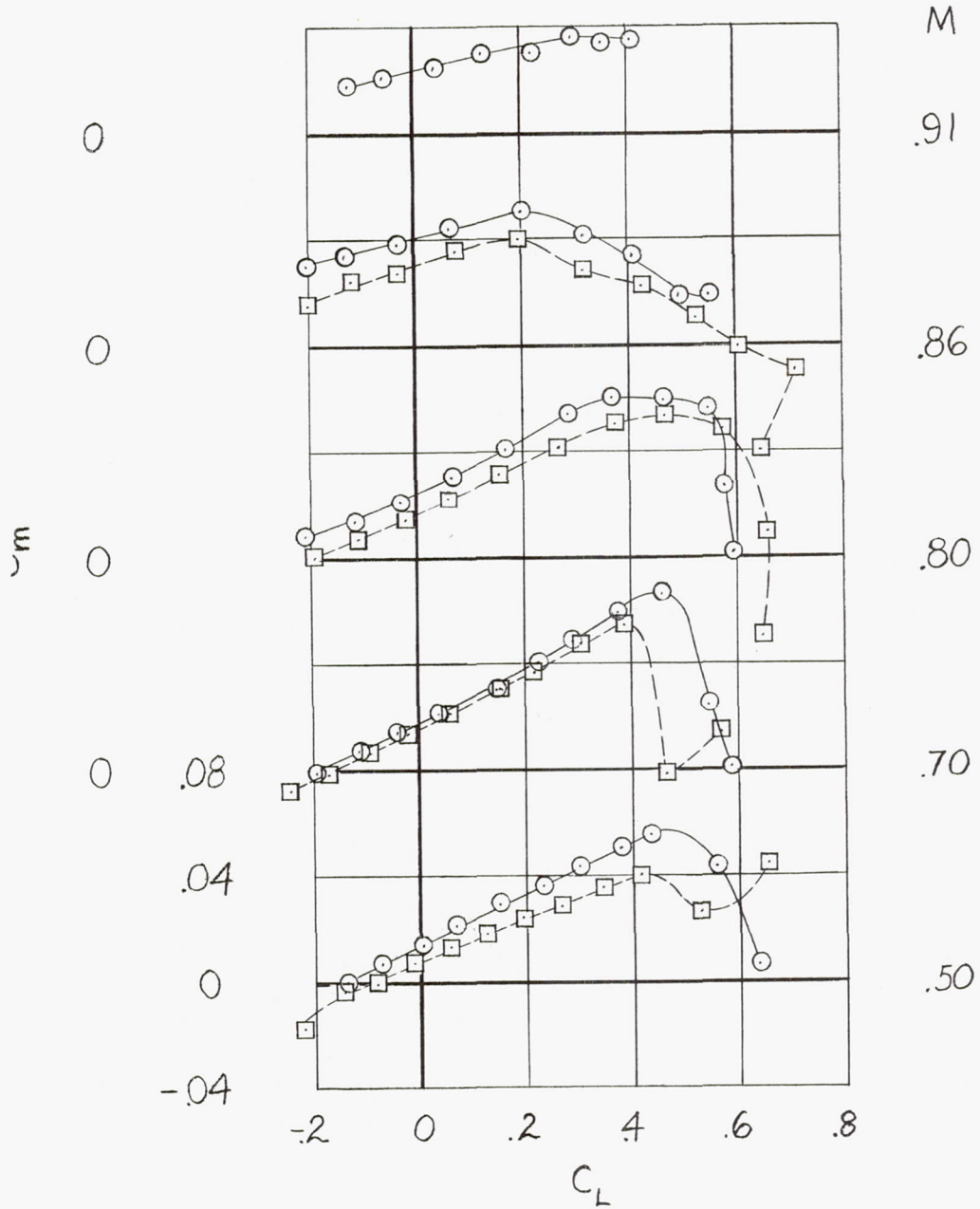
(a) Variation of α with C_L .

Figure 10.- Aerodynamic characteristics of unswept-wing model with bodies located under wing on long 64A010-section pylons.



○ — Fins off

□ — Fins on

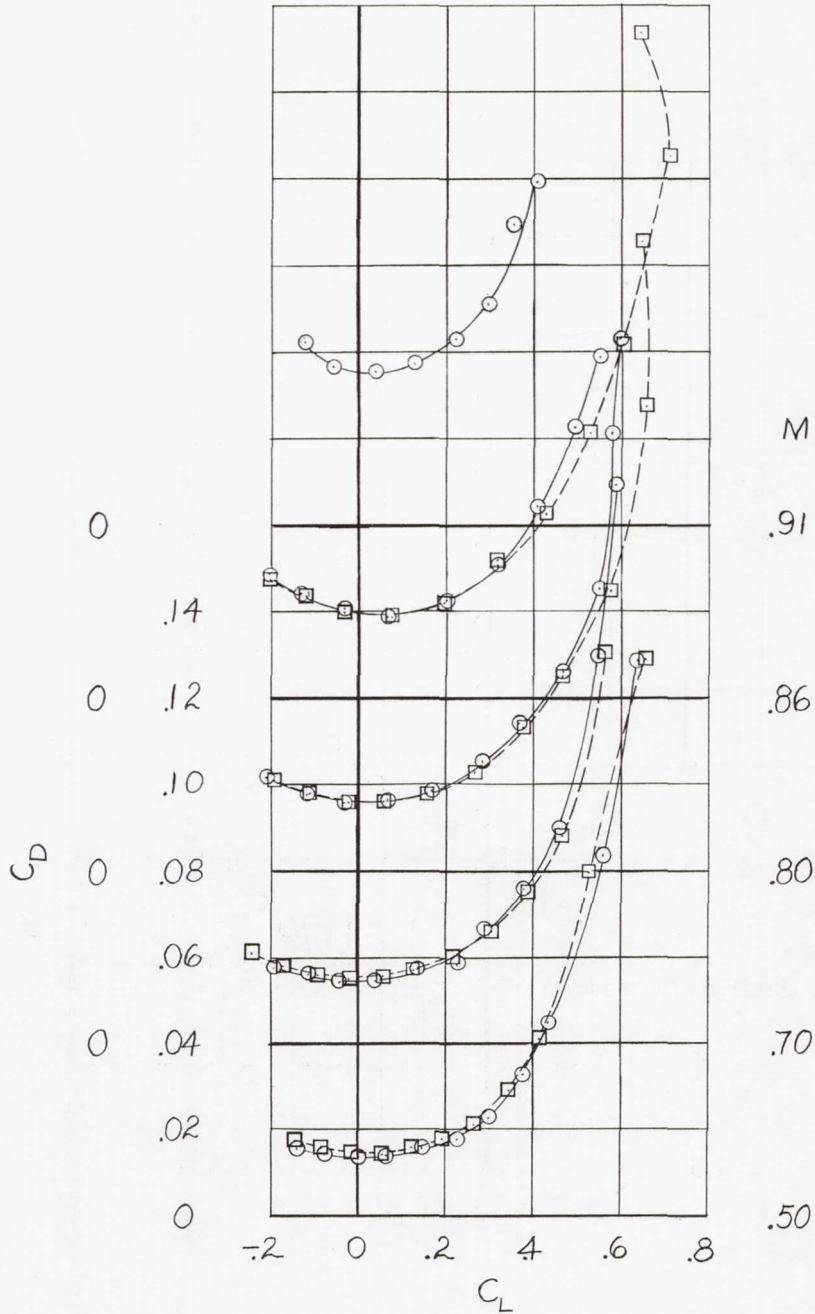


(b) Variation of C_m with C_L .

Figure 10.- Continued.

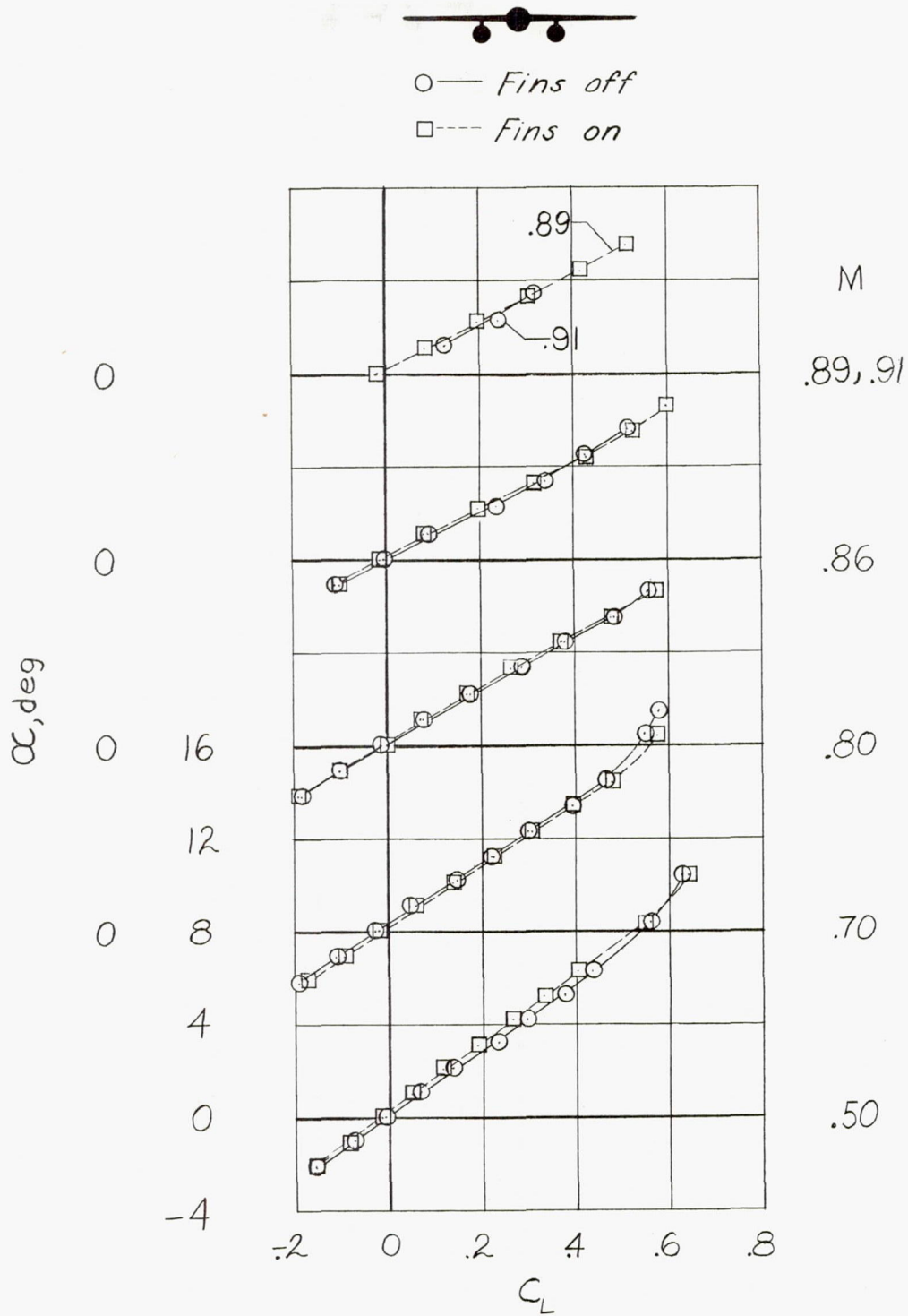


○ — Fins off
□ — Fins on



(c) Variation of C_D with C_L .

Figure 10.- Concluded.



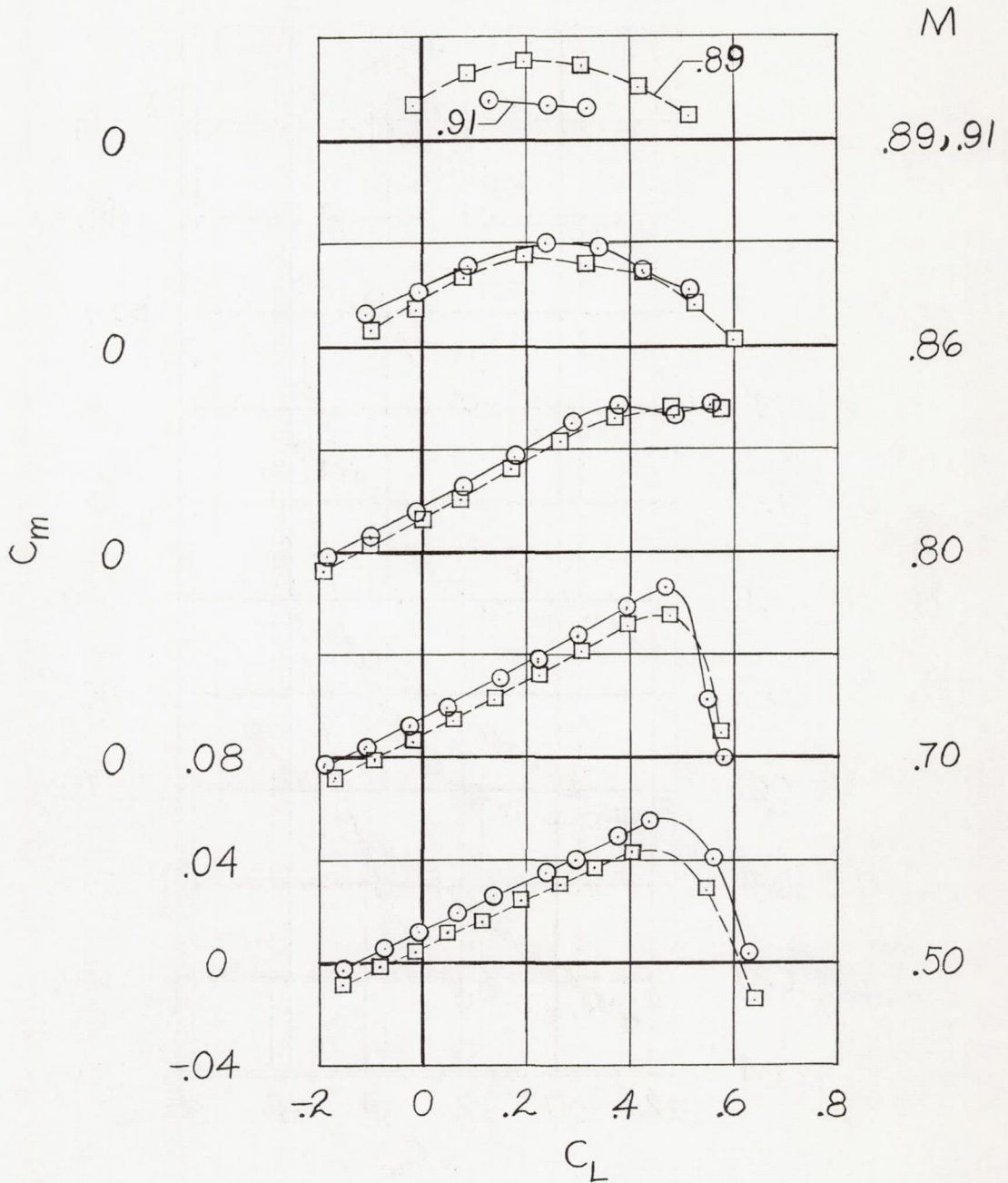
(a) Variation of α with C_L .

Figure 11.- Aerodynamic characteristics of unswept-wing model with bodies located under wing on short 64A010-section pylons.



○ — Fins off

□ — Fins on

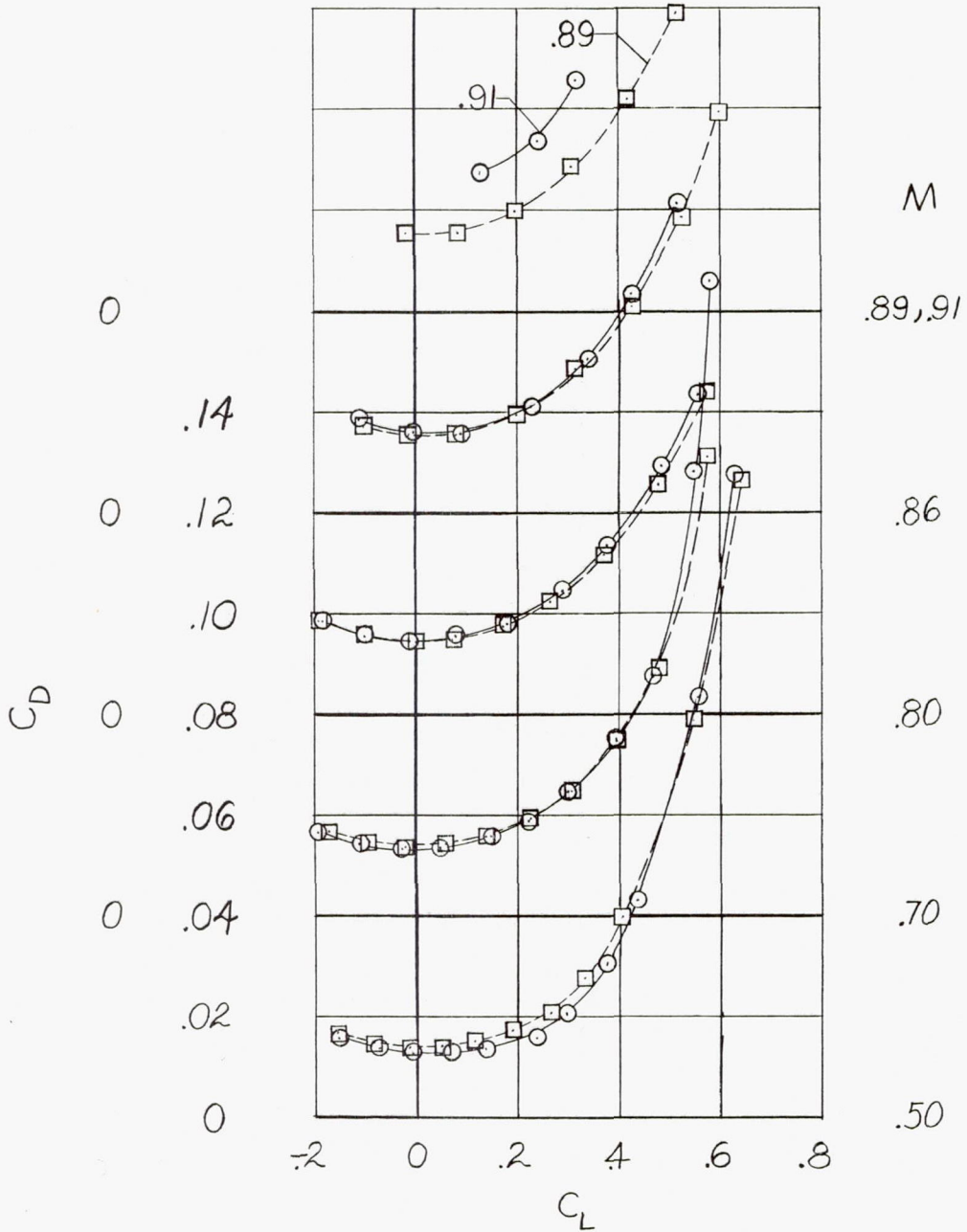


(b) Variation of C_m with C_L .

Figure 11.- Continued.

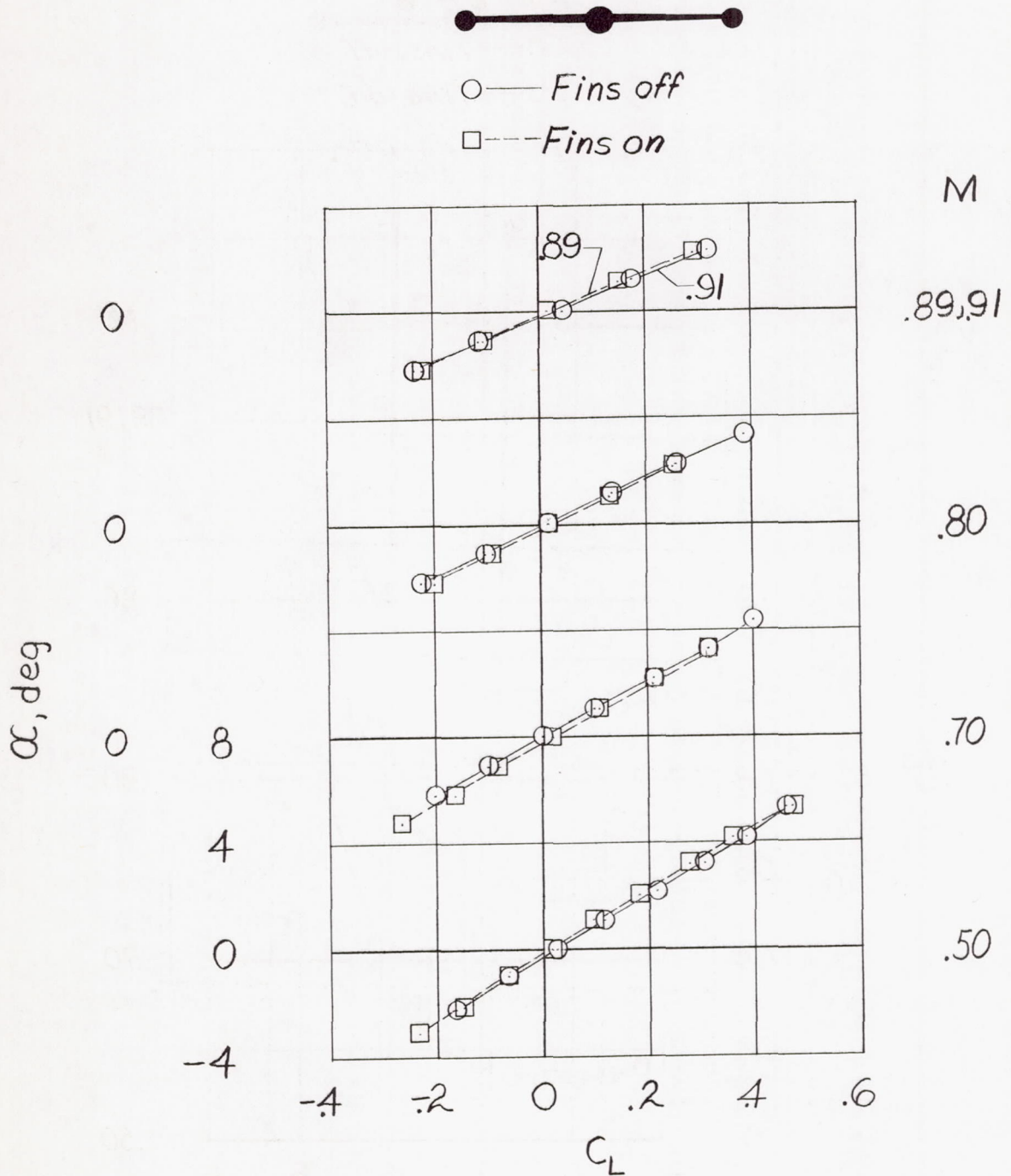


○ — Fins off
 □ — Fins on



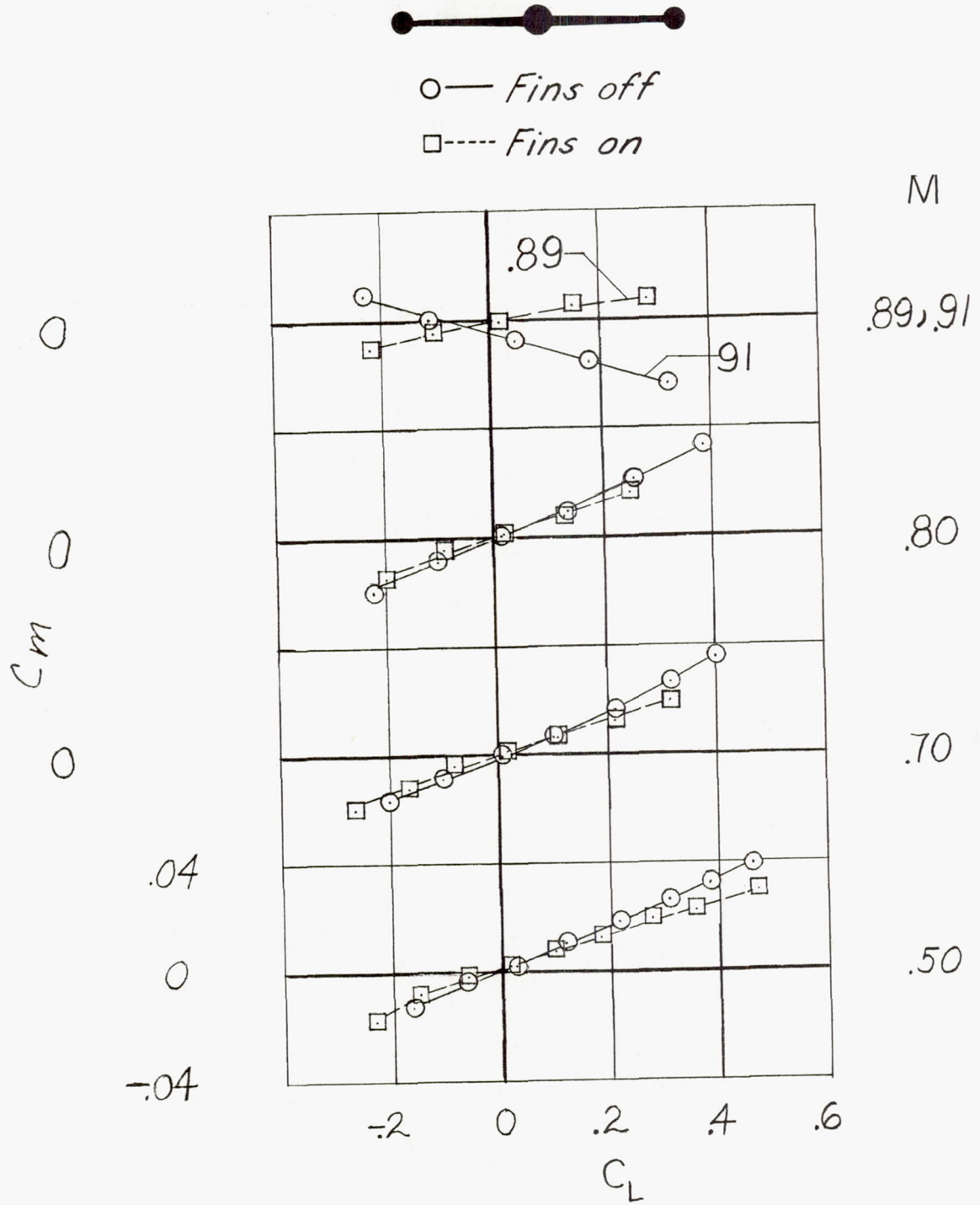
(c) Variation of C_D with C_L .

Figure 11.- Concluded.



(a) Variation of α with C_L .

Figure 12.- Aerodynamic characteristics of unswept-wing model with bodies tip-mounted.



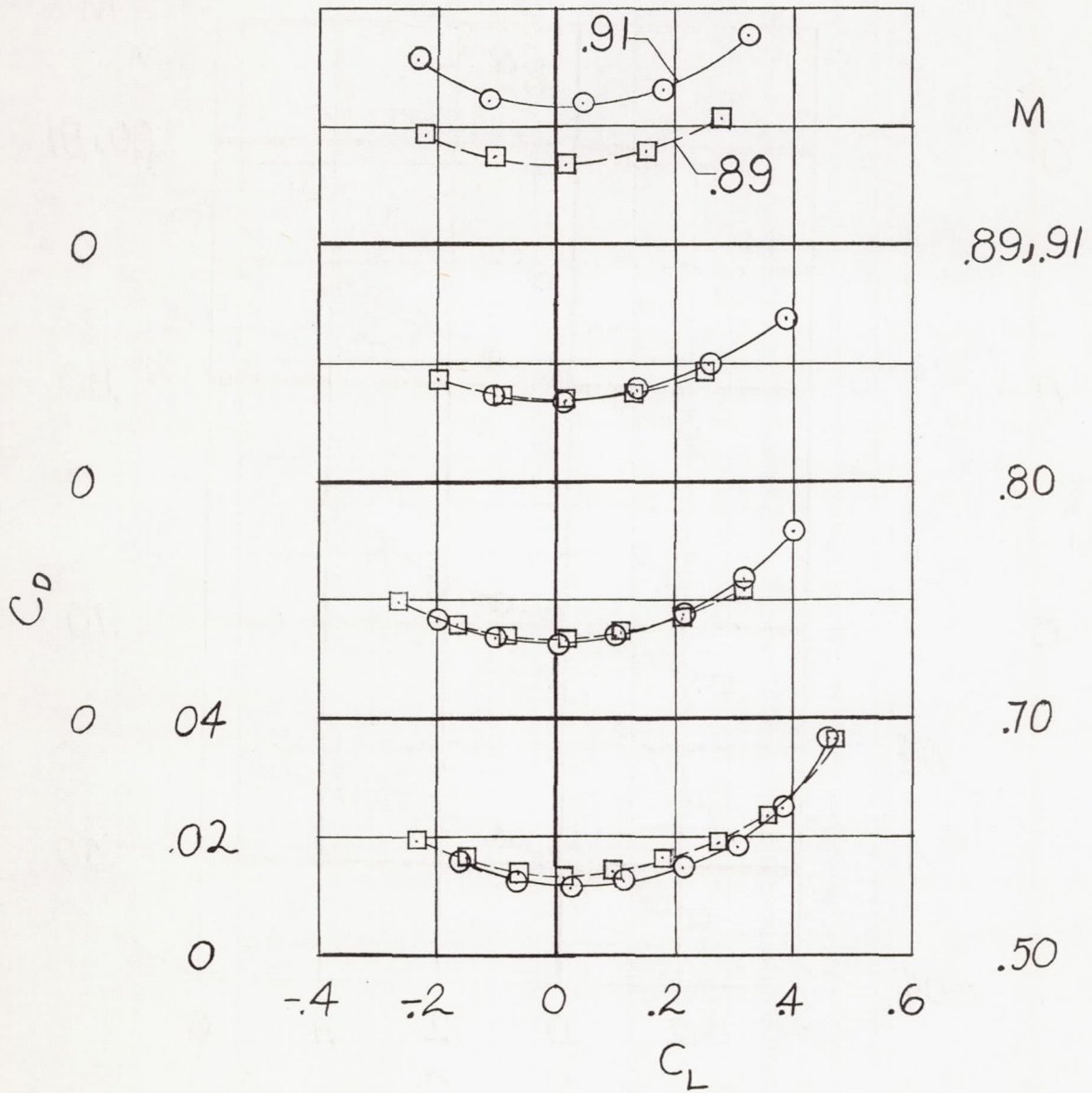
(b) Variation of C_m with C_L .

Figure 12.- Continued.



○ — Fins off

□ - - - Fins on



(c) Variation of C_D with C_L .

Figure 12.- Concluded.

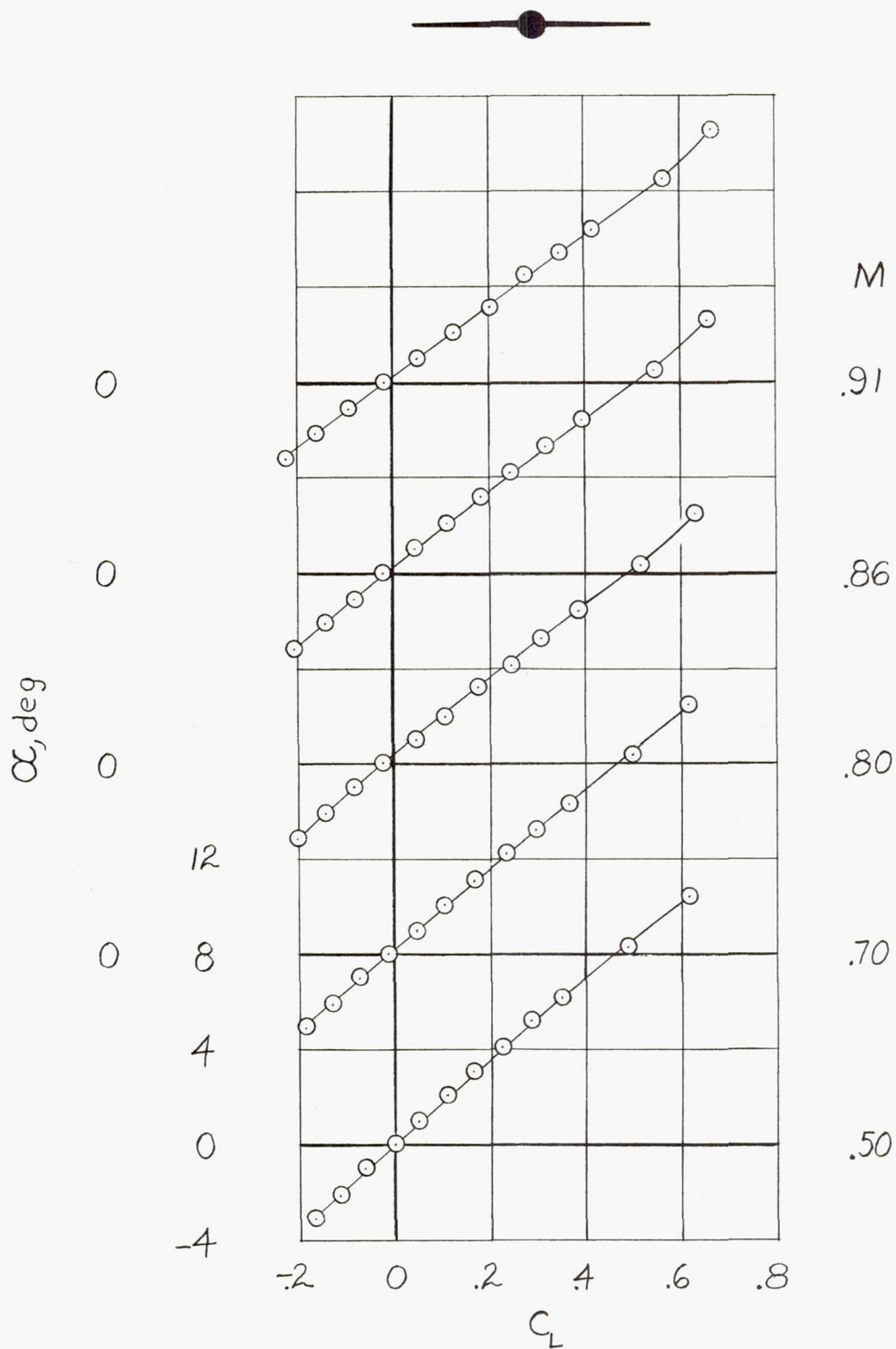
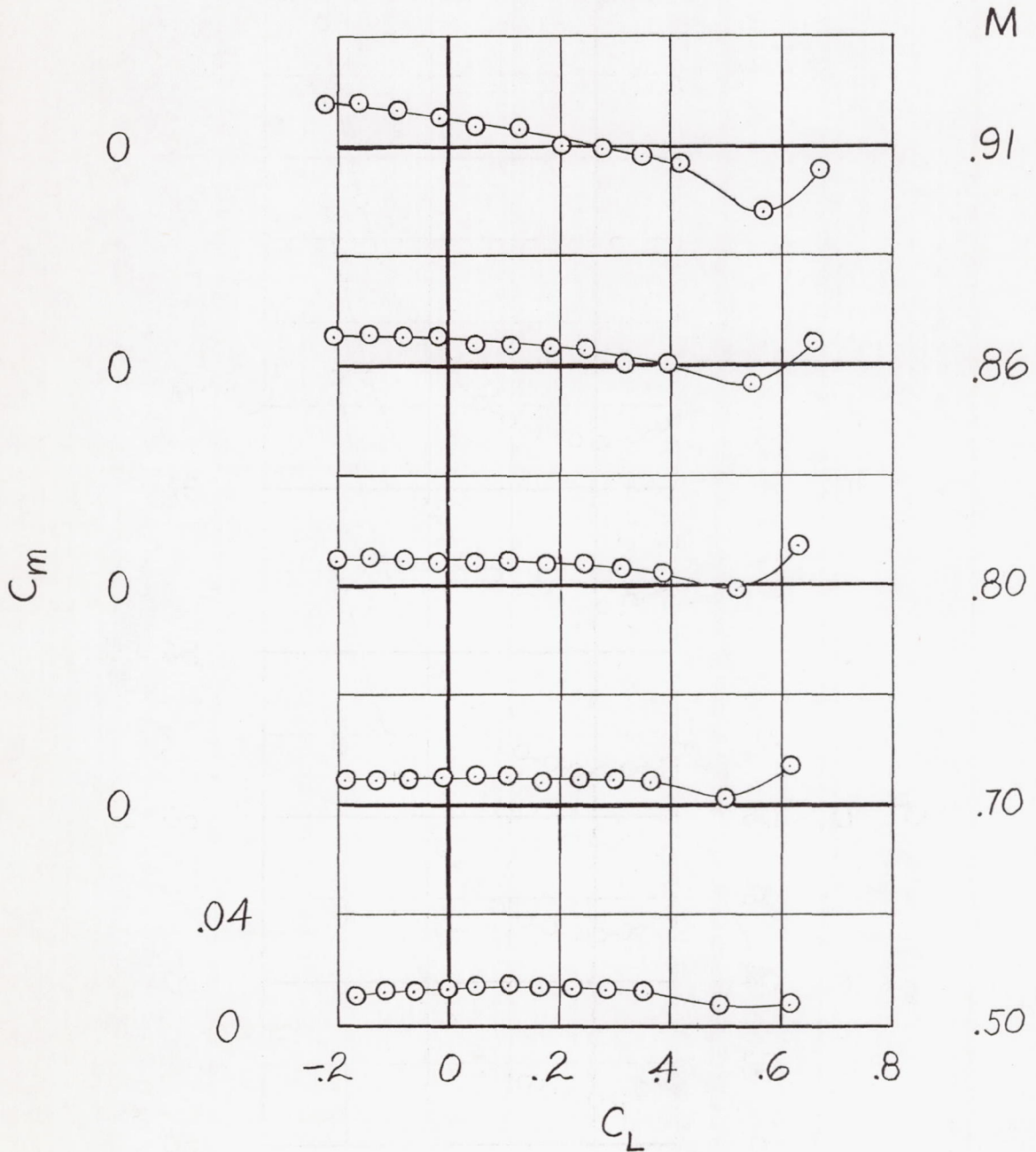
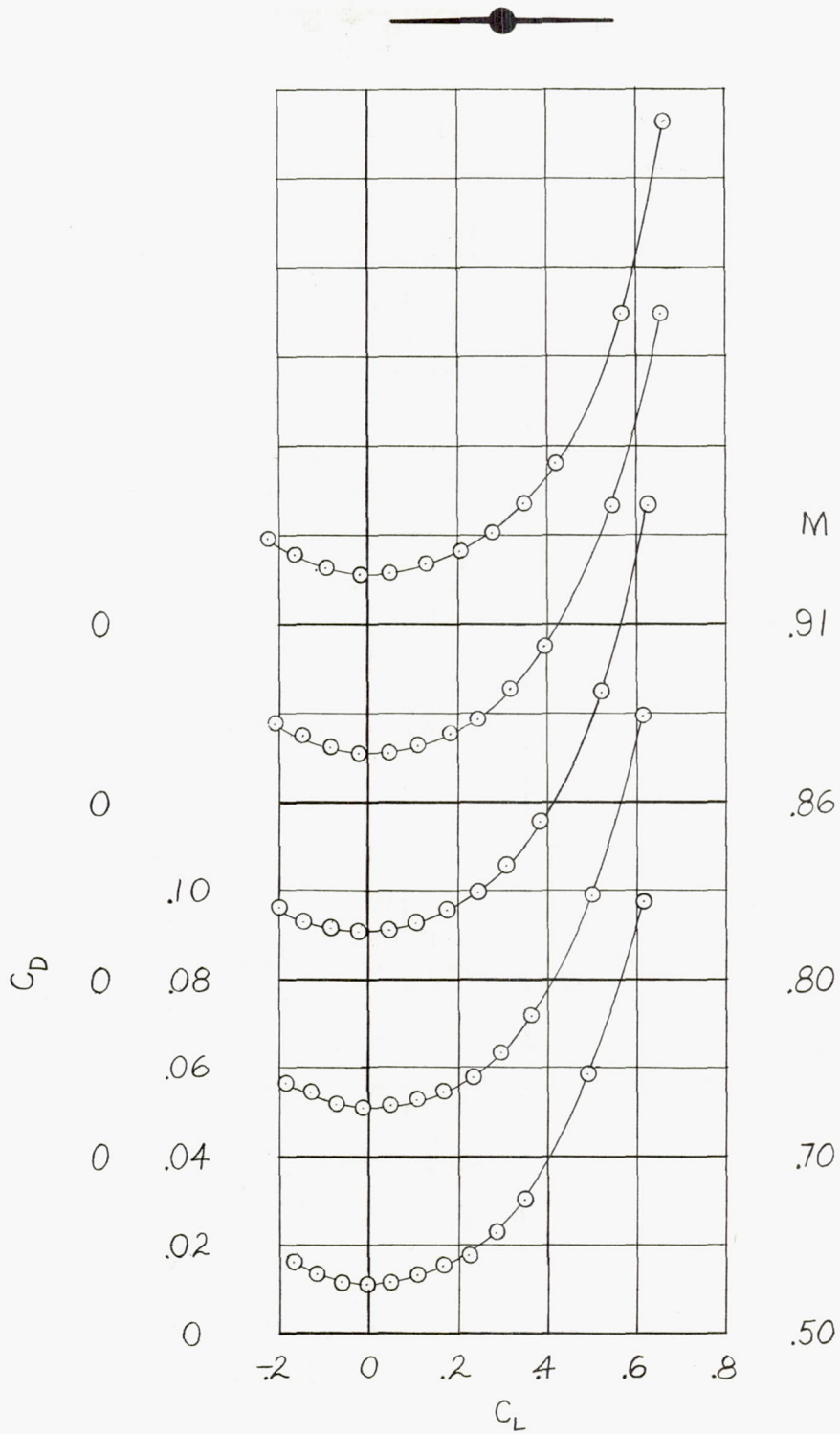
(a) Variation of α with C_L .

Figure 13.- Aerodynamic characteristics of basic swept-wing model.



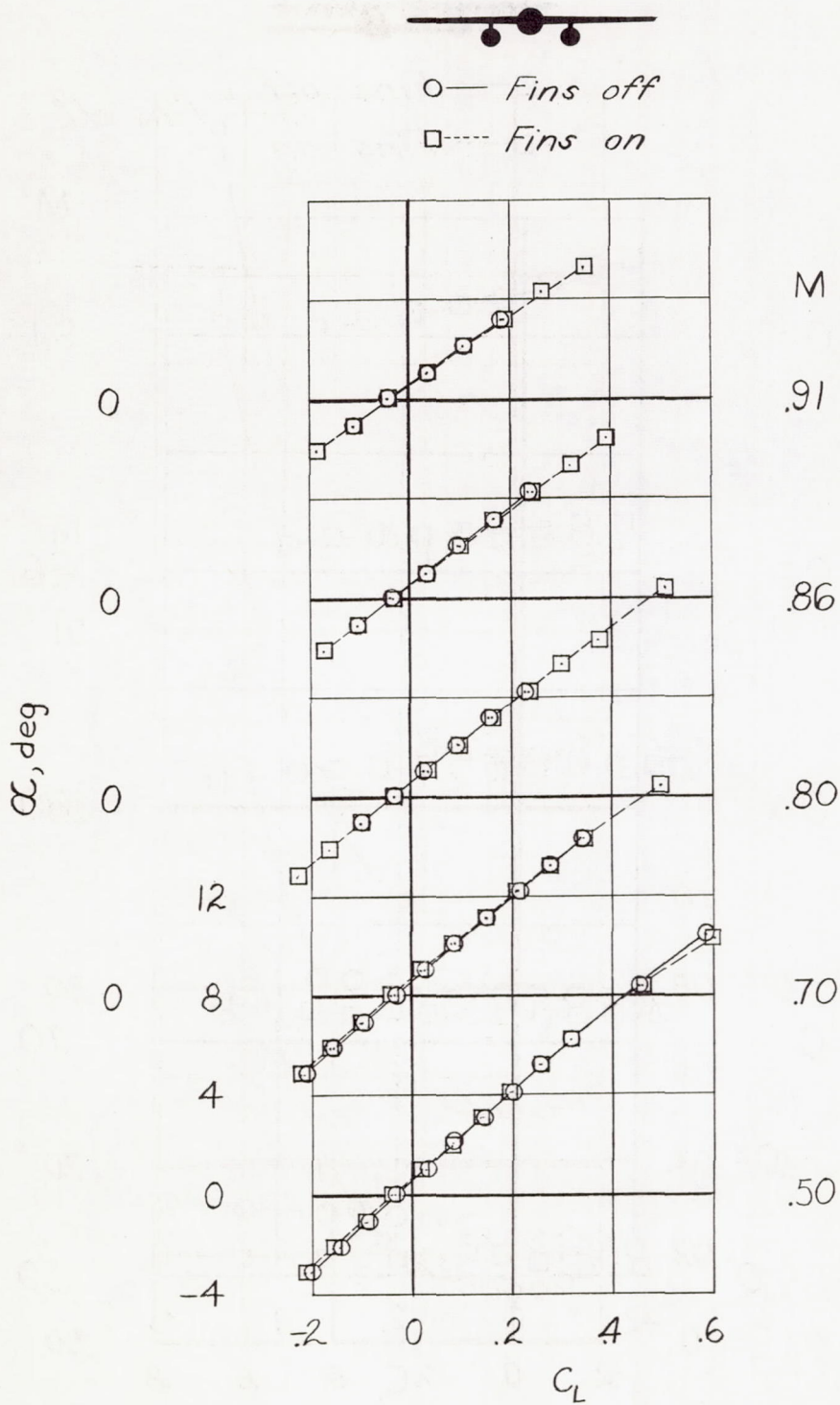
(b) Variation of C_m with C_L .

Figure 13.- Continued.



(c) Variation of C_D with C_L .

Figure 13.- Concluded.



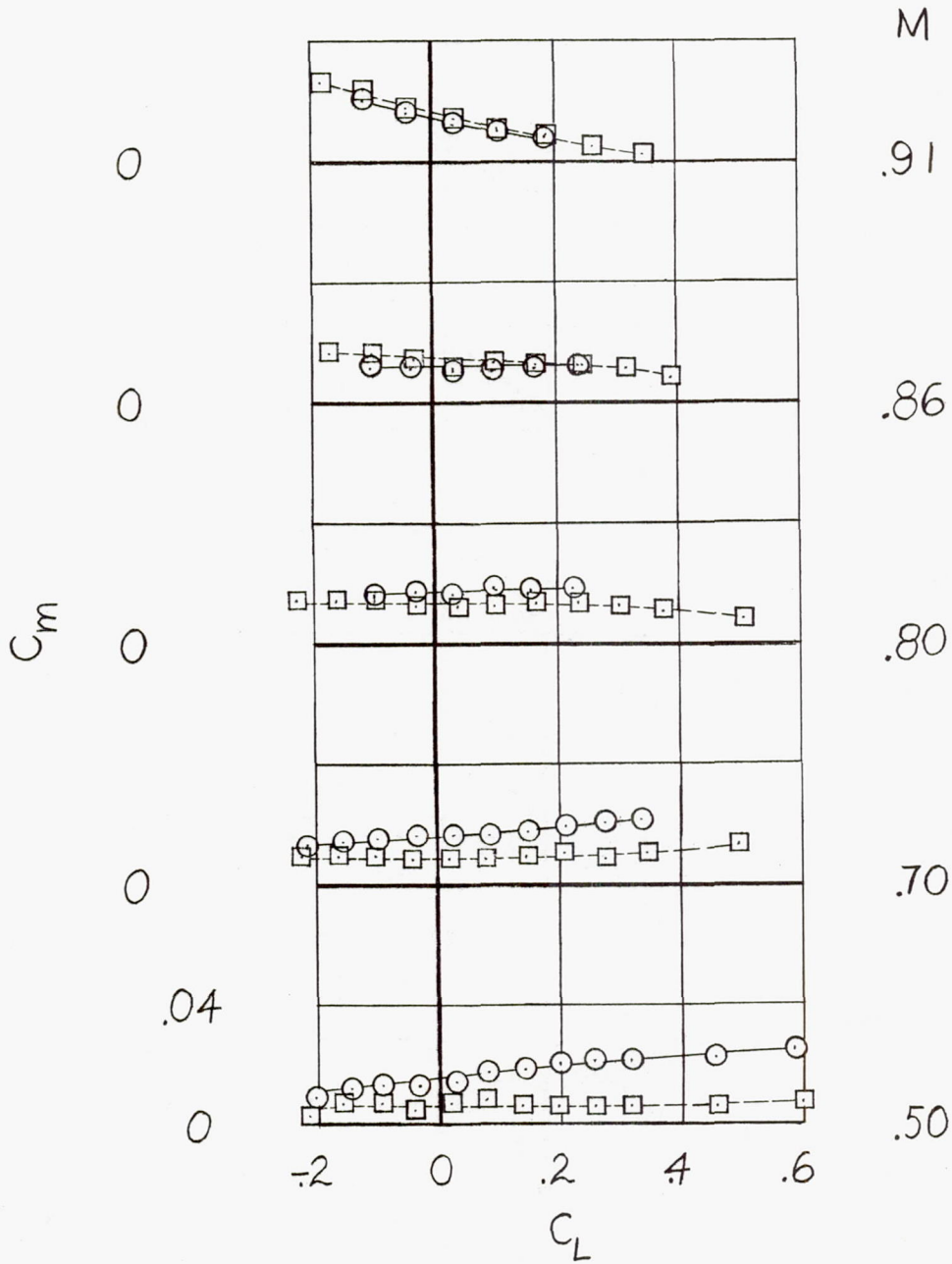
(a) Variation of α with C_L .

Figure 14.- Aerodynamic characteristics of swept-wing model with bodies located under wing on short 64A010-section pylons.



○ — Fins off

□ — Fins on

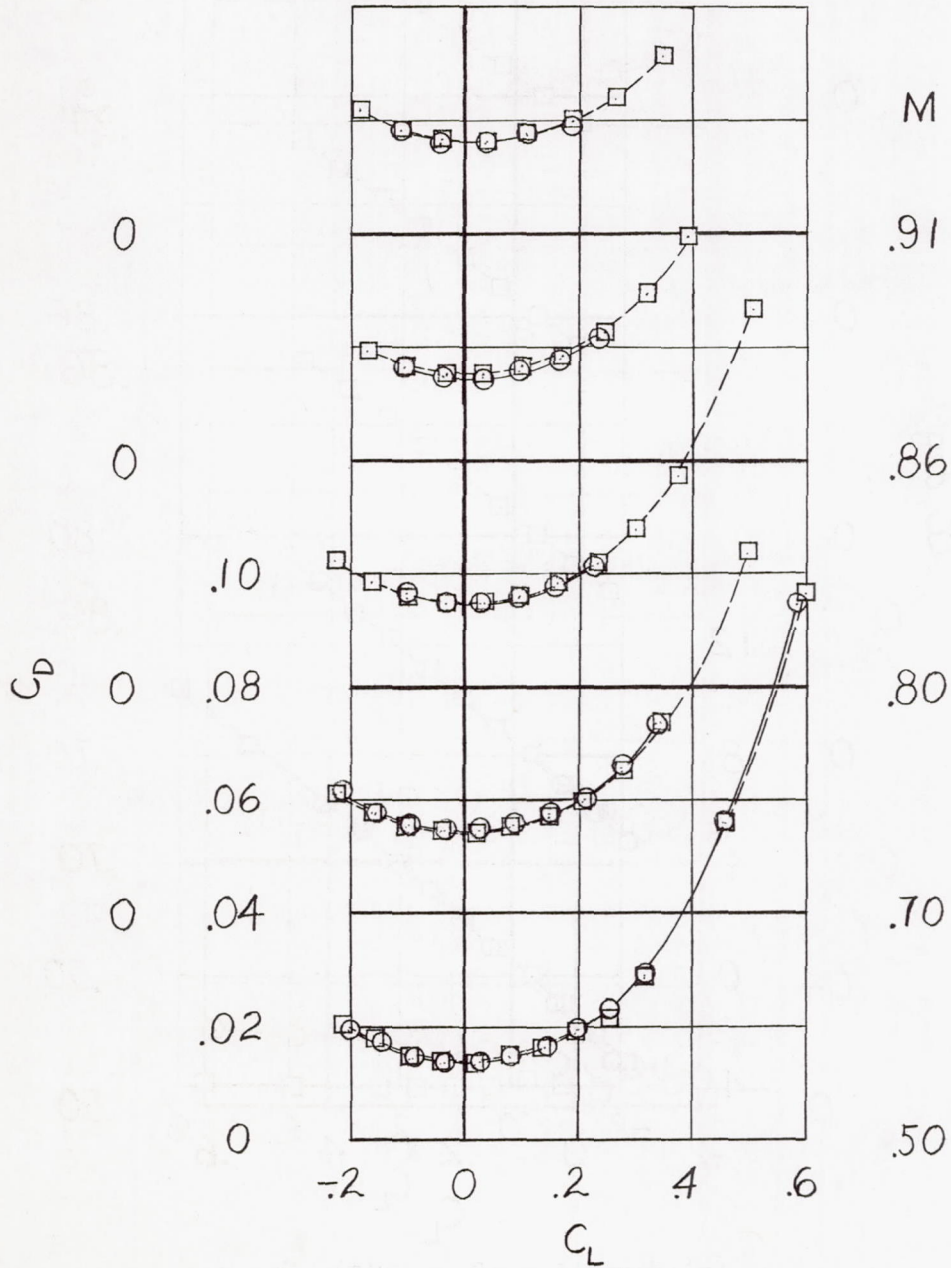


(b) Variation of C_m with C_L .

Figure 14.- Continued.

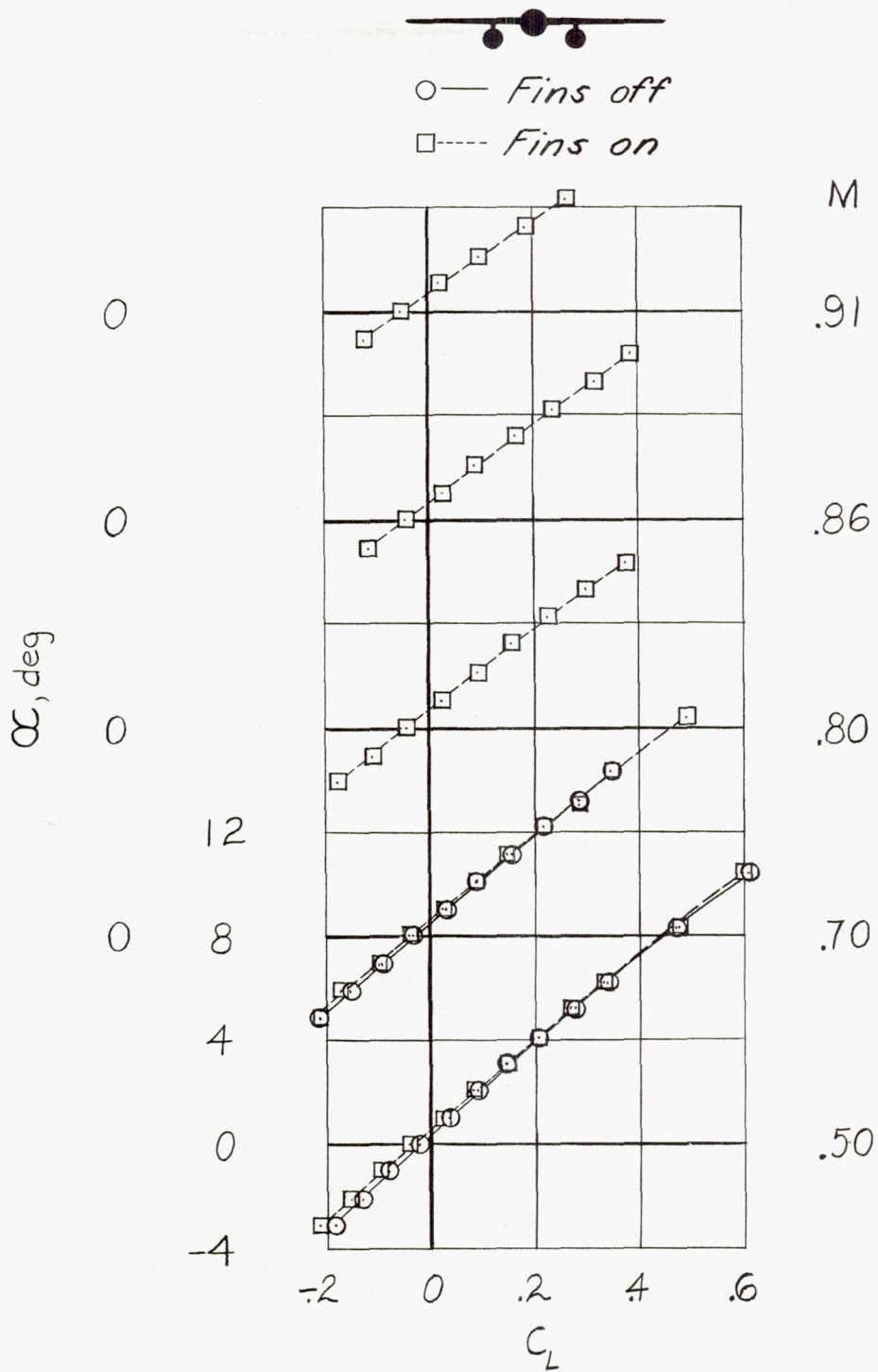


○ — Fins off
 □ — Fins on



(c) Variation of C_D with C_L .

Figure 14.- Concluded.



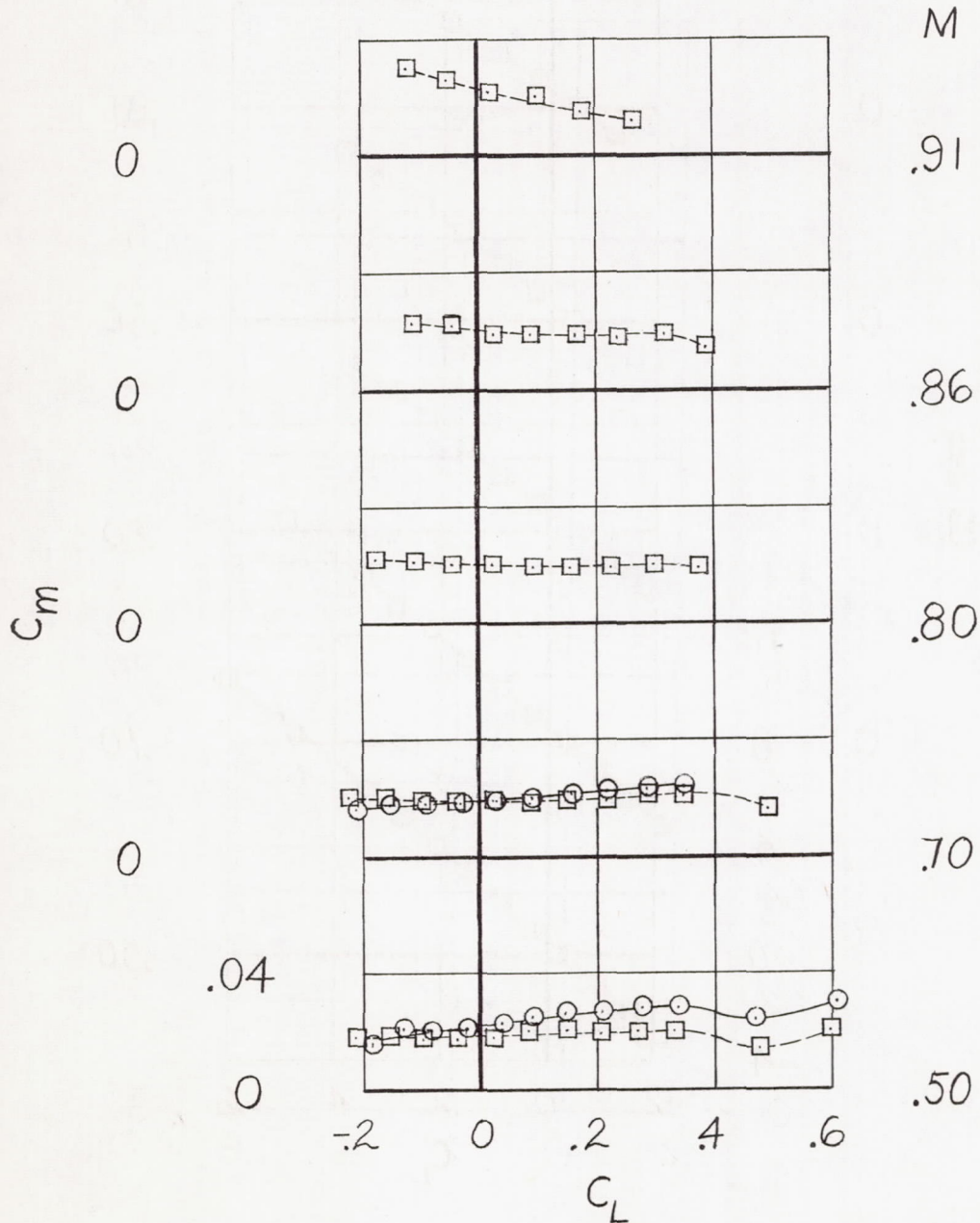
(a) Variation of α with C_L .

Figure 15.- Aerodynamic characteristics of the swept-wing model with bodies located under wing on short 64A010-section pylons with body tilted -5° with respect to fuselage center line.



○ — *Fins off*

□ — *Fins on*



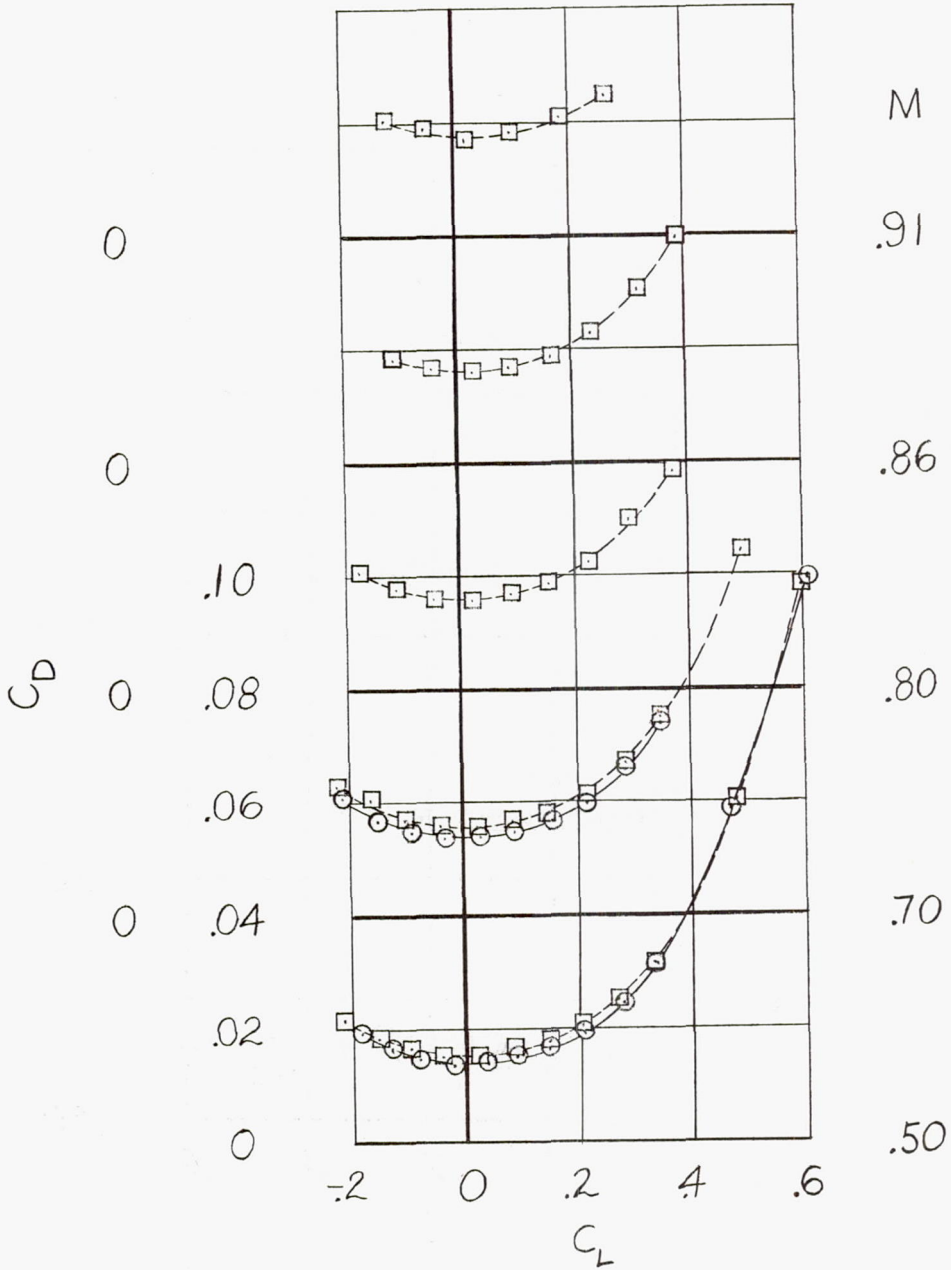
(b) Variation of C_m with C_L .

Figure 15.- Continued.



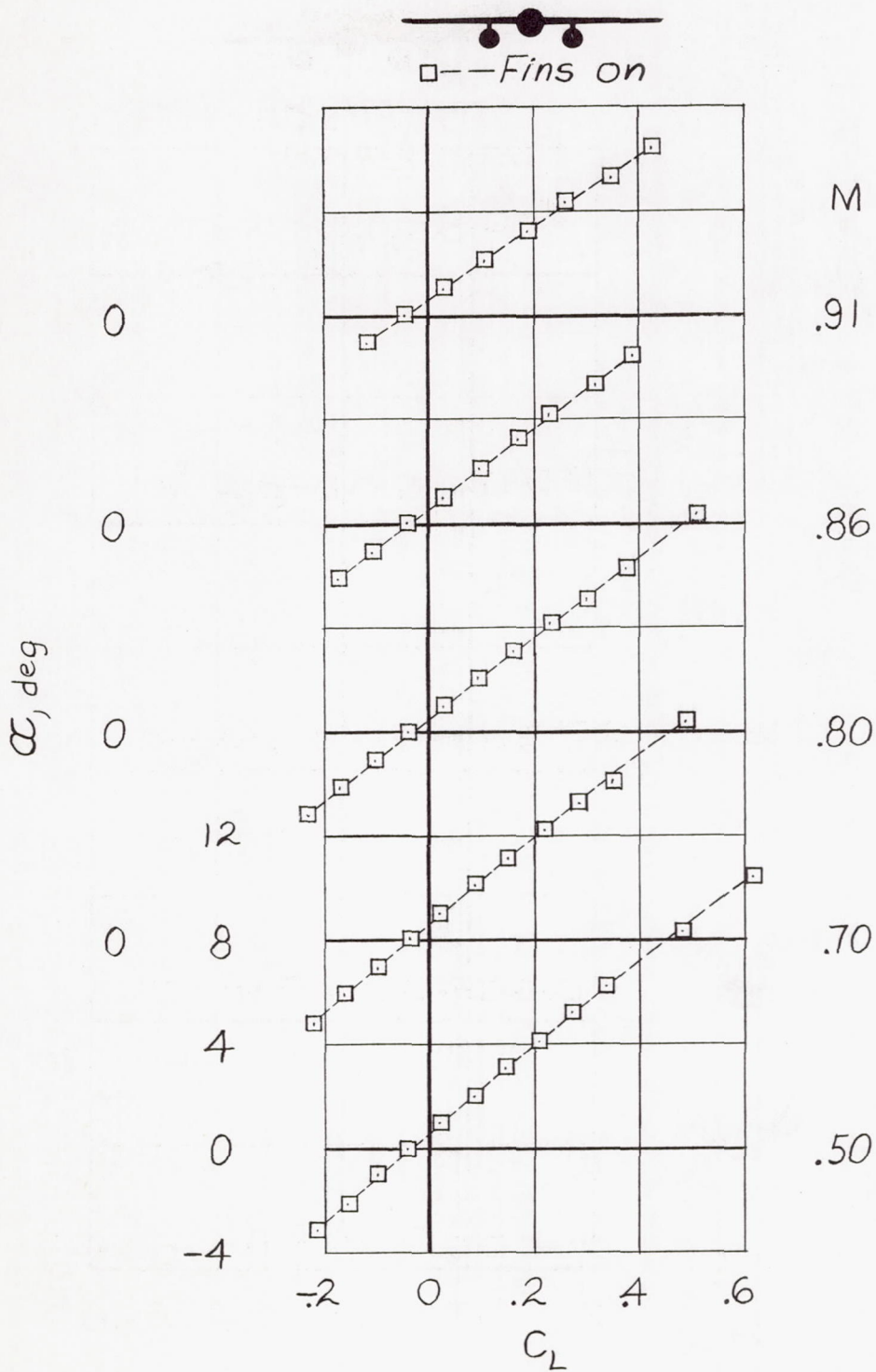
○ — Fins off

□ - - - Fins on



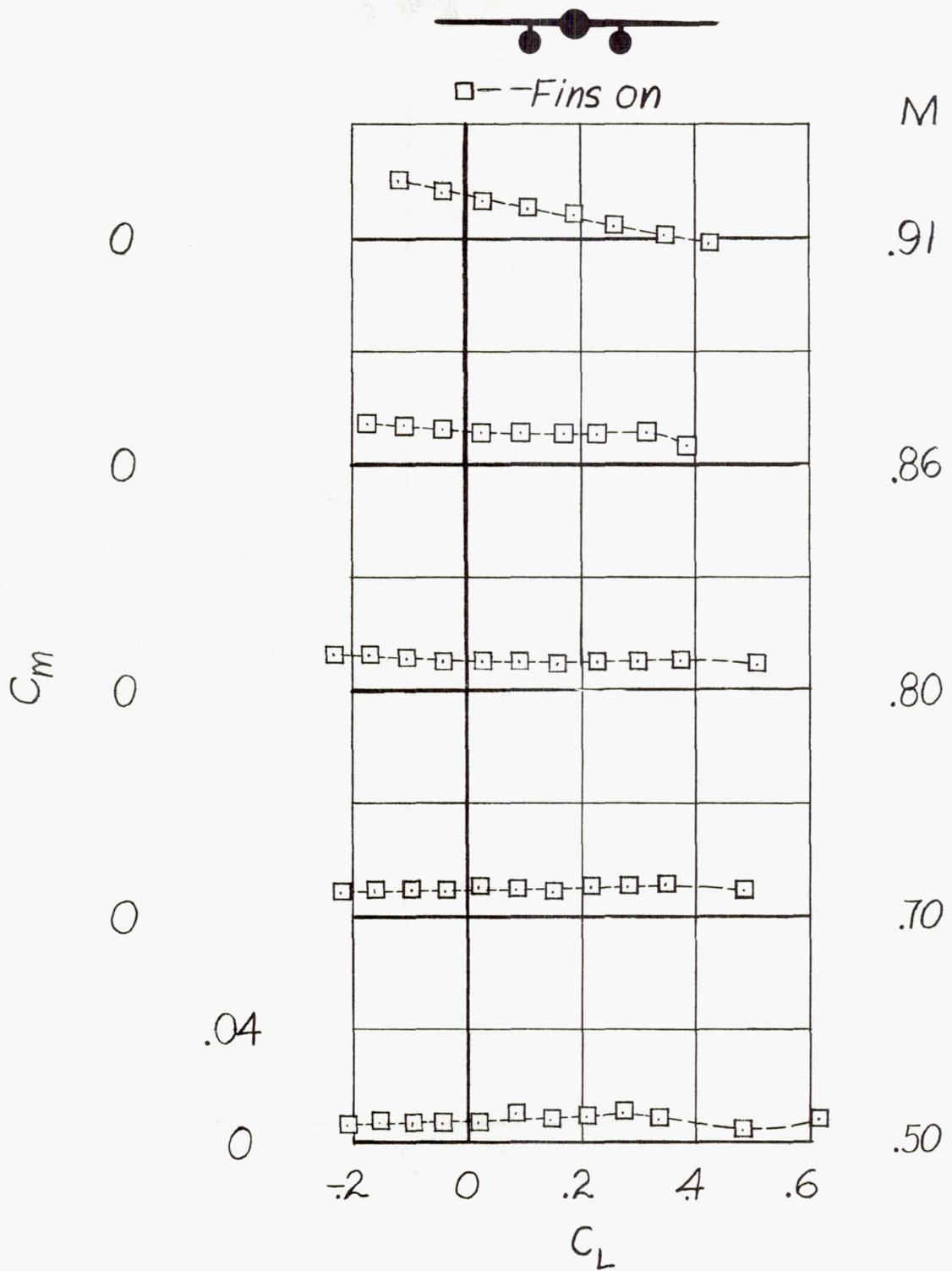
(c) Variation of C_D with C_L .

Figure 15.- Concluded.



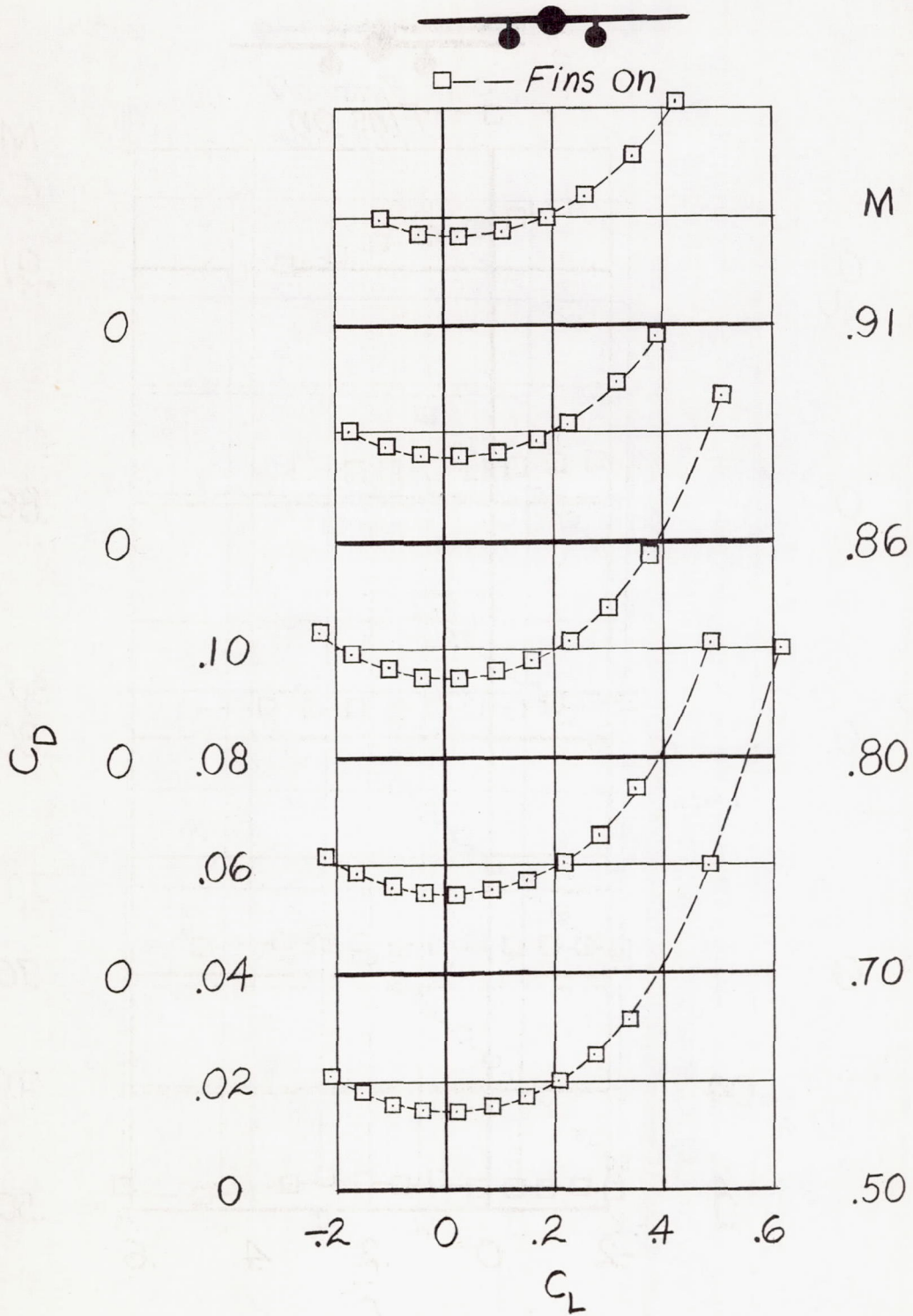
(a) Variation of α with C_L .

Figure 16.- Aerodynamic characteristics of swept-wing model with bodies located under wing on short flat pylons; fins on.



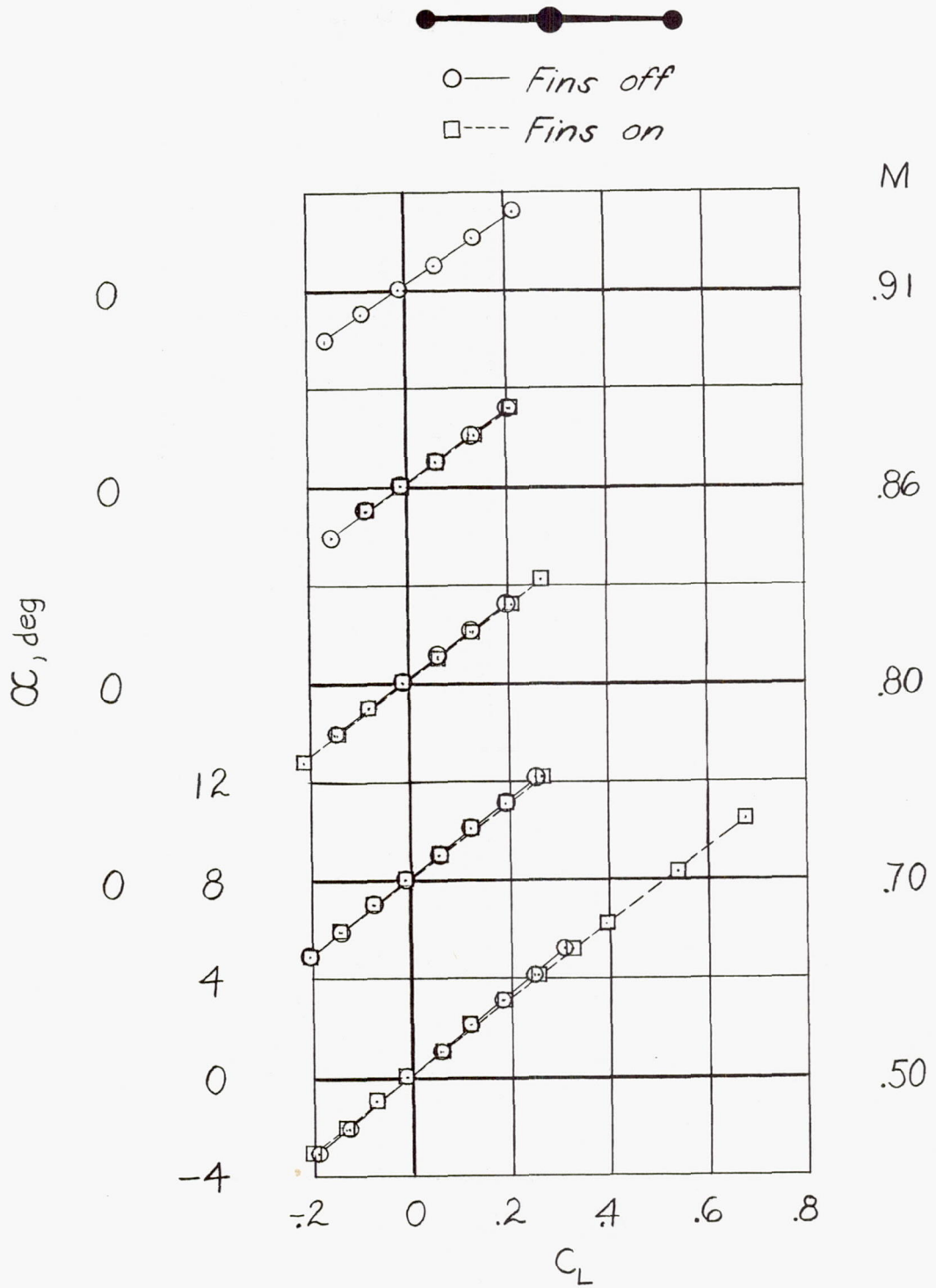
(b) Variation of C_m with C_L .

Figure 16.- Continued.



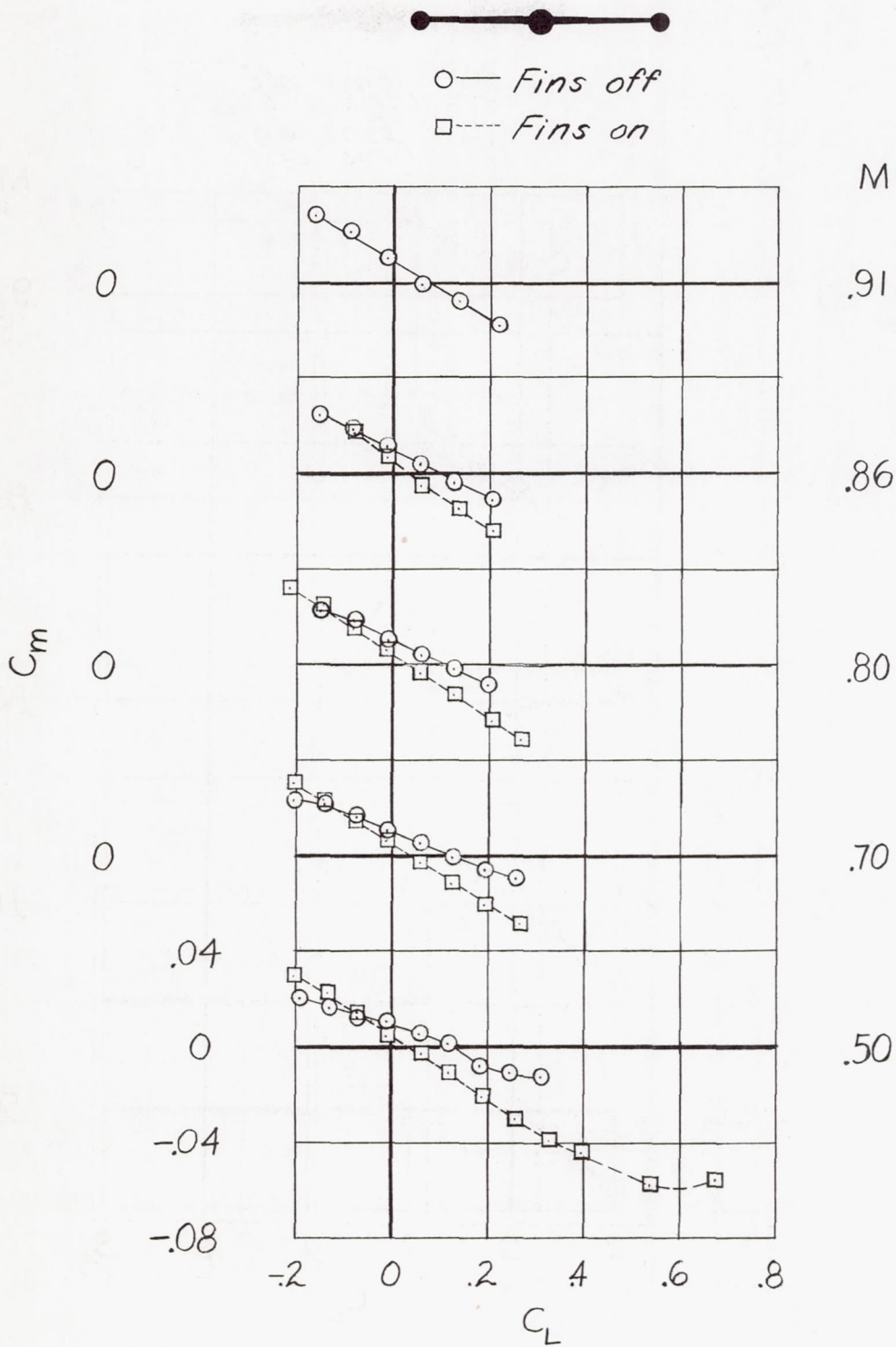
(c) Variation of C_D with C_L .

Figure 16.- Concluded.



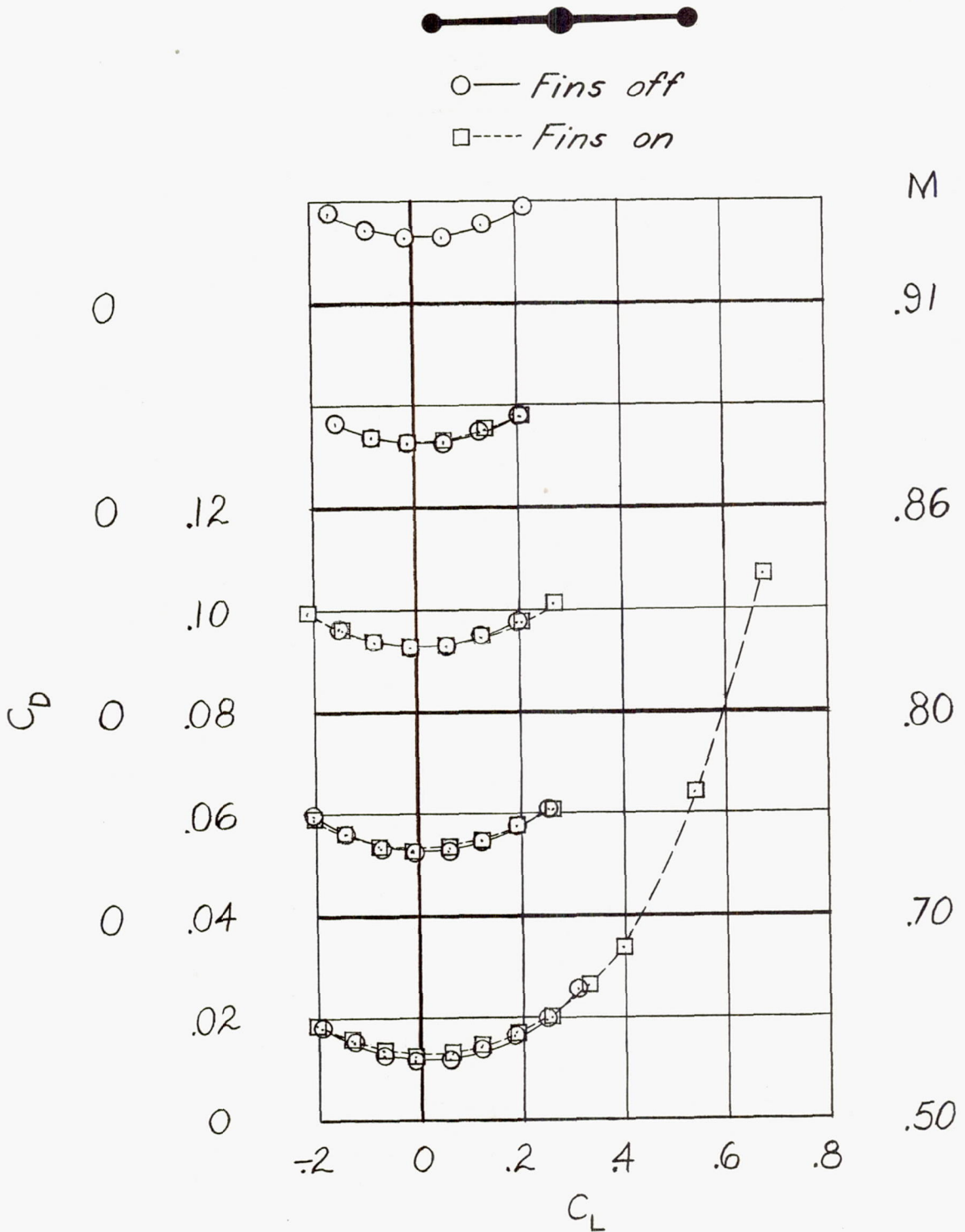
(a) Variation of α with C_L .

Figure 17.- Aerodynamic characteristics of swept-wing model with bodies tip-mounted.



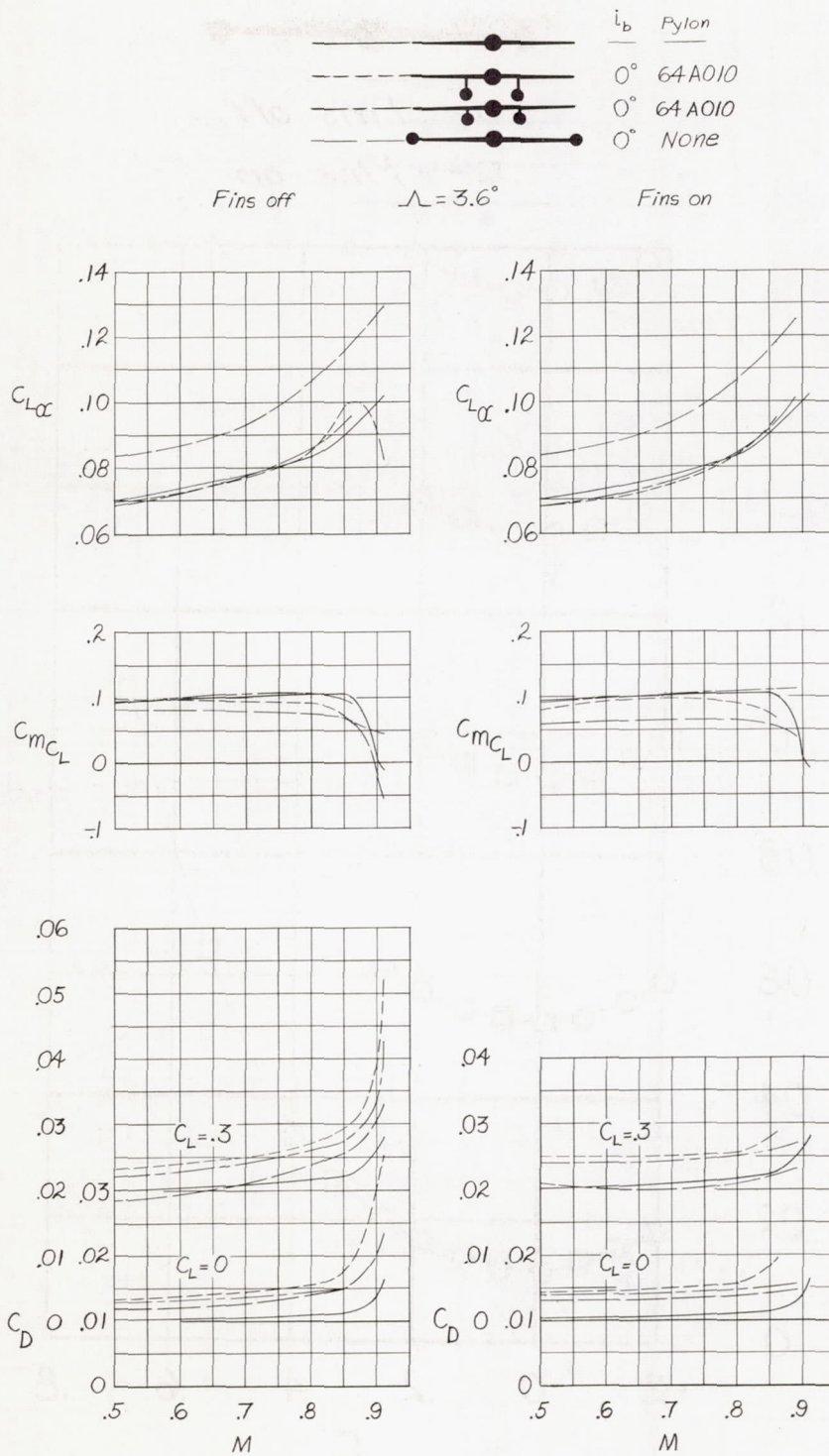
(b) Variation of C_m with C_L .

Figure 17.- Continued.



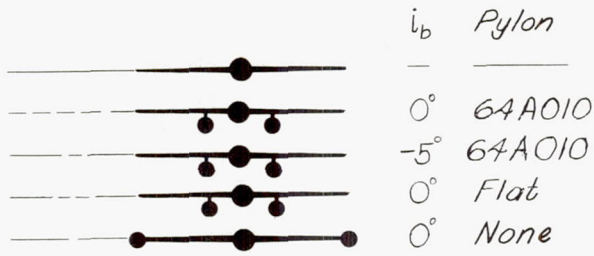
(c) Variation of C_D with C_L .

Figure 17.- Concluded.

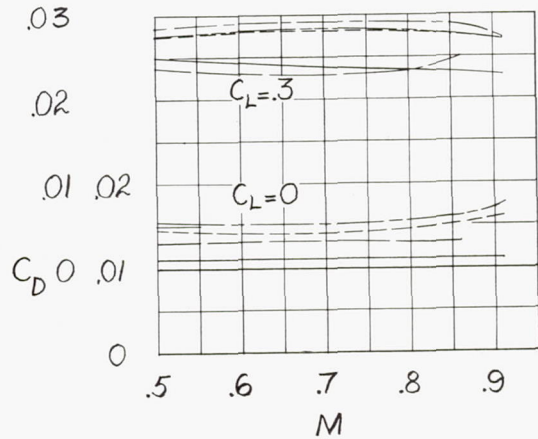
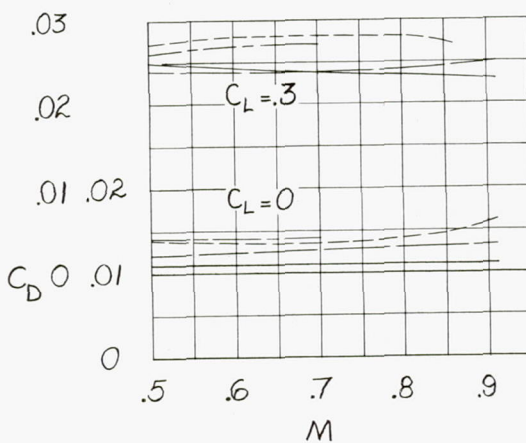
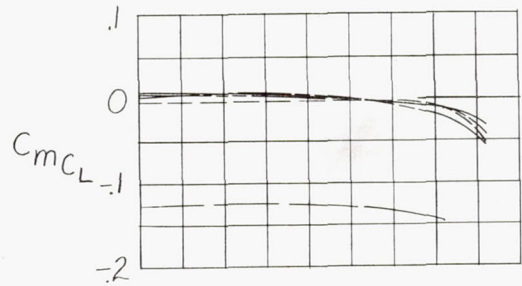
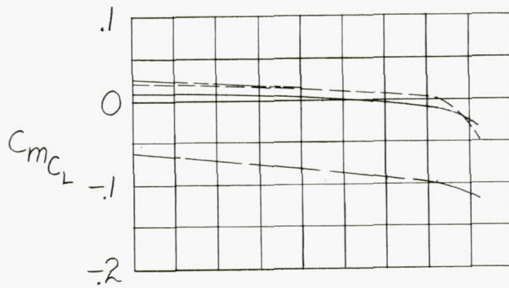
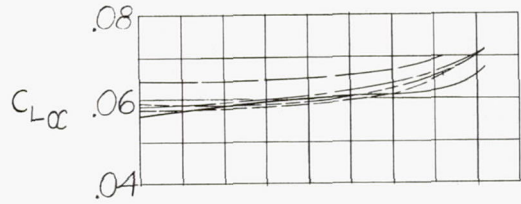
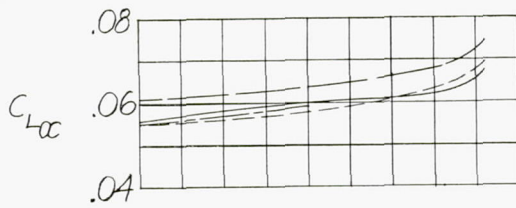


(a) Unswept-wing model.

Figure 18.- Summary of effects of body in several positions on aerodynamic characteristics of test models.



Fins off $\Lambda = 46.7^\circ$ Fins on

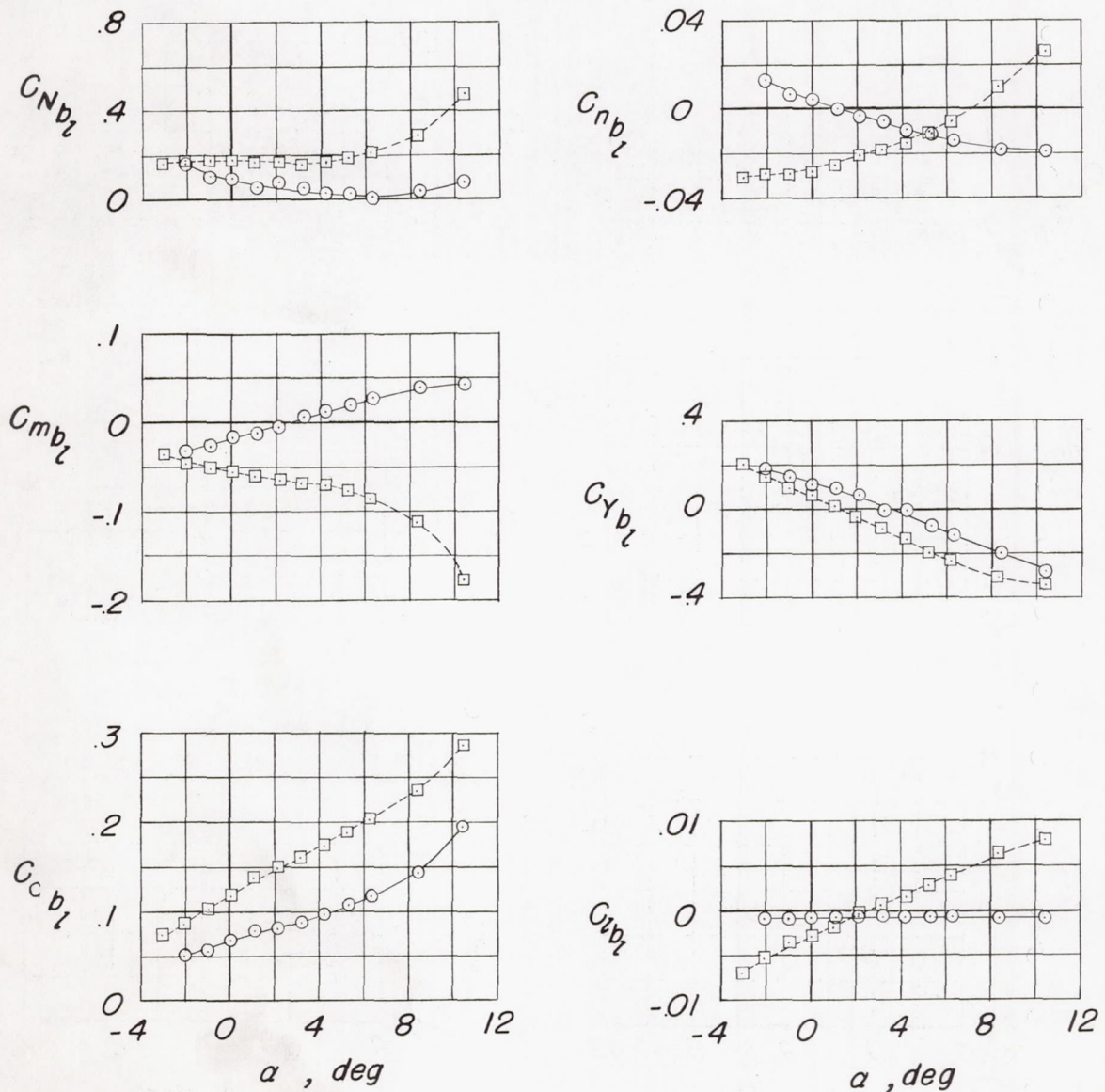


(b) Swept-wing model.

Figure 18.- Concluded.



○ — Fins off
 □ — Fins on



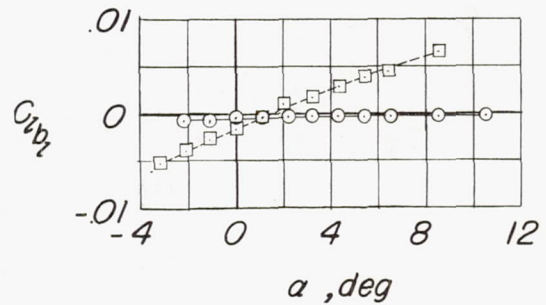
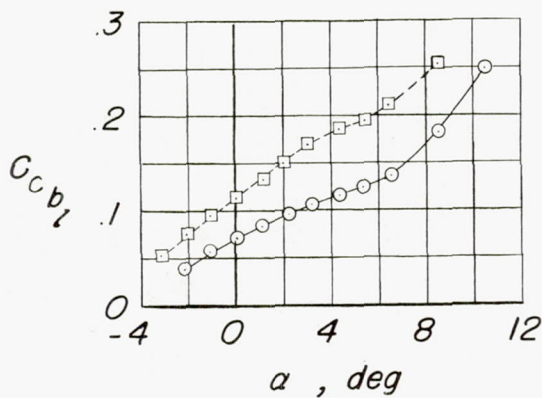
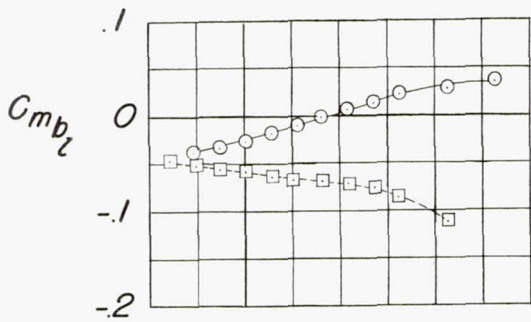
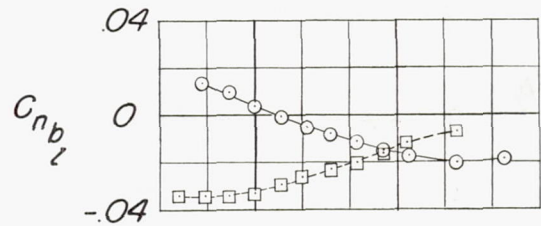
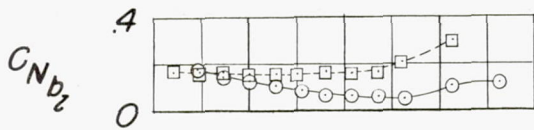
(a) $M = 0.50$.

Figure 19.- Aerodynamic characteristics of body on long 64A010-section pylon located on left wing of unswept-wing model.



○ — Fins off

□ — Fins on

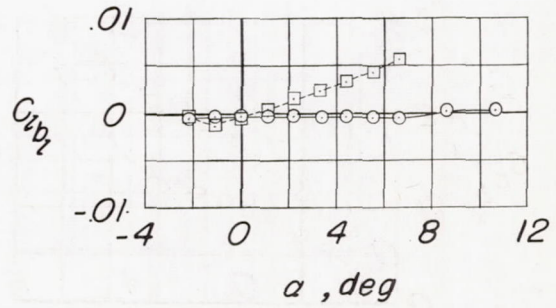
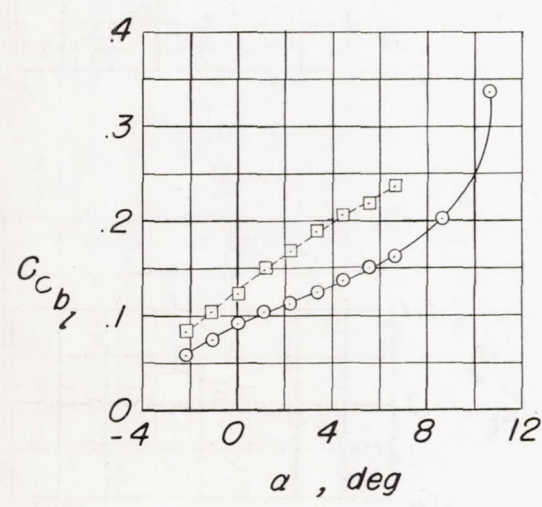
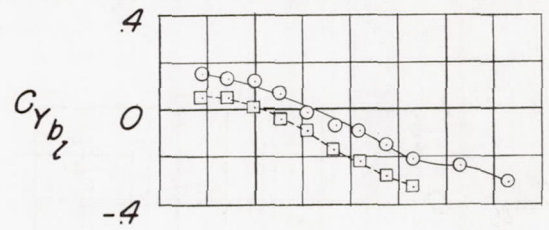
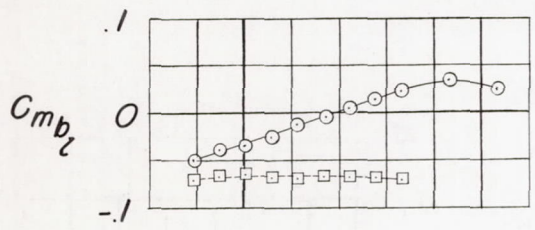
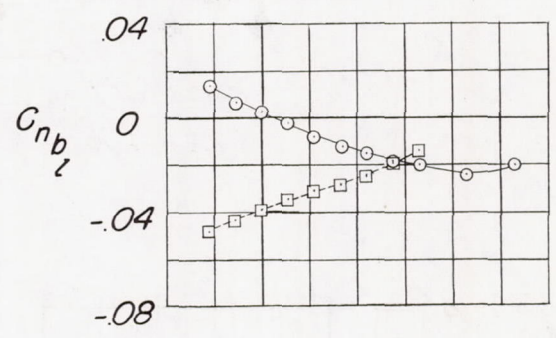
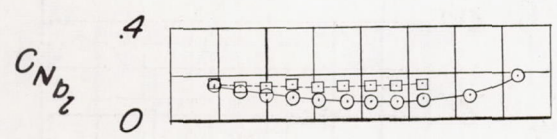


(b) $M = 0.70$.

Figure 19.- Continued.



○ — Fins off
 □ — Fins on

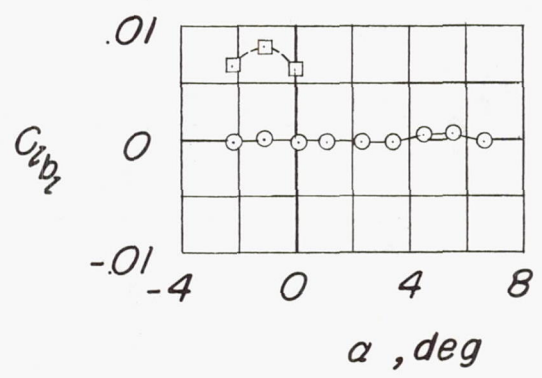
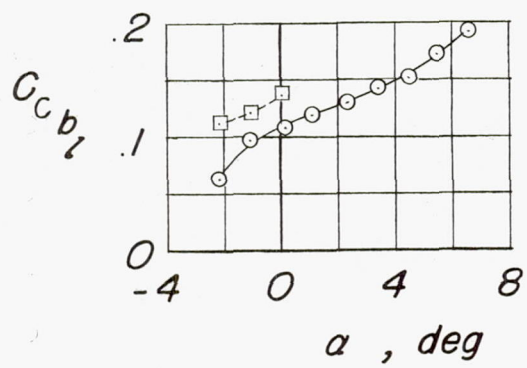
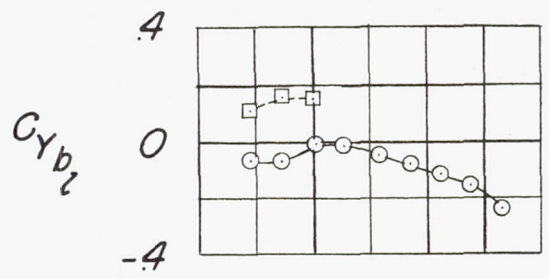
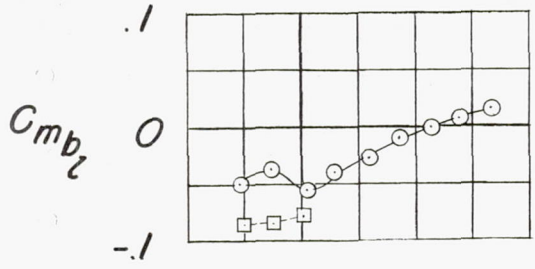
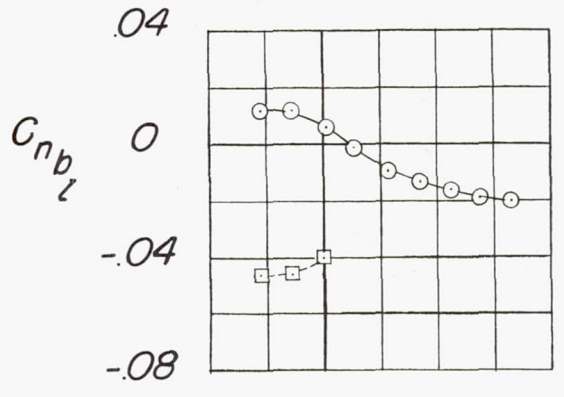
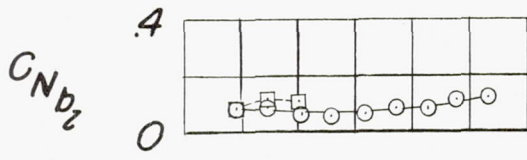


(c) $M = 0.80$.

Figure 19.- Continued.



○ — Fins off
 □ — Fins on

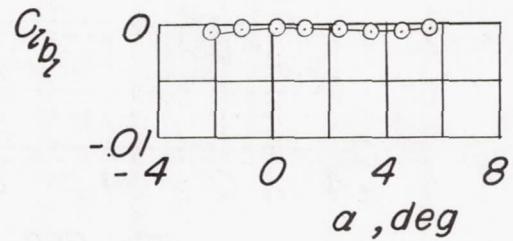
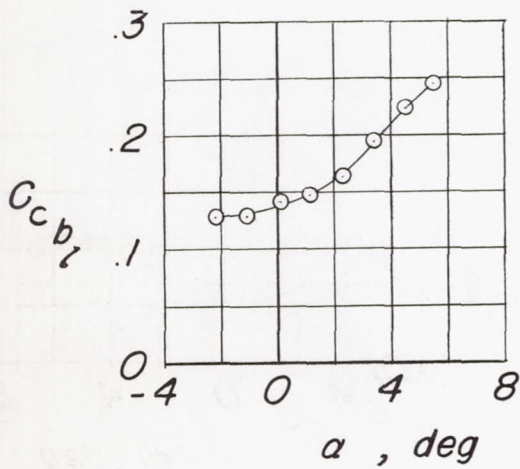
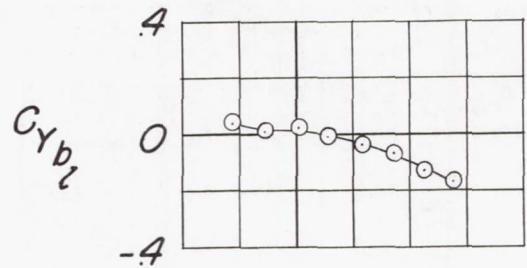
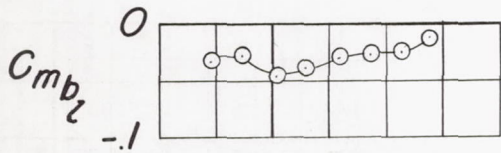
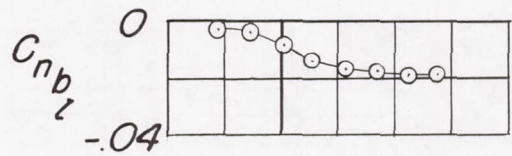
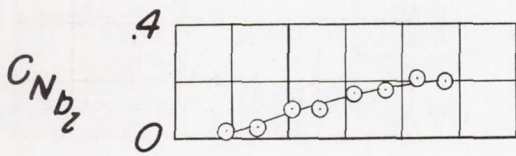


(d) M = 0.86.

Figure 19.- Continued.



○ — Fins off



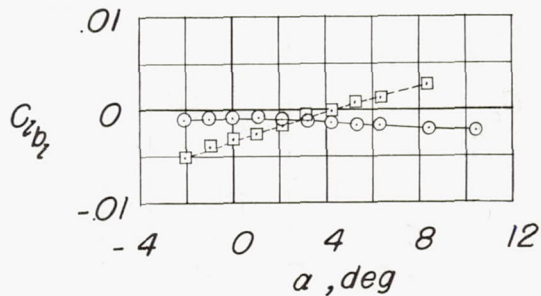
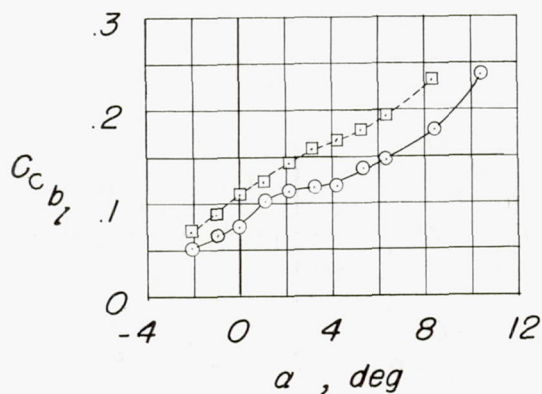
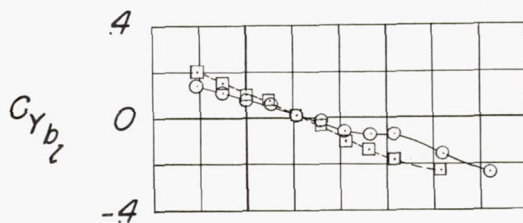
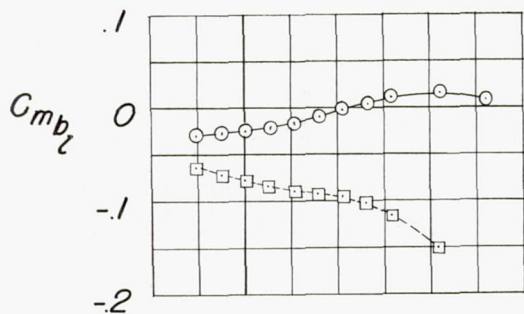
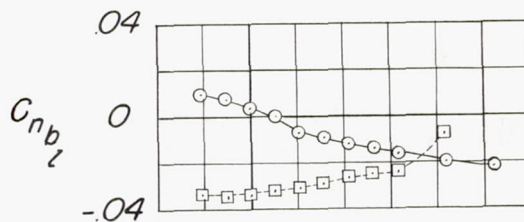
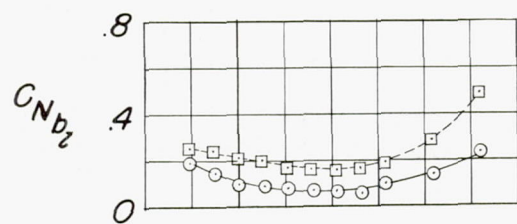
(e) $M = 0.91$.

Figure 19.- Concluded.



○ — Fins off

□ — Fins on

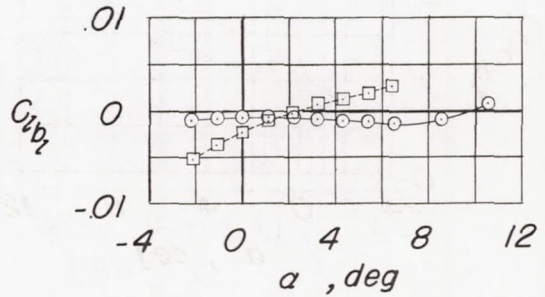
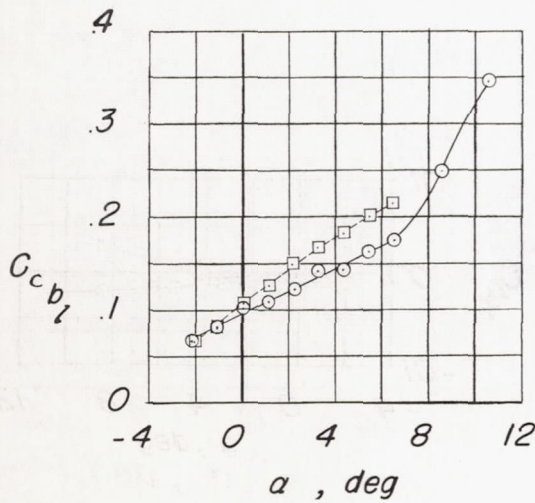
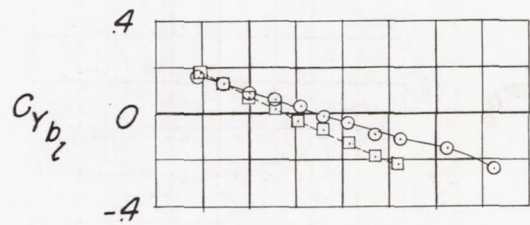
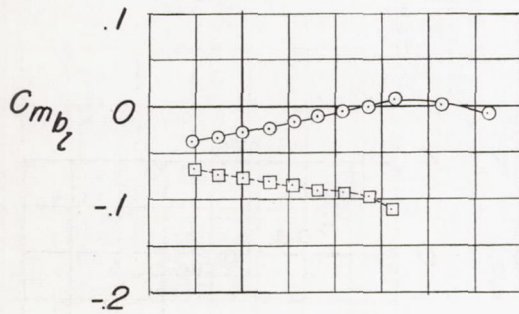
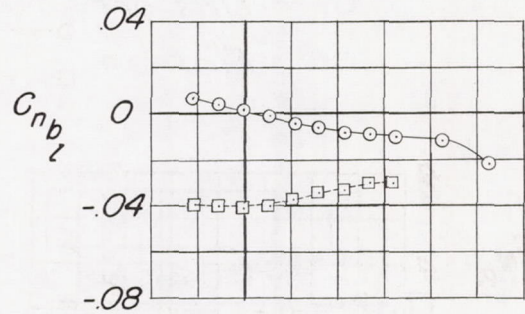
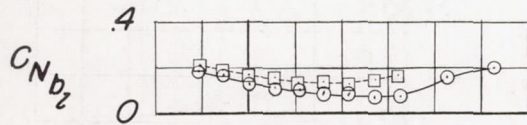


(a) $M = 0.50$.

Figure 20.- Aerodynamic characteristics of body on short 64A010-section pylon located on left wing of unswept-wing model.



○ — Fins off
 □ — Fins on

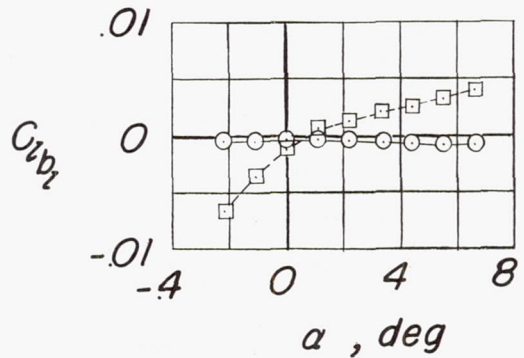
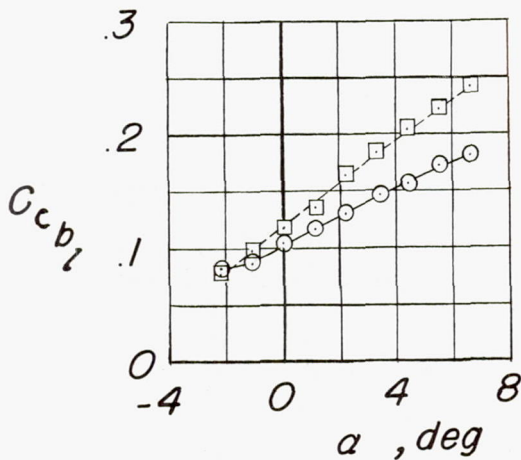
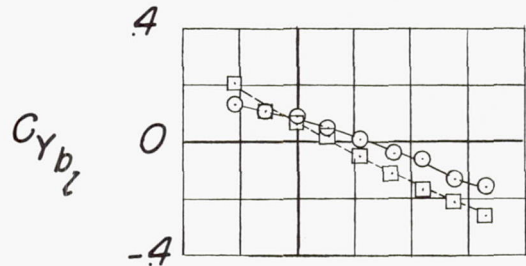
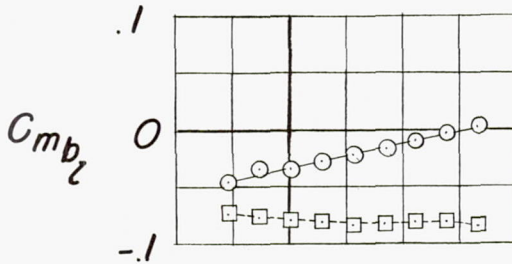
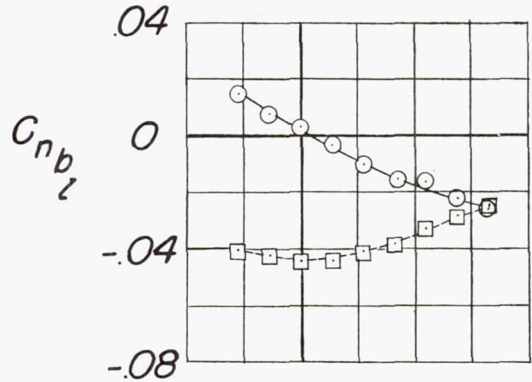
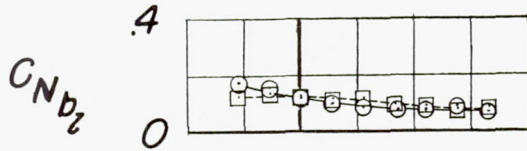


(b) $M = 0.70$.

Figure 20.- Continued.



○ — Fins off
 □ — Fins on

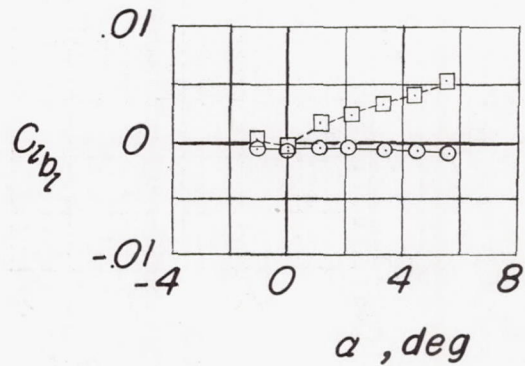
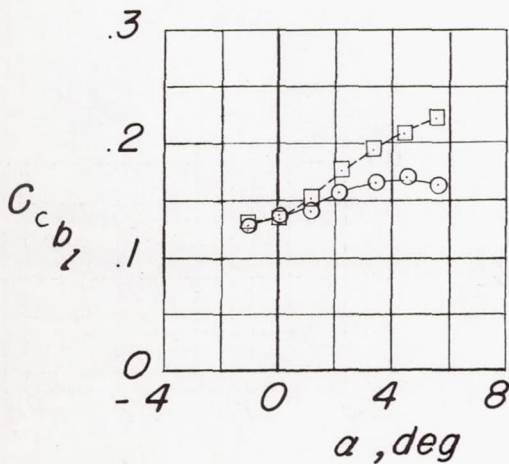
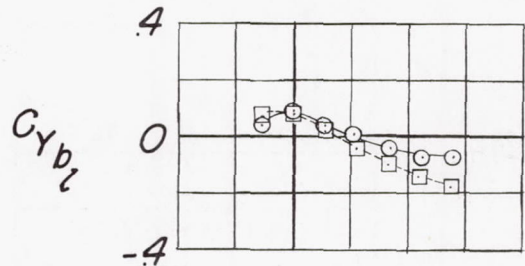
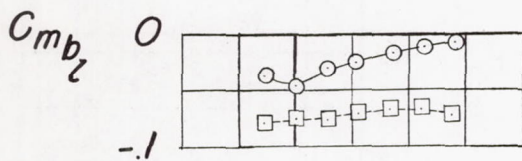
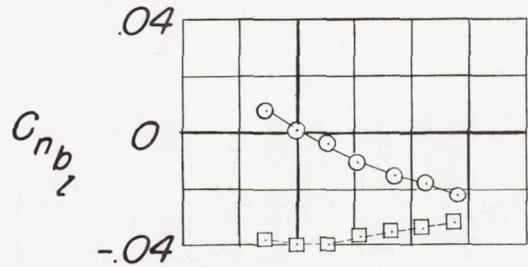
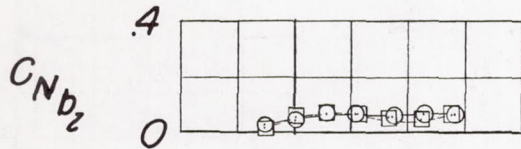


(c) M = 0.80.

Figure 20.- Continued.



○ — Fins off
 □ — Fins on



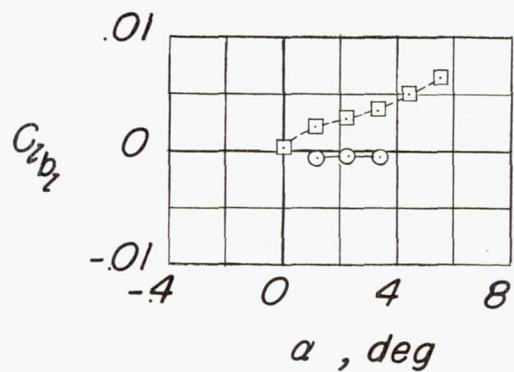
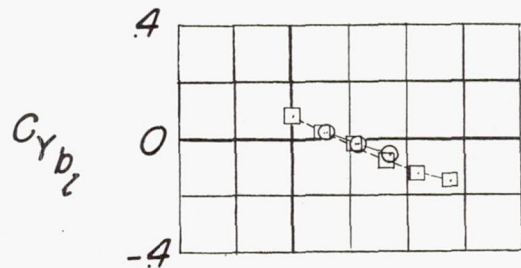
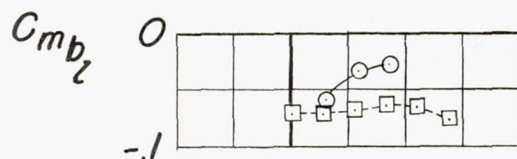
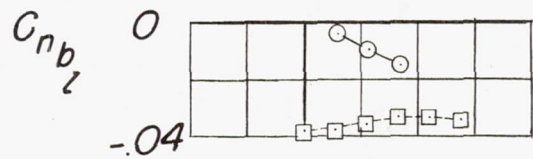
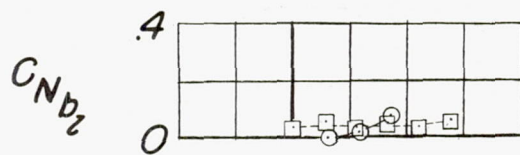
(d) $M = 0.86$.

Figure 20.- Continued.



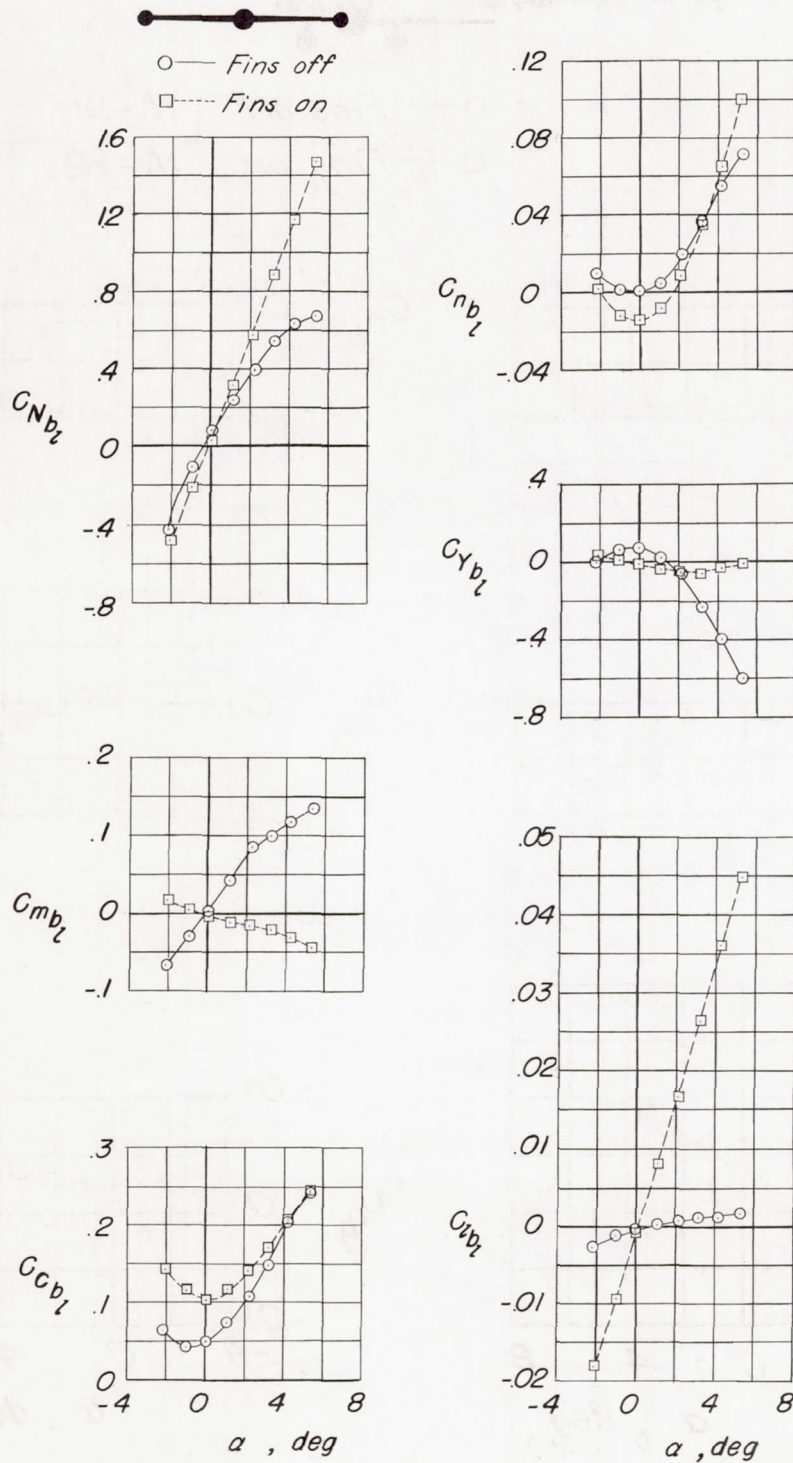
○— Fins off $M = .91$

□--- Fins on $M = .89$



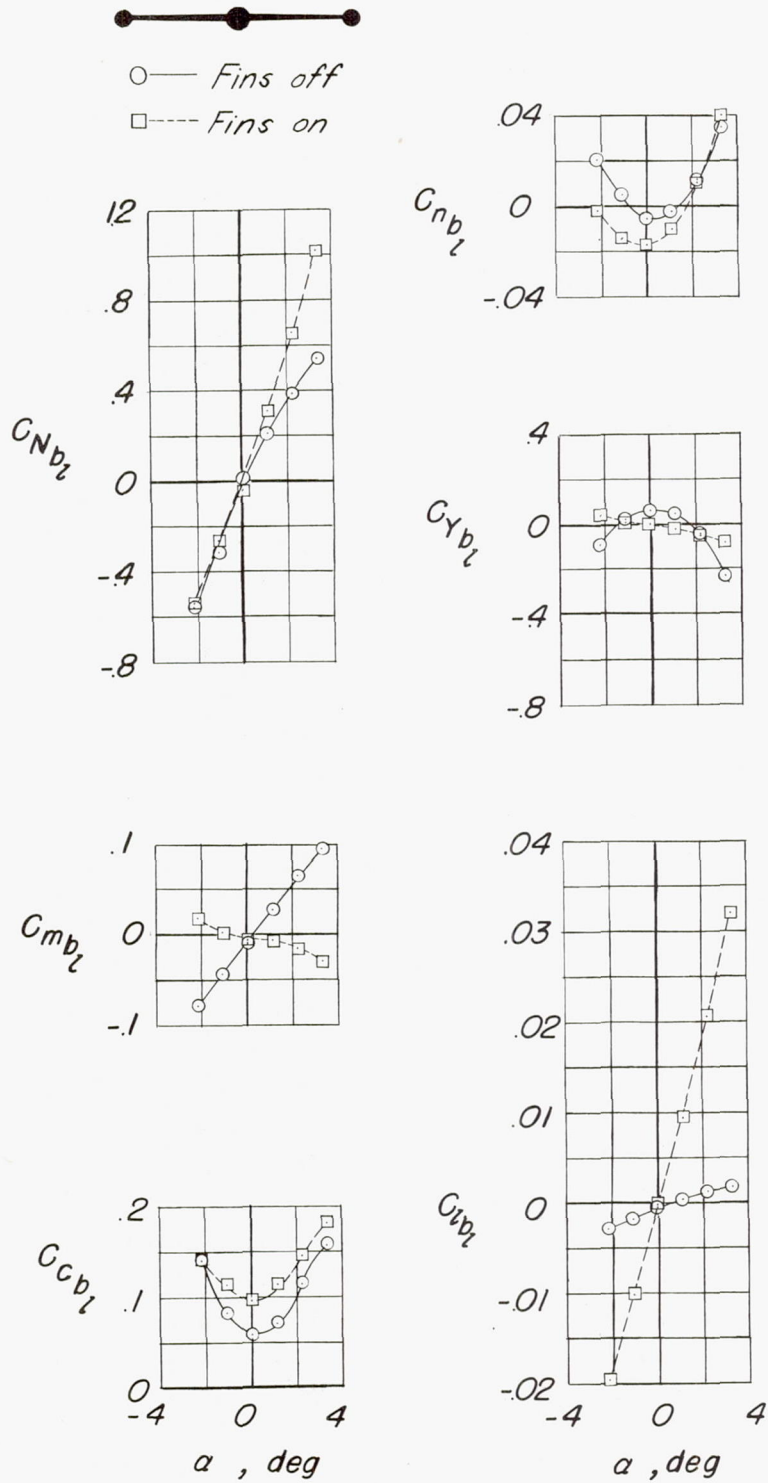
(e) $M \approx 0.90$.

Figure 20.- Concluded.



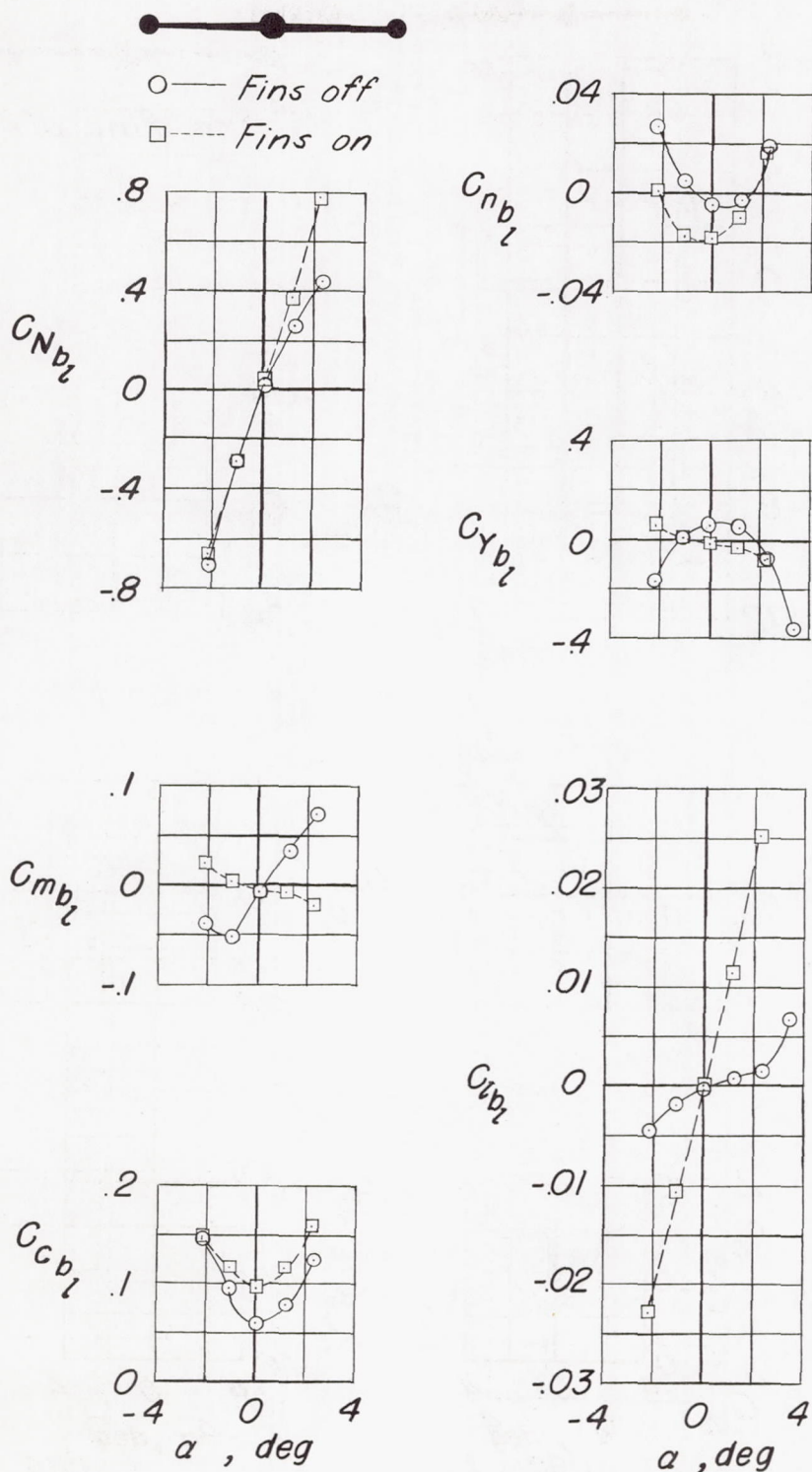
(a) $M = 0.50$.

Figure 21.- Aerodynamic characteristics of body located on left wing tip of unswept-wing model.



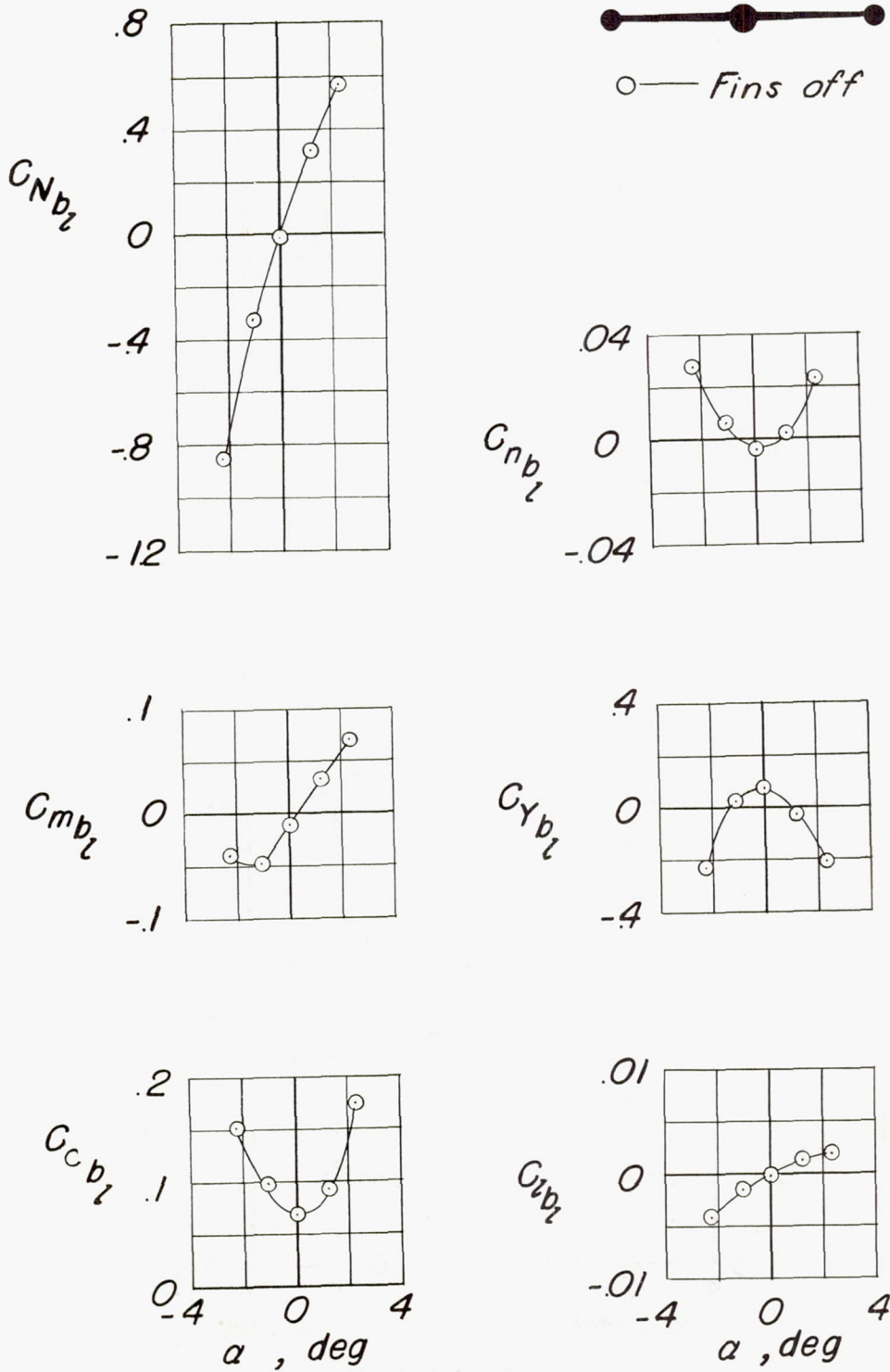
(b) $M = 0.70$.

Figure 21.- Continued.



(c) $M = 0.80$.

Figure 21.- Continued.



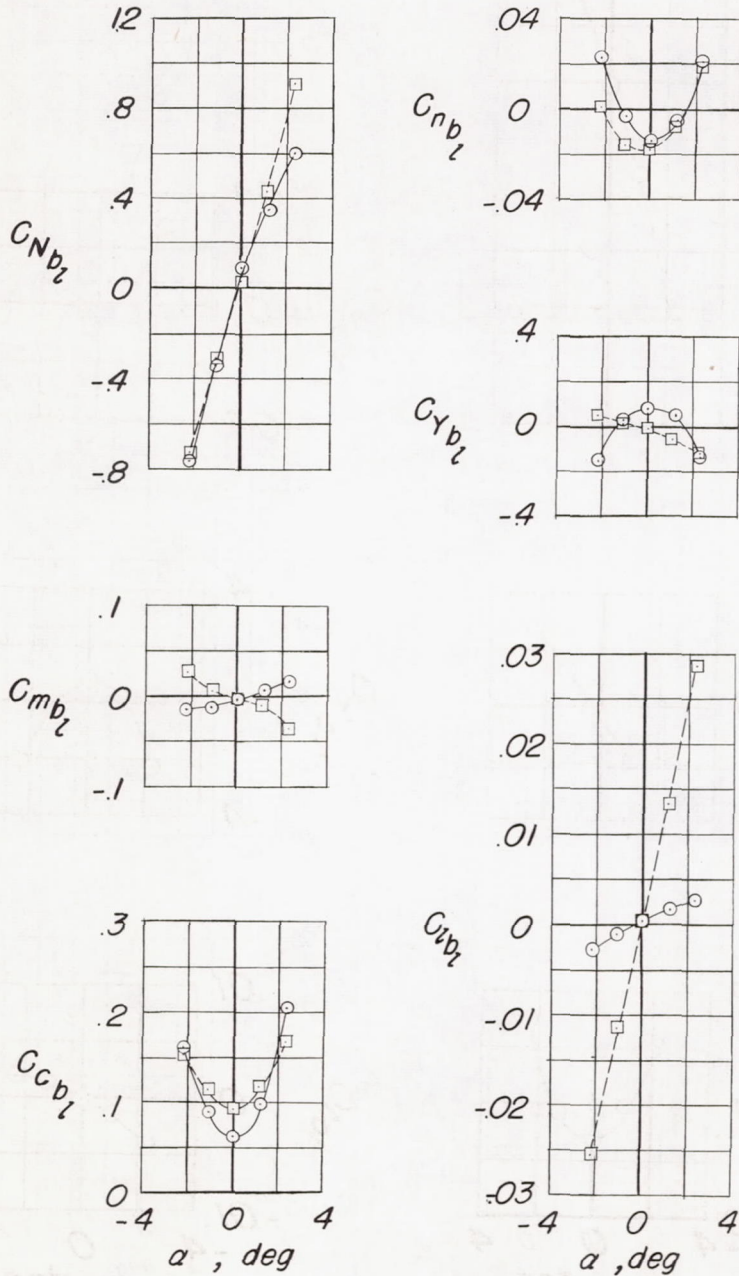
(d) · M = 0.86.

Figure 21.- Continued.



○— Fins off $M=91$

□--- Fins on $M=89$



(e) $M \approx 0.90$.

Figure 21.- Concluded.

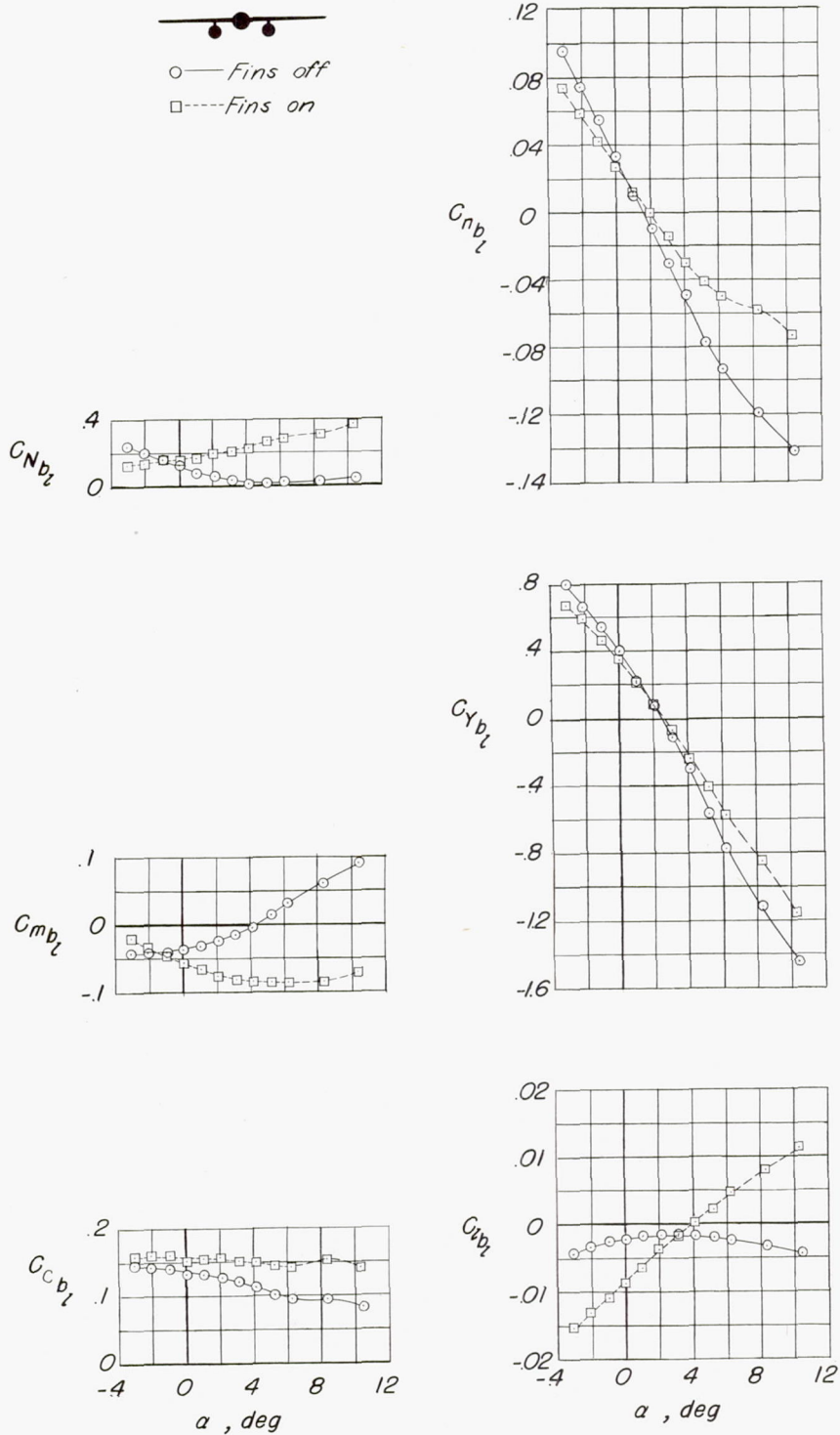
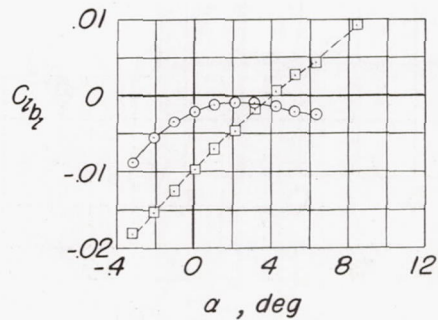
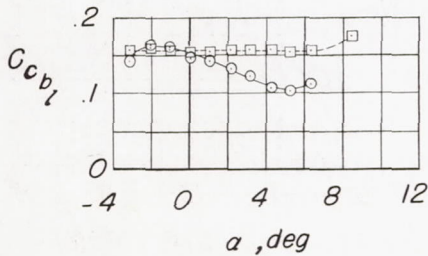
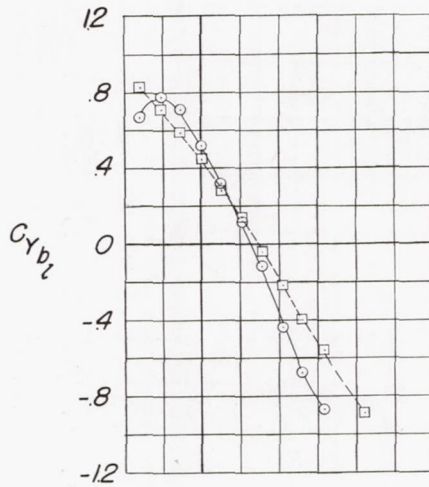
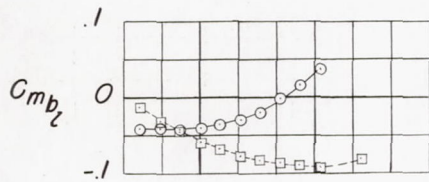
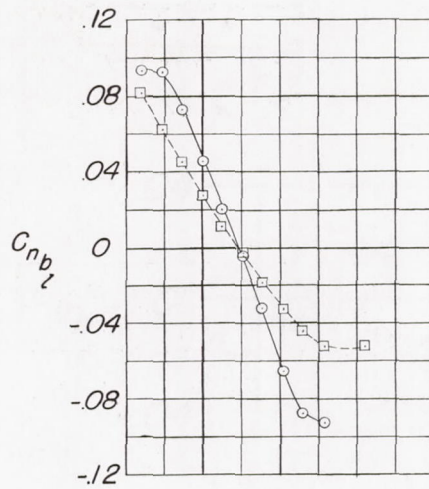
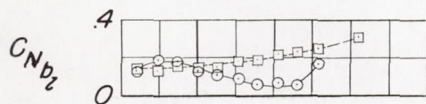


Figure 22.— Aerodynamic characteristics of body on short 64A010-section pylon located on left wing of swept-wing model.



○ — Fins off
 □ — Fins on



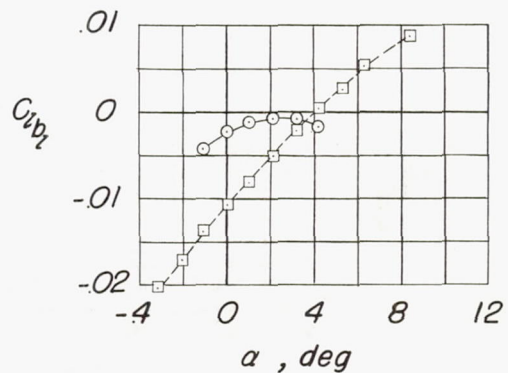
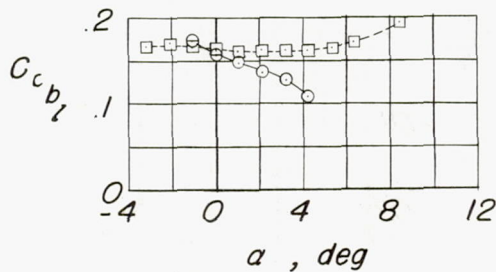
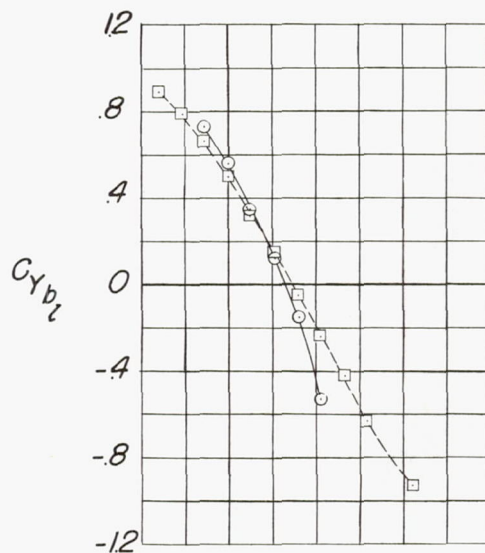
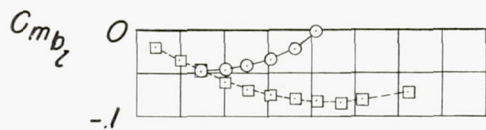
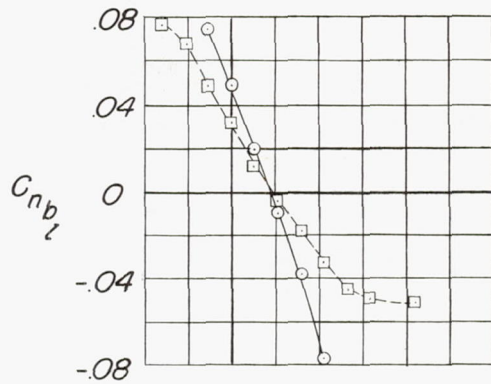
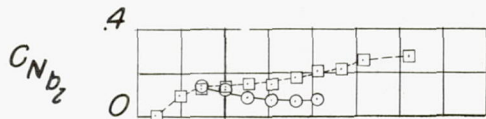
(b) $M = 0.70$.

Figure 22.- Continued.



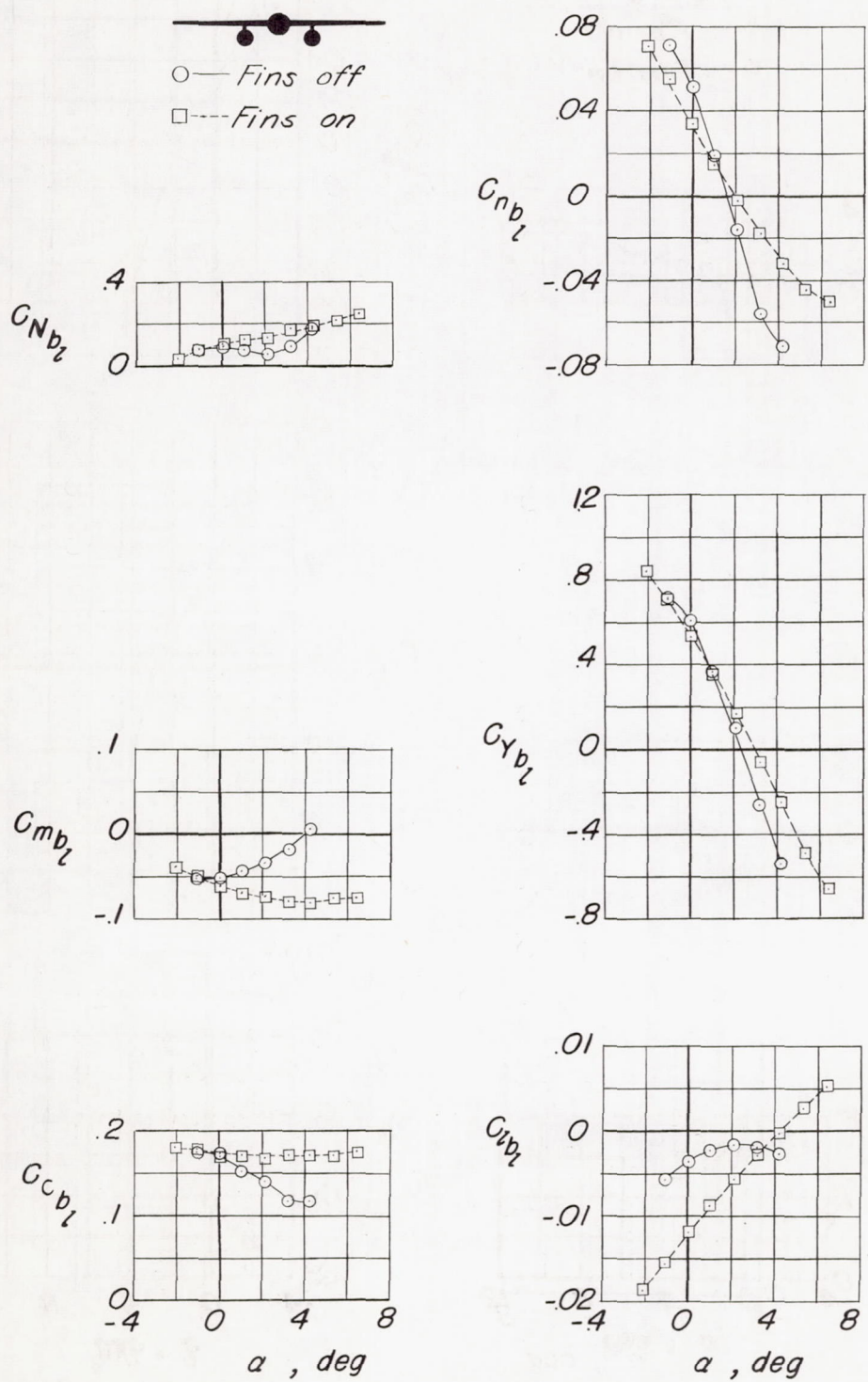
○ — Fins off

□ — Fins on



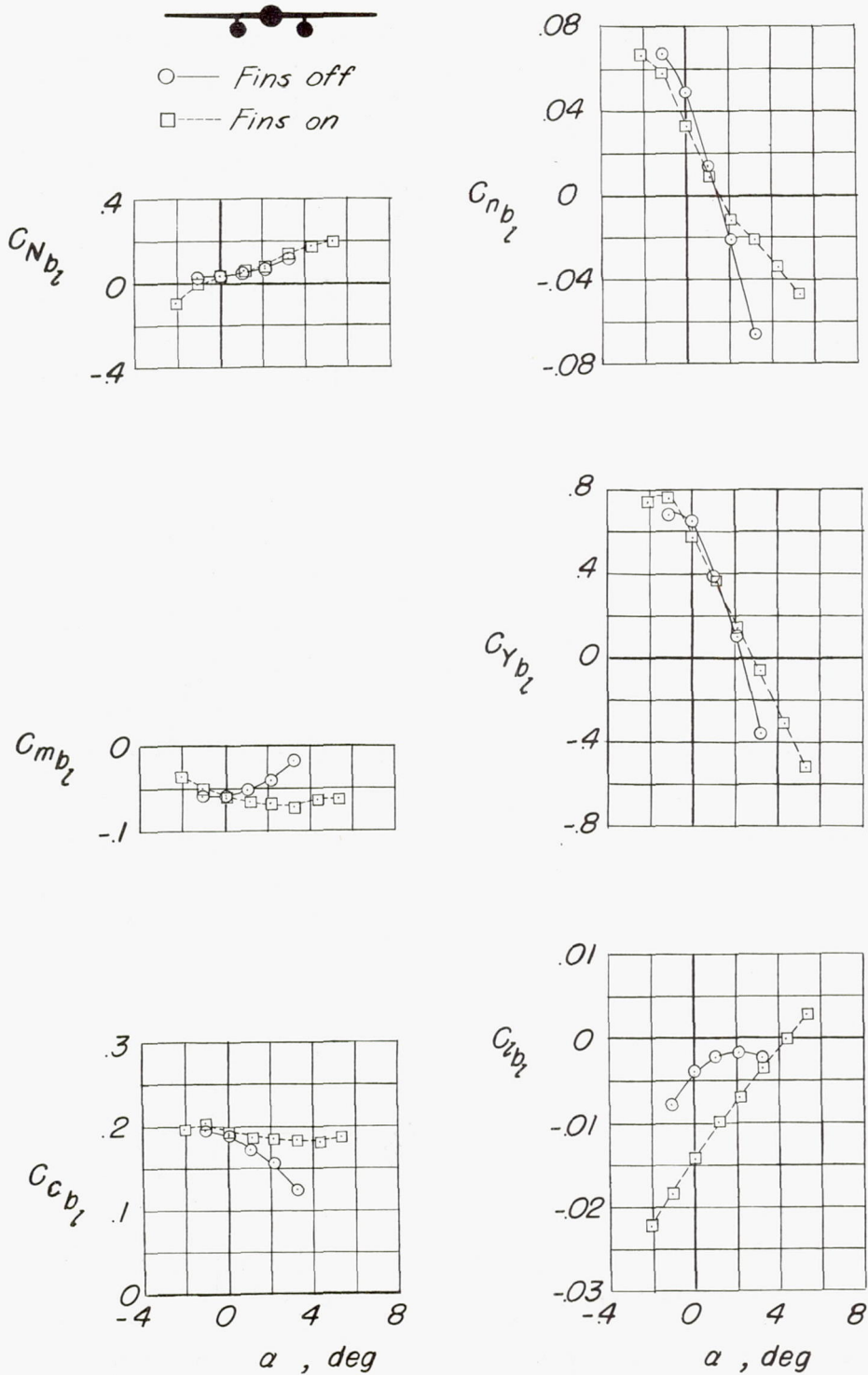
(c) M = 0.80.

Figure 22.- Continued.



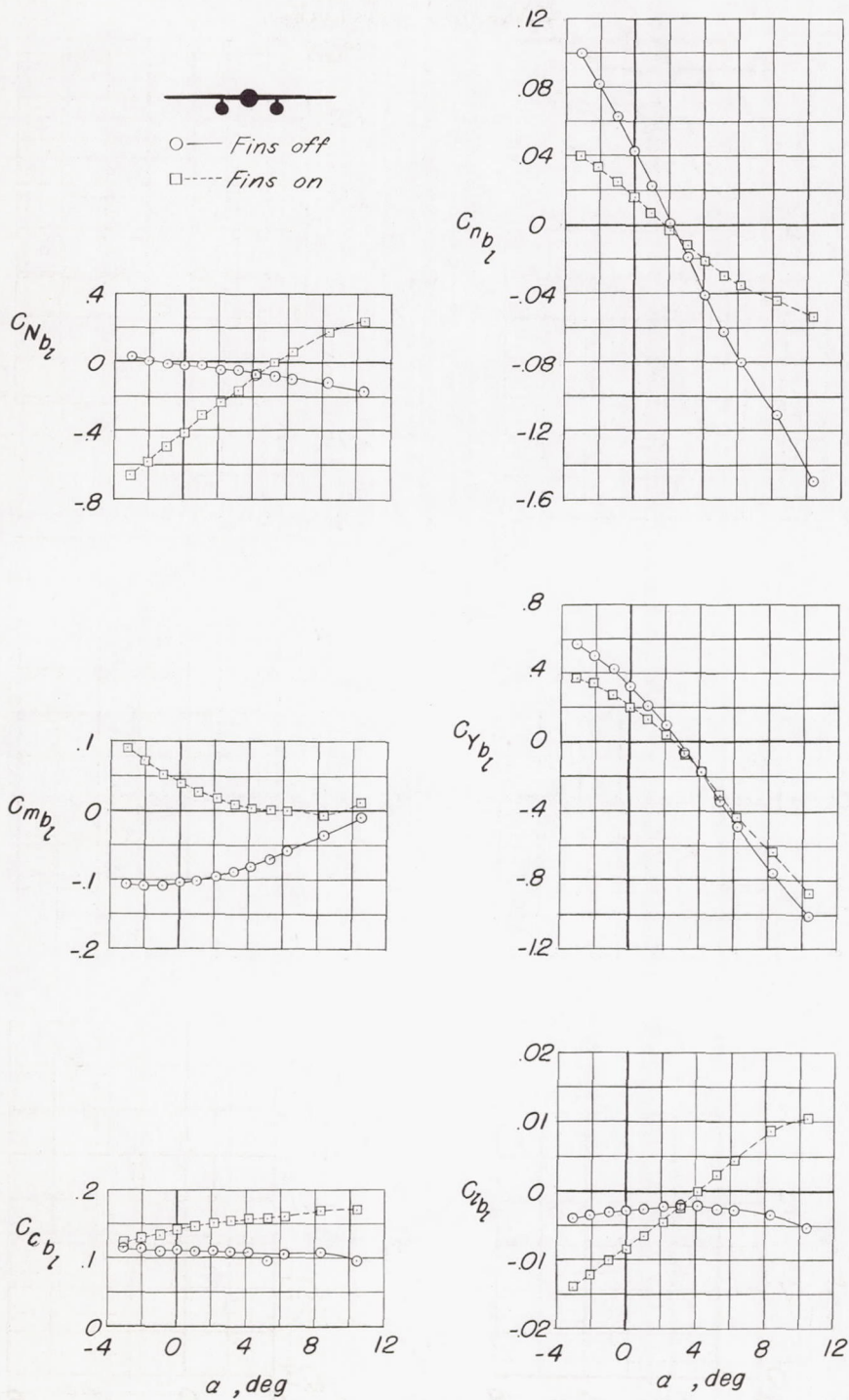
(d) $M = 0.86$.

Figure 22.- Continued.



(e) $M = 0.91$.

Figure 22.- Concluded.

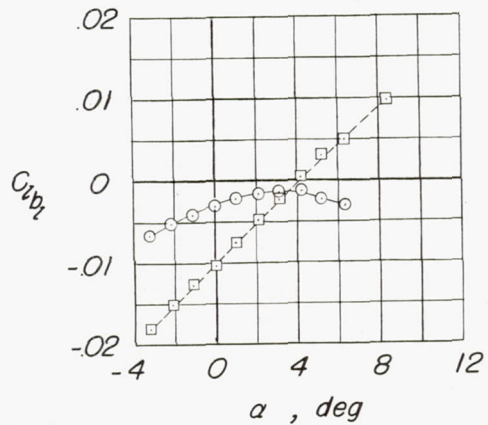
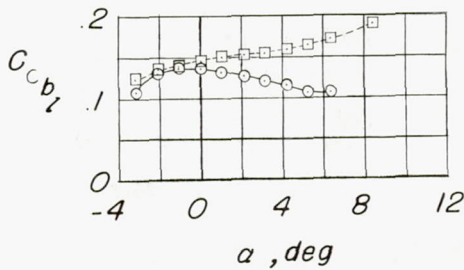
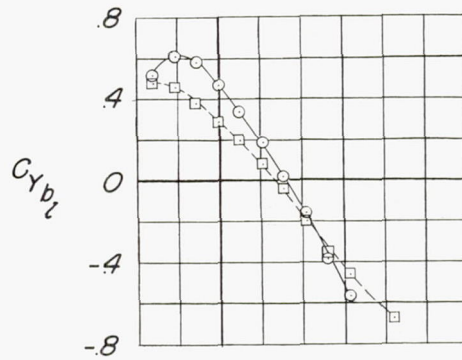
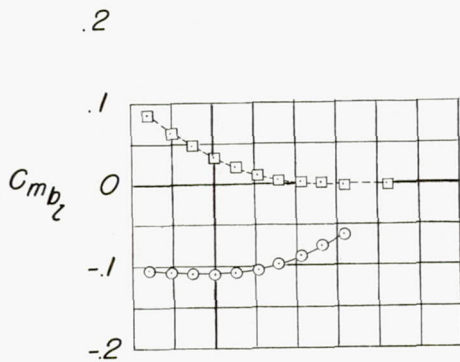
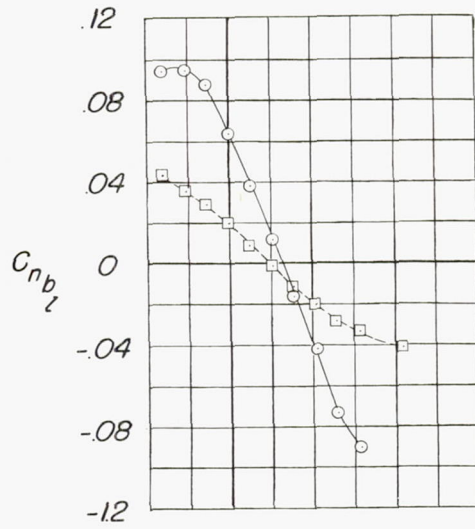
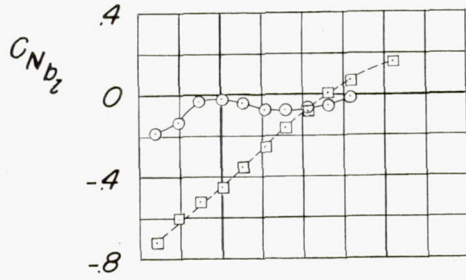


(a) $M = 0.50$.

Figure 23.- Aerodynamic characteristics of the body on the short 64A010-section pylon located on the left wing of the swept-wing model with body axis tilted -5° .



○ — Fins off
 □ — Fins on

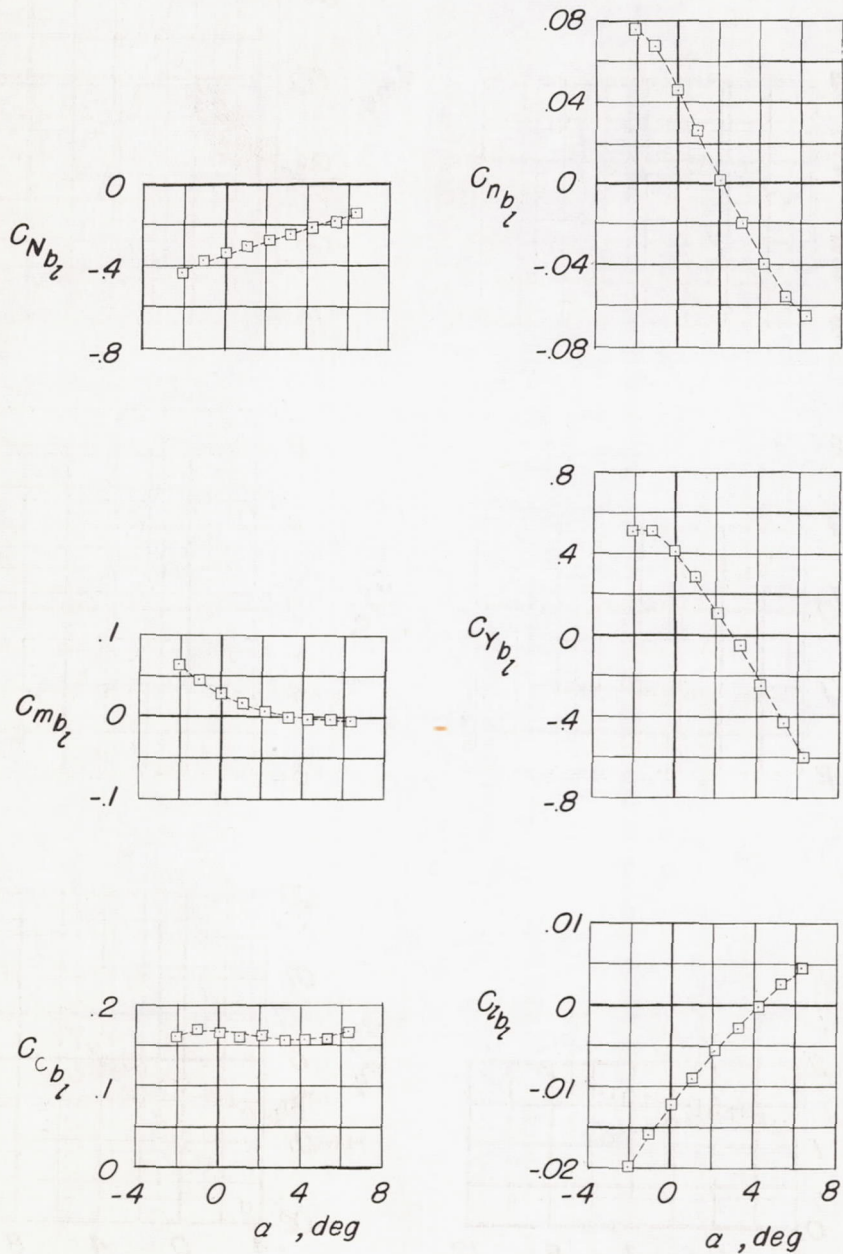


(b) M = 0.70.

Figure 23.- Continued.



□---Fins on

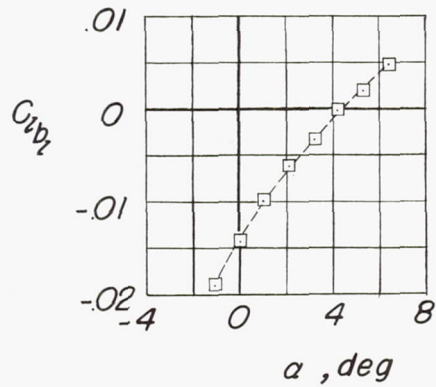
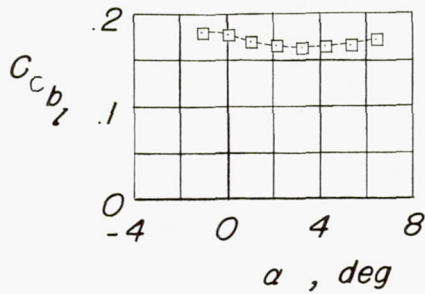
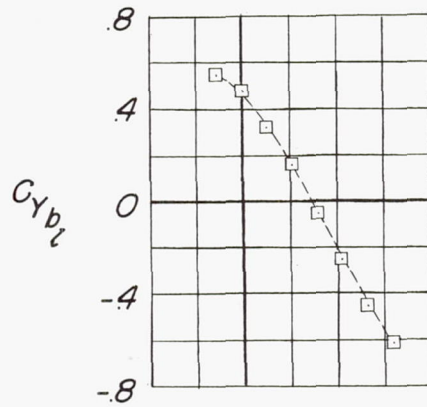
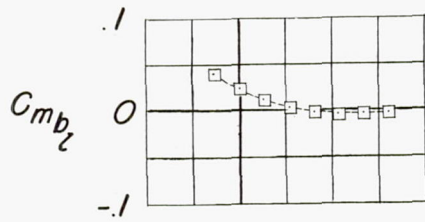
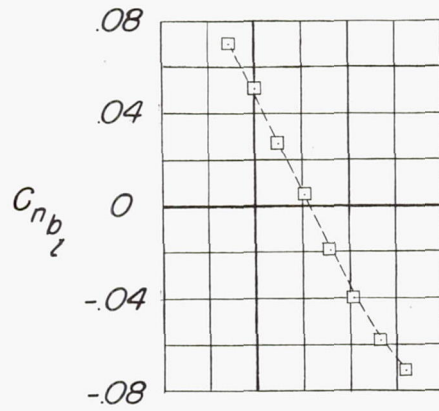
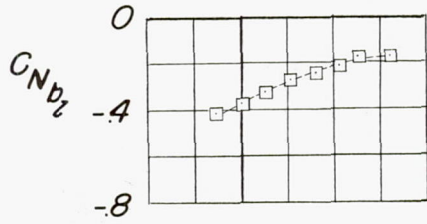


(c) $M = 0.80$.

Figure 23.- Continued.

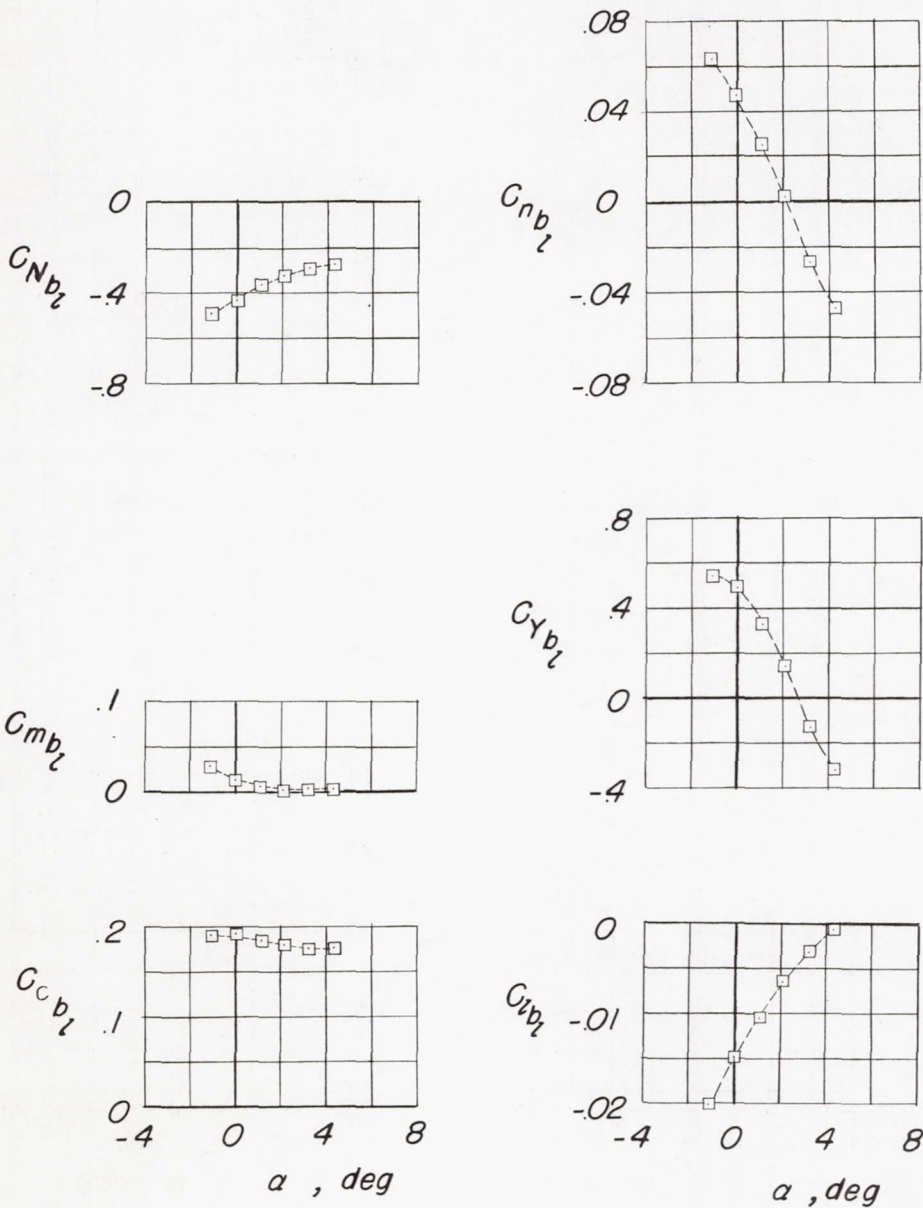
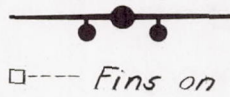


□-----Fins on



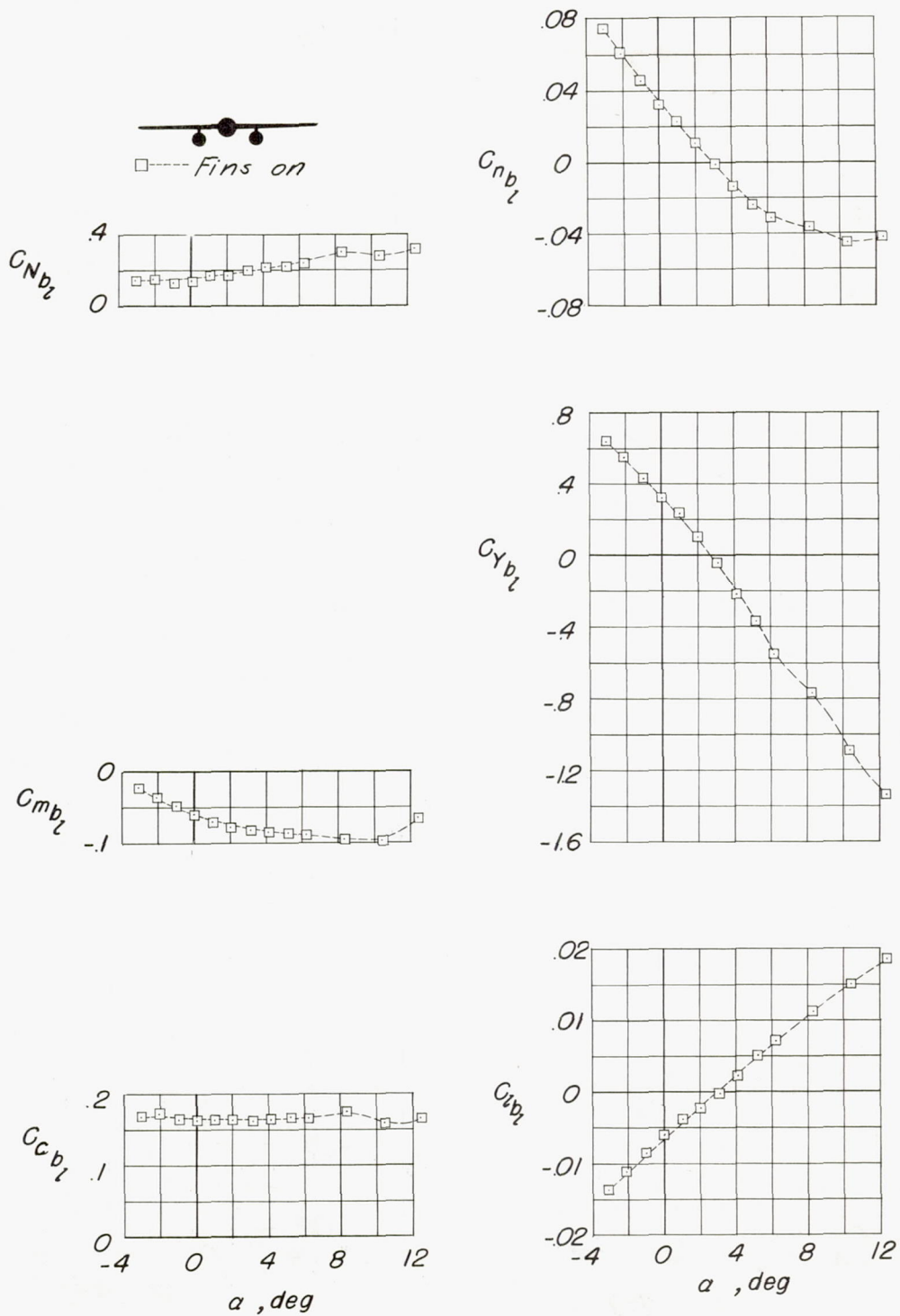
(d) $M = 0.86$.

Figure 23.- Continued.



(e) $M = 0.91$.

Figure 23.- Concluded.

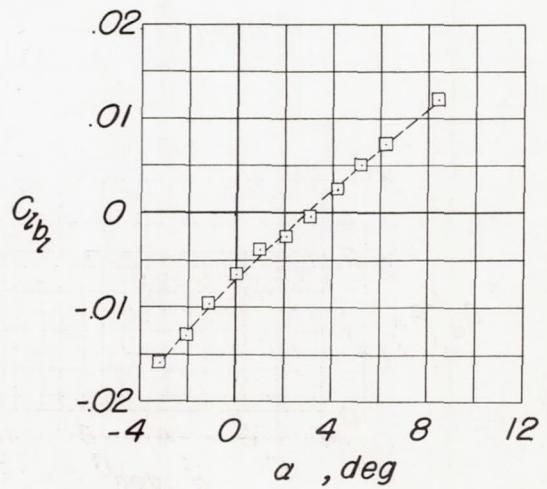
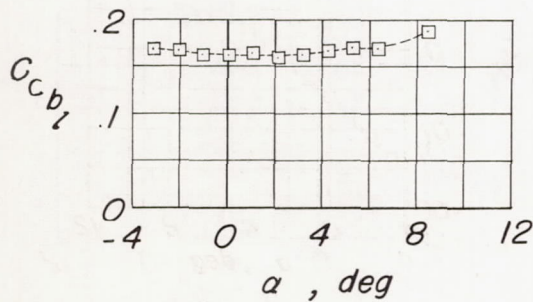
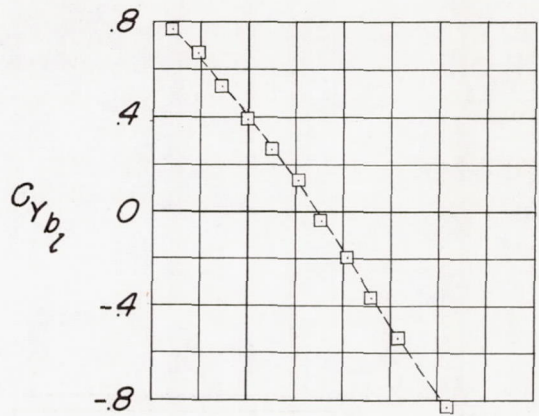
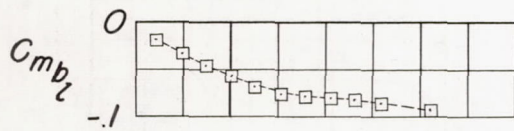
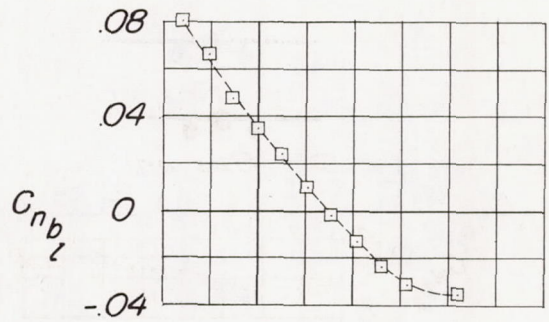
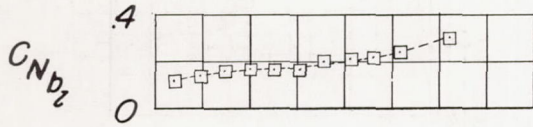


(a) $M = 0.50$.

Figure 24.- Aerodynamic characteristics of the body on the short flat pylon located on the left wing of the swept-wing model.

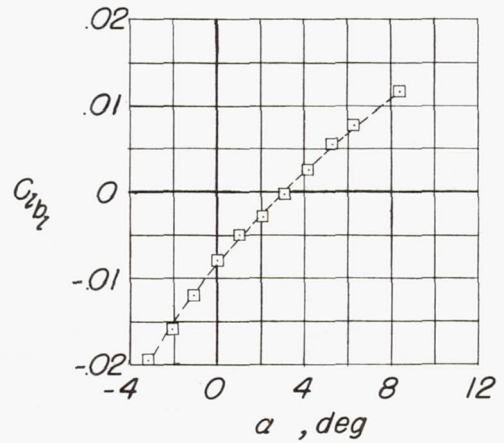
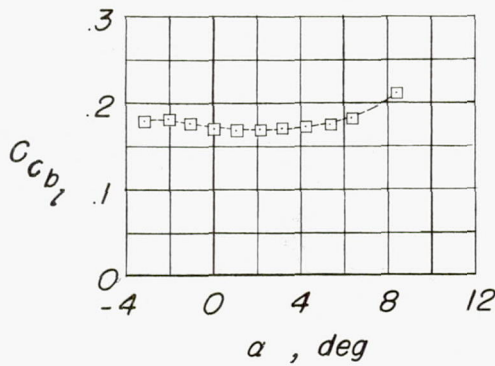
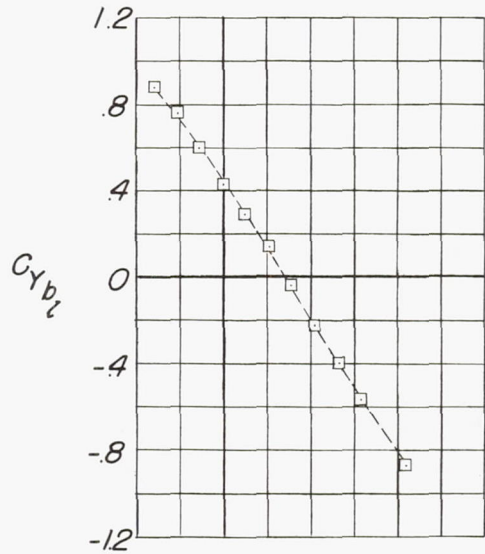
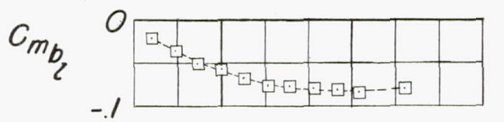
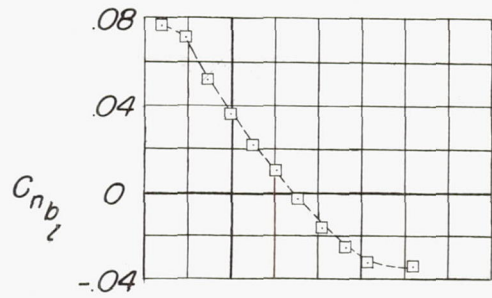
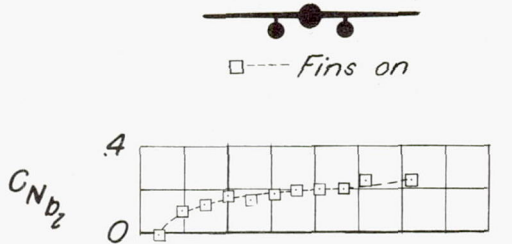


□ --- Fins on



(b) M = 0.70.

Figure 24.- Continued.

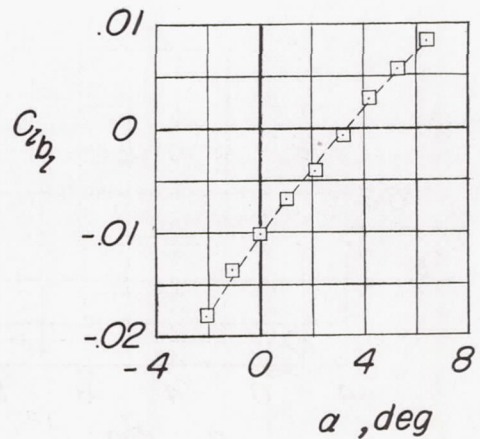
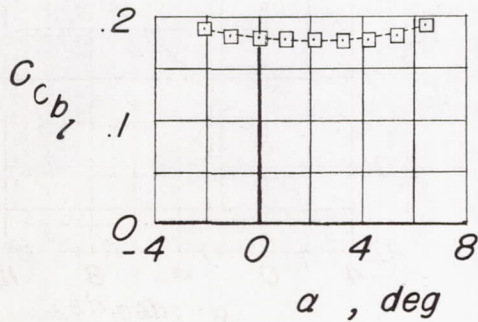
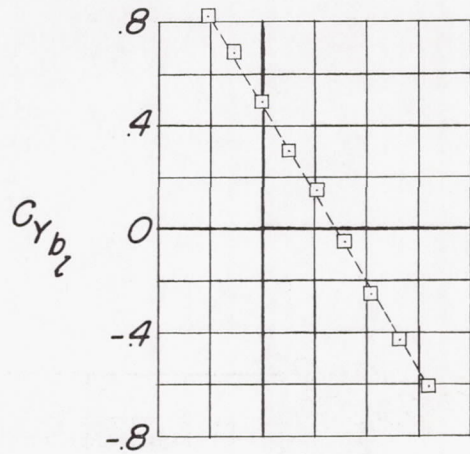
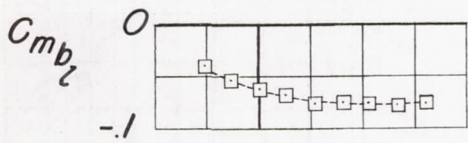
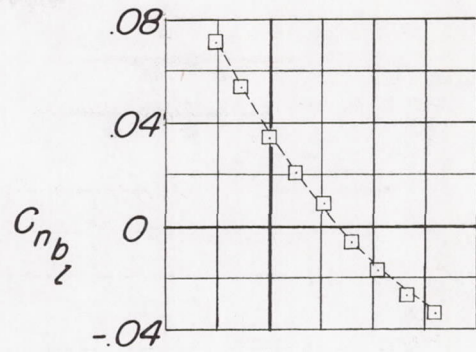
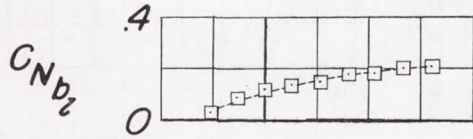


(c) $M = 0.80$.

Figure 24.- Continued.

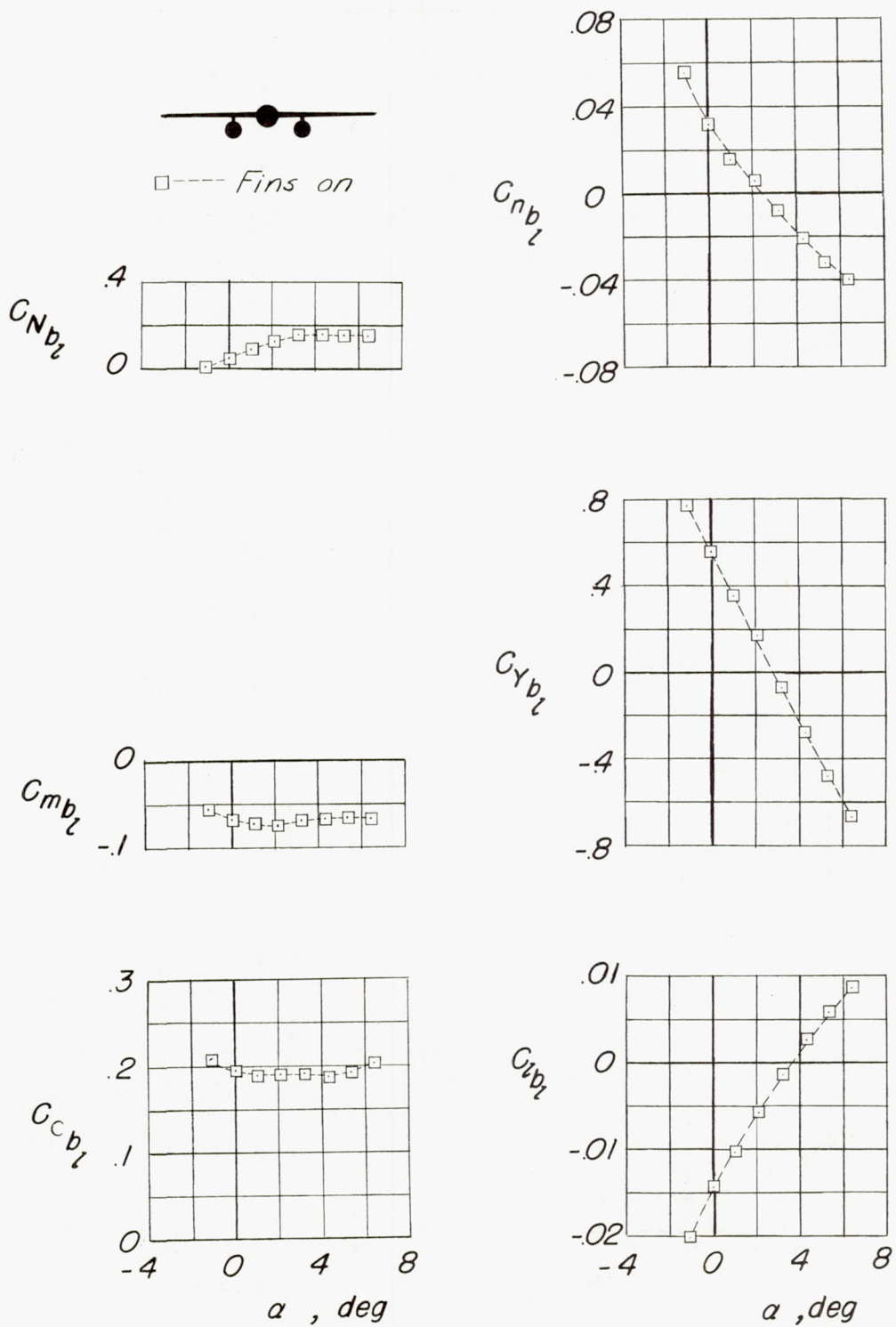


□ --- Fins on



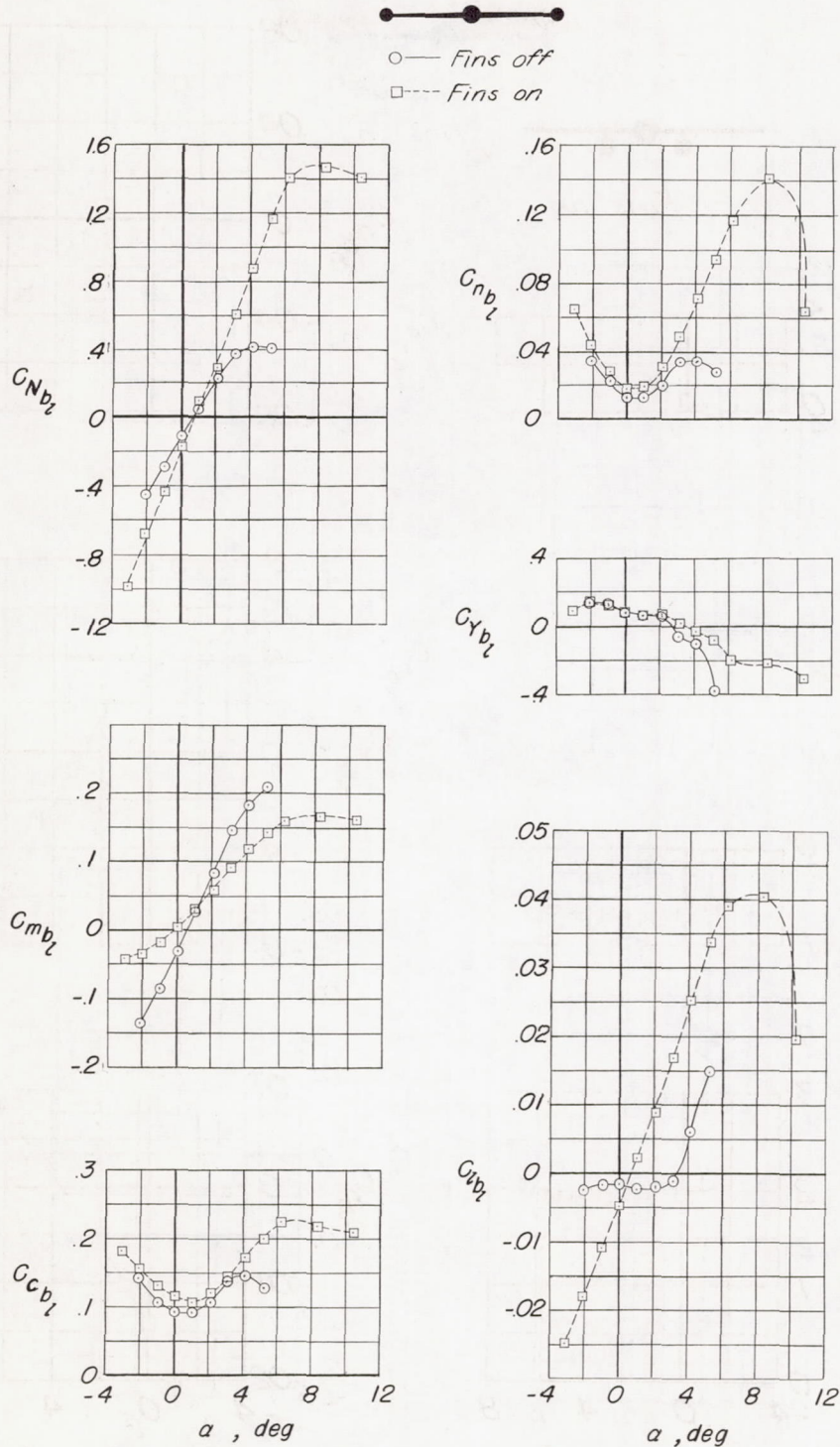
(d) M = 0.86.

Figure 24.- Continued.



(e) $M = 0.91$.

Figure 24.- Concluded.



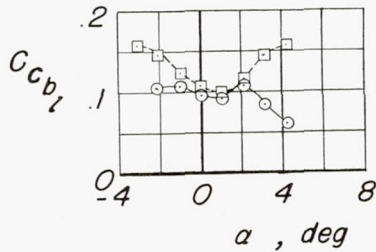
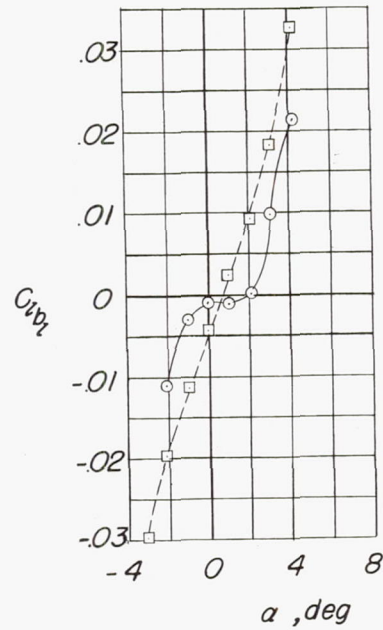
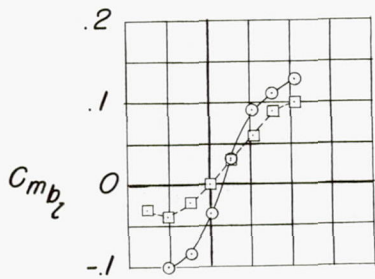
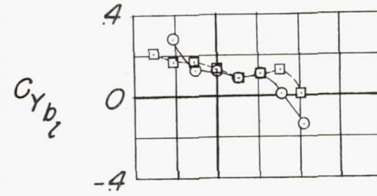
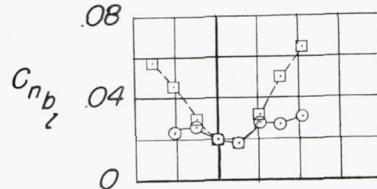
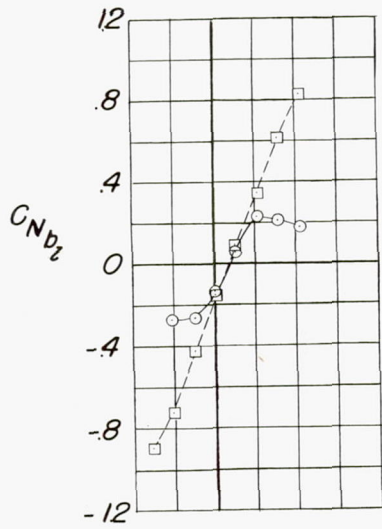
(a) $M = 0.50$.

Figure 25.- Aerodynamic characteristics of the body located on the left wing tip of the swept-wing model.



○ — Fins off

□ — Fins on

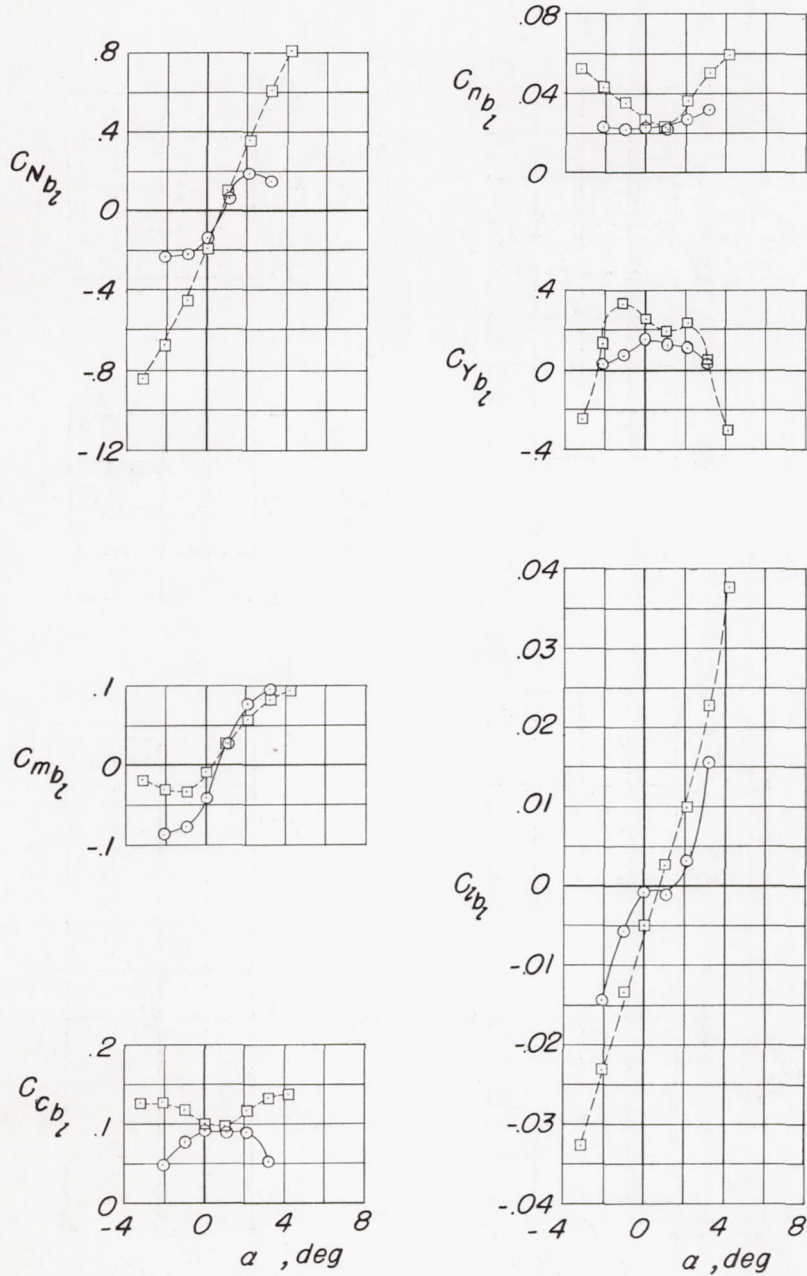


(b) M = 0.70.

Figure 25.- Continued.



○ — Fins off
 □ — Fins on



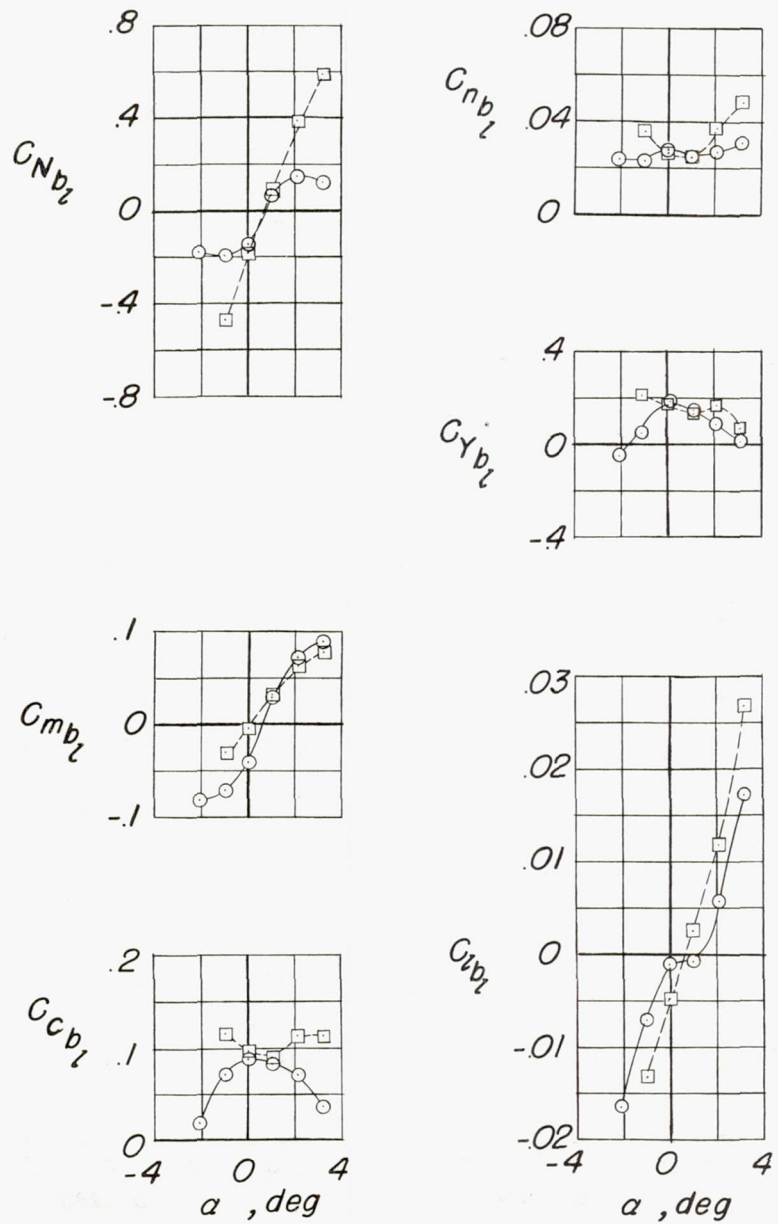
(c) $M = 0.80$.

Figure 25.- Continued.



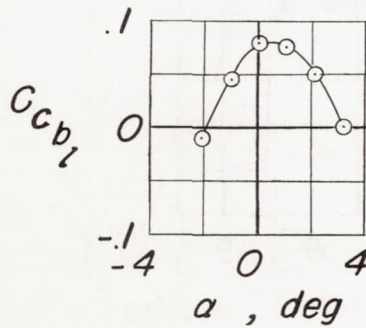
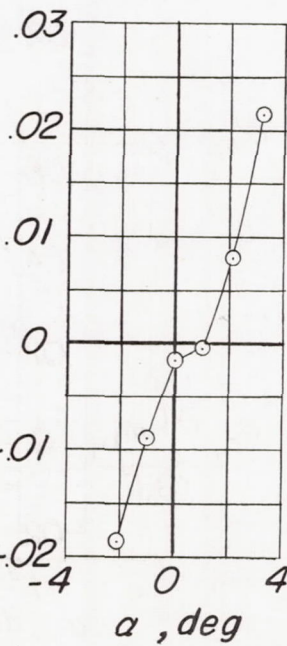
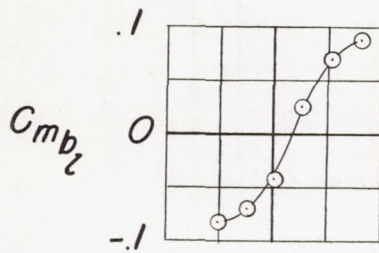
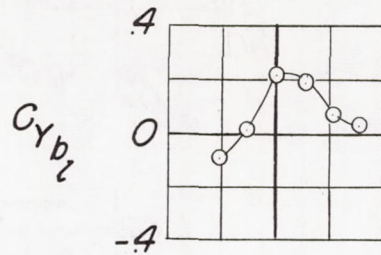
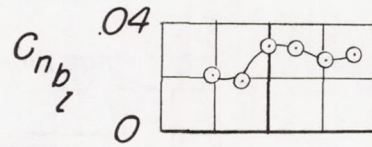
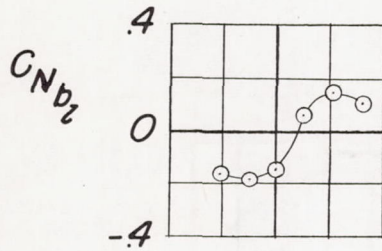
○ — Fins off

□ - - - Fins on



(d) $M = 0.86$.

Figure 25.- Continued.

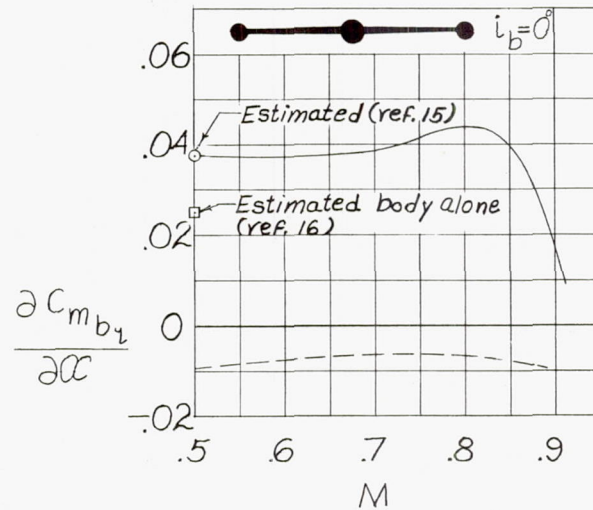
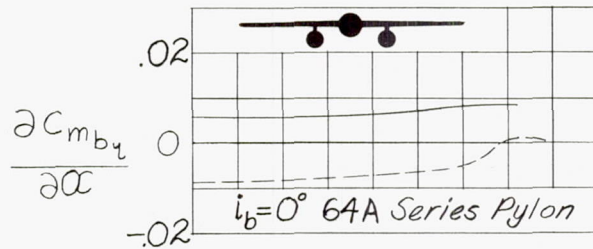
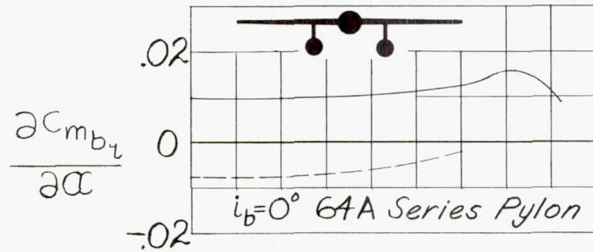


(e) $M = 0.91$.

Figure 25.- Concluded.

$$\Lambda = 3.6^\circ$$

Experiment Estimated
 Fins off ———— ○
 □
 Fins on - - - - -

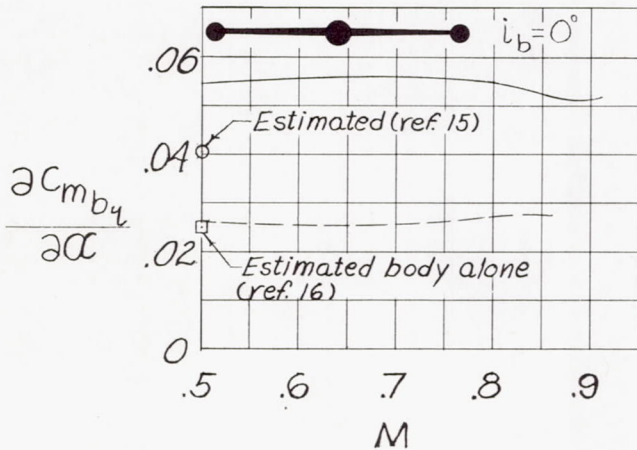
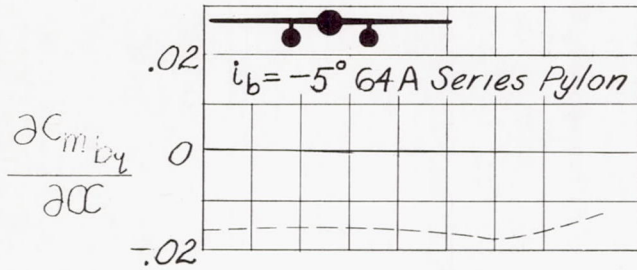
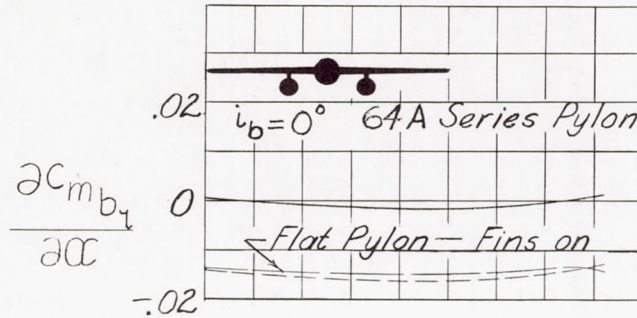


(a) In presence of unswept wing.

Figure 26.- Pitch characteristics of body in several positions on wing of models; $\alpha = 0^\circ$.

$$\Lambda = 46.7^\circ$$

Experiment Estimated
 Fins off ———— ○
 □
 Fins on - - - - -



(b) In presence of swept wing.

Figure 26.- Concluded.